Dark Energy Perturbations beyond Linear Perturbation Theory

Manvendra Pratap Rajvanshi

A thesis submitted for the partial fulfillment of

the degree of Doctor of Philosophy

Department of Physical Sciences,

Indian Institute of Science Education and Research Mohali

Knowledge city, Sector 81, SAS Nagar, Manauli PO, Mohali 140306, Punjab,

India.

June 10, 2021

Declaration

The work presented in this thesis has been carried out by me under the guidance of Prof. Jasjeet Singh Bagla at the Indian Institute of Science Education and Research, Mohali. This work has not been submitted in part or in full for a degree, a diploma, or a fellowship to any other university or institute. Whenever contributions of others are involved, every effort is made to indicate this clearly, with due acknowledgment of collaborative research and discussions. This thesis is a bonafide record of original work done by me and all sources listed within have been detailed in the bibliography.

Manvendra Pratap Rajvanshi
(Candidate)

In my capacity as the supervisor of the candidate's thesis work, I certify that the above statements by the candidate are true to the best of my knowledge.

Jasjeet Singh Bagla
(Supervisor)

Acknowledgements

I would like to acknowledge the kind guidance and support of my Ph.D. guide Prof. Jasjeet S. Bagla. He has been a very kind and helpful mentor. I acknowledge IISER Mohali for providing all the necessary facilities for this Ph.D. project. I thank Govt. of India for providing fellowships for all my undergraduate and doctoral studies. I am thankful to my Ph.D. thesis committee members for their valuable inputs. I would like to thank Dr. H.K. Jassal and Dr. Avinash Singh for fruitful collaborations. I am also thankful to my colleagues at the IISER Mohali Astro group. I would like to use this opportunity to thank all my friends, who have been there to support me in various phases of my life. I would like to express my gratitude to my family (my parents, sister, and brother-in-law) for their constant support, love, and motivation.

Abstract

Two of the most prominent challenges for modern cosmology are dark matter and dark energy. Observations show that rate of expansion of the Universe is increasing. Our current theory of gravitation: Einstein's General Relativity (GR) cannot account for this accelerated expansion if the Universe contains only normal matter and radiation. For GR to explain this late time acceleration, one needs to assume the presence of a new constituent in the energy budget. This constituent is dubbed "Dark Energy (DE)" and needs to have unusual properties like negative pressure. A number of DE models have been proposed. The "standard" model of cosmology (ΛCDM) has the Cosmological Constant (Λ), that acts as dark energy with a constant density and pressure. In contrast, there are theories of dark energy e.g. quintessence, chaplygin gas, tachyonic field, k-essence, etc. where density and pressure can vary in space-time. Although, ΛCDM is consistent with data, theoretical basis of such a constant is problematic. There are issues like the fine-tuning problem, coincidence problem, etc. This provides motivation for models beyond Λ. Methods need to be developed that can help distinguish between these models. Study of perturbations can help achieve this as perturbations might evolve differently in different models. Perturbations are studied at varying levels of approximation, e.g., linear theory approximation, spherical/ellipsoidal symmetry, N-body simulations, etc. This sets the context for this thesis. In this thesis, we study perturbations in scalar field based dark energy models: quintessence and tachyonic fields. We do relativistic, spherically symmetric simulations for both fields, with minimal assumptions. We derive equations in spherically symmetry, starting directly from action, without imposing any additional limitation on clustering properties of dark energy. We numerically calculate the evolution of this system for several lengthscales for initially overdense and underdense halos. We find that, even though we start with a homogeneous scalar field, perturbations are induced in quintessence because of minimal coupling. Induced perturbations grow with time but the amplitude remains small even when matter perturbations become nonlinear. DE density and equation of state (w) become functions of space-time. We also show that at late times, perturbation growth rate is slightly faster than that predicted by linear theory. Dark energy perturbations are stronger in large voids. Length scales play an important role as perturbations at large scales show faster growth for the same dark matter perturbation amplitude. We also study the prospects of distinguishing these two models using results from spherical collapse and linear perturbation theory. For the purpose of comparison between models we need methods of reconstructing potentials to reproduce a given expansion his-

tory. For quintessence and tachyonic fields we reconstruct potentials for a given $w(z)$. We show that closed form expressions for $V(\phi)$ can be obtained only for a limited classes of $w(z)$. We derive the necessary equations and then outline a numerical schema for reconstructing potentials for any general $w(z)$. This scheme is based on numerical interpolation technique of cubic splines. We also reconstruct potential for a coupled quintessence model, where background expansion mimics the ΛCDM model. A unique investigation that we carry out is this: if the background cosmology for two different models is tuned exactly, so that observations like supernovae cannot distinguish these, can the two models be distinguished by perturbations (linear and spherically symmetric nonlinear)? We do a systematic comparison of quintessence and tachyonic scalar fields. This is done using methodologies for reconstruction of potentials for two field models, given a particular background expansion. This allows us to delineate differences coming from different background and those coming from differences in dynamics of perturbations, owing to different nature of Lagrangians for quintessence and tachyonic models. We find that differences in dark matter and metric perturbations are weak and dependent on deviation of background from $w = -1$. Expansion histories that deviate significantly from Λ or $w = -1$, show large differences while models close to $w = -1$ show very little difference. Dark energy perturbations do show differences between the two classes of models, but these remain too weak to affect the metric/matter fluctuations. For the background expansions constrained by current data, the prospects of distinguishing models just on the basis of perturbations are not promising.

We also consider the question of distinguishing tachyonic and quintessence models with the same expansion history using Cosmological (Linear) Perturbation Theory. We show that while dark energy perturbations show differences, these are insignificant for effects on observables. Consistent with results from previous chapter, we find that for expansion histories allowed by data, distinguishing two models is extremely difficult on the basis of dark energy perturbations. To validate this result, we use parametric form for effective speed of sound for tachyonic and quintessence models, modify CMB code CLASS, and try to constrain these parameters. We find that the parameters remain unconstrained by present data. We also use CMB data to constrain common tachyonic models.

List of Publications

- Manvendra Pratap Rajvanshi and J.S. Bagla,
  Nonlinear spherical perturbations in quintessence models of dark energy,
  Journal of Cosmology and Astroparticle Physics, Volume 2018, June 2018
  doi: 10.1088/1475-7516/2018/06/018 [arXiv:1802.05840]

- Manvendra Pratap Rajvanshi, J. S. Bagla
  Reconstruction of dynamical dark energy potentials: Quintessence, tachyon and interacting models, J Astrophys Astron (2019) 40: 44. [arXiv:1905.01103]

- Manvendra Pratap Rajvanshi, J. S. Bagla
  Non-linear spherical collapse in tachyon models and a comparison of collapse in tachyon and quintessence models of dark energy.
  Classical and Quantum Gravity, Volume 37, Number 23
  doi:10.1088/1361-6382/abbb63 [arXiv:2003.07647]

- Manvendra Pratap Rajvanshi, Avinash Singh, H.K. Jassal, and J.S. Bagla,
  Tachyonic vs Quintessence dark energy: linear perturbations and CMB data.
  [arXiv:2104.00982]

Contents

Chapter 1

Introduction

1.1 Cosmology

The Universe and astronomical objects have been a source of wonder and have aroused human curiosity. What started as the identification of heavenly bodies and the pattern they follow, has transformed into various disciplines with varying levels of mathematical rigor. Cosmology is the study of the Universe at the largest scales. It has been known, since Newton's time, that gravitation is the key force in the dynamics of extraterrestrial bodies. At these scales and beyond, any theoretical description of the dynamics of the Universe is intertwined with the theory of gravitation. On one hand, the theory of gravitation forms the foundation for cosmology, and on the other hand, cosmology provides tests of gravitation at the largest scales that can be probed in the Universe.

The first three decades of the 20th century revolutionized both: our concepts of gravitation as well as our understanding of the cosmos. On the theoretical front, the development of General Theory of Relativity (GR) ([1, 2, 3]) completely changed the perspective on gravitational dynamics while observations by Hubble, Slipher, and others ([4, 5]) established the case for an expanding universe. At the time, it was debated if the Universe is static and ever-lasting. Einstein found in his new theory that the Universe cannot be static unless he introduced a new constant in his theory. This new constant was called the "Cosmological Constant (Λ)". Even then the perturbations in the Universe were not static and hence the static model is unstable. Observational work by Hubble, Slipher, etc. showed that Universe was indeed expanding. Hence there was no need for Λ to make the static model viable [6].

The simplest models (see 1.1.2) of the Universe, based on the ideas of isotropy and homogeneity, use the General Theory of Relativity (GR) to predict the average expansion of the Universe. The expansion rate can be measured using luminosity and spectral shifts of astrophysical objects. Calculations that only consider dark matter, radiation, and baryons lead to an ever-slowing expansion rate. In the 1980s and late 1990s, observations from galaxy correlation functions and supernova suggested that the expansion rate is accelerating. This "accelerated expansion" required the introduction of a new component, with the unusual property of negative pressure. This new component was said to represent a new form of energy called "dark energy". Theoretical modeling of this component, simulations of these models, and comparison with observations, form one of the core themes of modern Cosmology and Physics, in general.

The Dark Sector (Dark Energy and Dark Matter) of the Universe is one of the biggest challenges for modern physics. Observations are effectively passive in the sense that we can not set up the phenomena or design a laboratory experiment, we have to be content with information coming to us and try to observe. Besides the observational/experimental limits, there are mammoth challenges on the theoretical side. Calculations/simulations in General Relativity (or its modifications) are extremely complicated. Besides a few very simplified scenarios, almost all calculations require approximations (even when solving on computers). Dark Energy physics brings its own theoretical complexities. Simulations have to be done with various degree of approximations and validity of these have to be tested. Dark Energy models can have perturbations and studying the influence of these on cosmological observables is a very important area of research. Any predicted and confirmed deviations from the standard ΛCDM paradigm will open the doors for new physics.
The study of perturbations in dynamical dark energy models, is mostly done at linear approximations. Nonlinear regime can be simulated in only simplified scenarios. This is the context of this thesis. Here we look into simulations of nonlinear and linear perturbations in scalar field dark energy models.

This chapter sets the context and gives a quick overview of cosmology. We briefly look at some important building blocks of modern cosmology that are relevant to this work. We start by discussing some simple cosmological models. Then we introduce the "accelerated expansion" and henceforth dark energy. This is followed by an introduction to scalar field models of quintessence and tachyonic field.

The remaining sections discuss tools/methodology that are needed for studying dark energy perturbations. The last section describes the layout of this thesis.

1.1.1 General Theory of Relativity (GR)

As mentioned earlier, gravitation is the dominant force at extra-galactic scales. So we need a theoretical description of gravity to build any theoretical model of the Universe. Newton's law of gravity ([7]) was the first founding stone of our understanding of gravity. It is an extremely successful theory across wide domains/scales of applications. However, Newtonian theory of gravity is not compatible with the special theory of relativity (SR)[8, 9]. Newton's law requires action at a distance, which is not allowed as per the principles of SR. So Einstein, who gave his theory of special relativity in 1905, formulated a relativistic theory of gravity, which generalized the special theory of relativity to include dynamics with accelerated observers. This "General Theory of Relativity" ([1, 2]), completely changed the notion of what are the variables of interest for dynamics. It made space-time itself a dynamical quantity that is sourced by the matter energy content of space-time.

In GR, dynamics is formulated in terms of space-time. In Newtonian theory, we start with the distribution of sources (masses), calculate potentials/forces, move the masses, and repeat the process as required. In GR, mass energy distribution acts upon space-time and the geometry of the space-time decides how the constituents evolve. In addition, there can be forces coming from non-gravitational interactions. In absence of other forces, massless particles move on null-geodesics while massive particles follow geodesics. The equations have to be solved simultaneously for metric coefficients as well as the matter and field constituents of the Universe.
In short, in GR, geometry of space-time becomes equivalent to gravity. Metric is related to constituents of that space-time through Einstein Field Equations:

$$G_{\mu\nu} = 8\pi G T_{\mu\nu} \tag{1.1}$$

Here $G_{\mu\nu}$, called the Einstein tensor, encodes the information of space-time geometry while on the right-hand side $T_{\mu\nu}$, called the stress-energy tensor or the stress-momentum tensor, represents the sources/constituents of the Universe.

1.1.2 Homogeneous and Isotropic Universe

Once we have a theoretical framework for gravitation (GR here), the simplest models of the Universe can be formulated using the Copernican Principle ([10]). Copernican Principle states that no observer is special in the entire cosmos. In the context of Cosmology, this is called "the Cosmological Principle", a term coined by Weyl. This can be made mathematically precise using concepts of isotropy and homogeneity of space. Important pioneering work was done by Friedmann, Lemaitre, Robertson, Walker, etc.[11, 12, 13, 14, 15, 16]. If we assume that the 3-space is invariant under translation and rotations, it can be shown rigorously[13, 14, 15, 16], that the only possible class of metrics is given by following general metric:

$$ds^2 = g_{\mu\nu}dx^\mu dx^\nu = dt^2 - a(t)^2\left(\frac{dr^2}{1-\kappa r^2} + r^2 d\Omega^2\right) \tag{1.2}$$

This metric is called the FLRW metric named after Friedmann, Lemaitre, Robertson, and Walker. Here we see that we have only one variable to solve for, $a(t)$ called the scale factor. Einstein's equations are used to obtain differential equations for $a(t)$. We need the form of the stress-energy tensor to solve Einstein's equations. Many cosmic components can be described by an effective fluid description. Stress energy tensor for a perfect fluid can be written as:

$$T_{\mu\nu} = (\bar{\rho} + \bar{p})u_\mu u_\nu - \bar{p}g_{\mu\nu} \tag{1.3}$$

Then the equations for $a(t)$ are:

$$\left(\frac{\dot{a}}{a}\right)^2 = \frac{8\pi G}{3}\sum_i \bar{\rho}_i - \frac{\kappa}{a^2} \tag{1.4}$$

$$\left(\frac{\ddot{a}}{a}\right) = -\frac{4\pi G}{3}\sum_i \bar{\rho}_i(1+3w_i) \tag{1.5}$$

where ρ_i and w_i is the average energy density and equation of state, respectively, of i_{th} constituent. w is defined as:

$$w \equiv \frac{\bar{p}}{\bar{\rho}} \tag{1.6}$$

These equations are known as Friedmann equations. These have to be solved along with continuity/dynamics equations for the evolution of source terms. These equations can be obtained either from respective Lagrangian by variational calculus or from the vanishing four divergence of stress-energy tensor:

$$T^{\mu}_{\nu\ ,\mu} = 0 \tag{1.7}$$

For a fluid with equation of state parameter w, the continuity equation is:

$$\dot{\rho} + 3H\rho(1+w) = 0 \tag{1.8}$$

where H is defined as:

$$H \equiv \frac{\dot{a}}{a} \tag{1.9}$$

Although we do observe in the real physical universe a lot of structure, the mathematical construct of a homogeneous and isotropic universe can be used as a proxy for studying dynamics of the Universe "on average". We assume that the observed Universe is **statistically** homogeneous & isotropic. Although there is no rigorous derivation that proves the equivalence of "metric isotropy & homogeneity" and "statistical homogeneity & isotropy", observationally the FLRW metric based calculations are consistent with observational data. There are a number of toy models that demonstrate that the differences are small.
Once we decide on contents of the Universe, Friedmann equations can be solved for $a(t)$. If there is only one component described by a single fluid with a constant w, we have:

$$\rho \propto a^{-3(1+w)} \tag{1.10}$$

$$a \propto t^{\frac{2}{3(1+w)}} \tag{1.11}$$

In general, we can solve Friedmann equations for any mix of constituents and put the theory to observational tests.

1.1.3 Some useful solutions of Friedmann Equations

An FLRW universe which only has pressure-less matter is called the Einstein-de Sitter universe[17]. Then the Friedmann equation is:

$$\frac{da}{dt} = H_0\sqrt{\Omega_0^m}\frac{a_0^{3/2}}{\sqrt{a}} \tag{1.12}$$

here H_0 is Hubble constant i.e. present value of H and Ω_0^m is present day density parameter for matter. Density parameter for a component is dimensionless measure of density contribution of that component to the total energy budget of the Universe. It is defined (for a component i with density ρ_i) as:

$$\Omega_i \equiv \frac{8\pi G\rho_i}{3H_0^2} \equiv \frac{\rho_i}{\rho_c} \tag{1.13}$$

where ρ_c is called critical density of the Universe and is defined as:

$$\rho_c = \frac{3H_0^2}{8\pi G} \tag{1.14}$$

For Einstein-de Sitter, matter density is equal to critical density. In this case the solution for a and H are:

$$a = \left(\frac{3H_0}{2}\right)^{2/3} t^{2/3} \qquad H = \frac{2}{3t} \tag{1.15}$$

In general, allowing for curvature, radiation and cosmological constant, Friedmann equation can be written as:

$$\left(\frac{\dot{a}}{a}\right)^2 = H^2 = H_0^2 \left(\Omega_0^r a^{-4} + \Omega_0^m a^{-3} + \Omega_\Lambda + \Omega_\kappa a^{-2}\right) \tag{1.16}$$

Evolution of density parameters and H is plotted for a particular set of parameters, in following figure (1.1)

1.1.4 Distances & Redshifts

Solving Friedmann equations one can obtain evolution of $a(t)$. Given the FLRW metric (1.2), equations of motion for photons can be calculated as massless particles move on null geodesics of a given geometry:

$$P^\alpha P^\beta_{,\alpha} = 0 \tag{1.17}$$

where P represents four momentum of a photon. From these equations, it can be shown that:

$$P^0 \propto a^{-1} \tag{1.18}$$

which can be translated into a relation between emitted wavelength and observed wavelength of photons. If λ_e is emitted wavelength of an electromagnetic signal

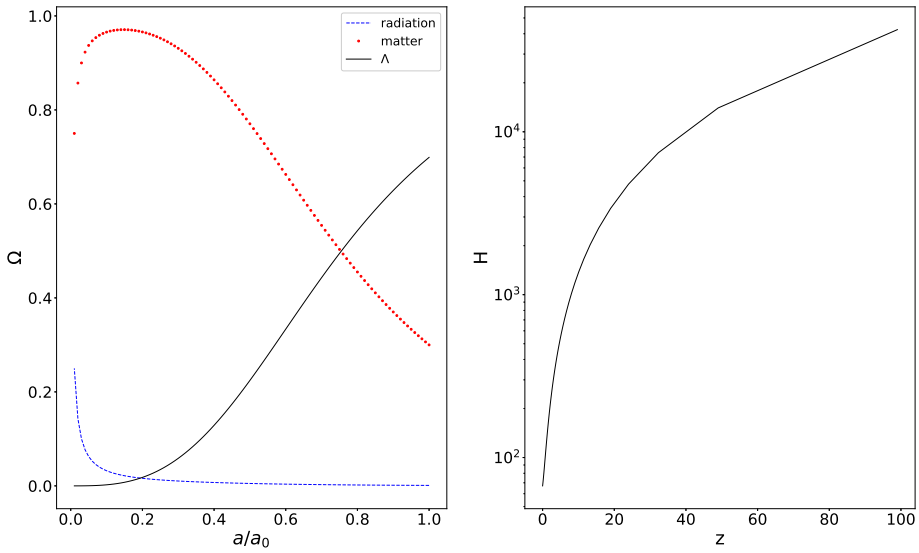

Figure 1.1: Left panel: Evolution of density contributions for different components. Matter density falls faster than Λ and eventually Λ comes to dominate giving late time acceleration. Right panel: Hubble parameter as function of redshift, while $\dot{a}$ begins to increase near $z = 0$, the ratio $\frac{\dot{a}}{a}$ continues to decrease.

at a_e, its observed wavelength is λ_o at a_o, then:

$$\frac{\lambda_o}{\lambda_e} = \frac{a_o}{a_e} \tag{1.19}$$

We define the redshift (z) of an epoch at a as:

$$z \equiv \frac{a_0}{a} - 1 = \frac{\lambda_0}{\lambda} - 1 \tag{1.20}$$

here a_0 is taken to be present value of a.

Light/electromagnetic radiations are one of the primary media for carrying out observations. As photons travel in this $FLRW$ space-time geometry their wavelengths are stretched and the relation between coordinate distances of source and the amount of wavelength change is dependent on the geometry of space-time. So it can be used as a test of the theory of space-time, in this case, the validity of dynamics coming from FLRW metric and associated equations, and hence also a check on GR.

For this purpose we need to identify variables in the theory that can be connected to observations. Different notions of distances[18] can be defined/used in Cosmology depending upon the observation being made. The simplest one is the

comoving distance. Let's write $FLRW$ metric 1.2 in a new form:

$$ds^2 = g_{\mu\nu}dx^\mu dx^\nu = dt^2 - a(t)^2\left[d\chi^2 + f_\kappa(\chi)^2 d\Omega^2\right] \tag{1.21}$$

with

$$r = \begin{cases} \sin(\chi) & (\kappa = 1) \\ \chi & (\kappa = 0) \\ \sinh(\chi) & (\kappa = -1) \end{cases}$$

and

$$f_\kappa(\chi) = \begin{cases} \sin(\chi) & (\kappa = 1) \\ \chi & (\kappa = 0) \\ \sinh(\chi) & (\kappa = -1) \end{cases}$$

For photons moving on null paths, the interval ds is zero and we have (for photons and other massless particles originating at $\{\chi = \chi_e, t = t_e\}$ moving along the radial direction):

$$d_c \equiv -\int_{t_o}^{t_e} \frac{dt}{a(t)} = \chi_e \tag{1.22}$$

Here subscript o represents present epoch/observer. d_c is called the comoving distance to an emitter at t_e and is a marker of a particular location in space. Writing the above relation in terms of redshifts (z):

$$d_c = \frac{1}{a_o}\int_0^z \frac{dz}{H(z)} \tag{1.23}$$

Redshifts of sources can be estimated directly using spectroscopic observations. Another useful distance, called the luminosity distance (d_l), can be composed out of z and comoving distance χ. d_l is defined as:

$$d_l^2 \equiv \frac{L_e}{4\pi F_o} \tag{1.24}$$

where L_e is luminosity of the source and F_o is observed flux covering all frequencies. F_o is also called the bolometric flux. d_l is related to the comoving distance χ as:

$$d_l = a_o f_\kappa(\chi)(1+z) \tag{1.25}$$

hence,

$$d_l = \frac{1+z}{\sqrt{-\kappa}} sinh\left(\sqrt{-\kappa}\int_0^z \frac{dz}{H(z)}\right) \tag{1.26}$$

If we independently know the luminosity of a light source, then using the observed flux, we can estimate the luminosity distance. Redshifts can be obtained from spectroscopic analysis. Then using eq. 1.26 along with Friedmann equations, we can compare theory with observations as we have (d_l, z) from observations as well as from theory. This is one of the ways a theory of cosmological space-time can be tested/constrained. But for this, we need an estimate of luminosity. Supernova type Ia have been used to good effect in the last 25 years for this purpose.

1.2 Accelerated Expansion and the Cosmological Constant

As discussed in the previous subsection, we need to know the luminosity of a source along with an independent measure of redshift to constrain cosmological dynamics. Supernova of type Ia serve this purpose. Such sources are known as "standard candles" of cosmology.

In the late 90s, studies of these types of supernova indicated that the expansion rate of the Universe is increasing. Studies that established this results were done by HSST team (Riess et. al[19]), SCP team (Perlmutter et. al[20]) and Schmidt et al ([21]). As we saw in subsection 1.1.3 that if we have only normal/dark matter with a positive equation of state parameter, we can not have accelerated expansion. From Friedmann eq. 1.5:

$$\left(\frac{\ddot{a}}{a}\right) = -\frac{4\pi G}{3}\sum_i \bar{\rho}_i(1+3w_i)$$

we can see that for $\ddot{a}$ to be positive the dominating energy component needs to have $w < -1/3$, which is very strange requirement in the context of standard physics. Recall that w is ratio of pressure to density, and this requirement makes pressure negative.

1.2.1 Return of the Cosmological Constant

When Einstein studied cosmological implications of the General Theory of Relativity, he found[3, 22] that he could only have a quasi-static universe if he introduced an additional term in his field equations:

$$G_{\mu\nu} - \Lambda g_{\mu\nu} = 8\pi G T_{\mu\nu} \tag{1.27}$$

He later abandoned it in light of observations that the Universe is expanding, not static. But the observations that suggested accelerated expansion brought back Λ into Cosmology. Even before supernovae observations established the case for a Λ-like component, there was indirect observational evidence combined with theoretical arguments, which suggested the presence of Λ[23, 24, 25, 26]. Einstein's equations with cosmological constant, considering matter and curvature, are:

$$\left(\frac{\dot{a}}{a}\right)^2 = \frac{8\pi G}{3}\bar{\rho}_m + \frac{\Lambda}{3} - \frac{\kappa}{a^2} \tag{1.28}$$

Using definitions of critical density and density parameters (Ω):

$$H^2 = H_0^2\left(\Omega_{m0}\frac{a_0^3}{a^3} + \Omega_\Lambda - \frac{\Omega_\kappa}{a^2}\right) \tag{1.29}$$

For early universe (high redshifts), radiation needs to be taken into account in above two equations. The form as stated above is appropriate at low redshifts. This model of the Universe with Λ and Cold Dark Matter (CDM) is the current standard model of Cosmology called the ΛCDM model. It not only provides a phase of late time acceleration suggested by supernova data, but it also gives an excellent fit to a wide variety of direct/indirect astrophysical data [27, 28, 29].

While the cosmological constant model is in great agreement with data, there are some "theoretical caveats" associated with cosmological constant, which make modern cosmology both challenging and interesting[30]. There is a possible theoretical basis for Λ coming from vacuum energy. But the predicted energy density associated with Λ is of order $\rho_{vac} \approx 10^{74}\ GeV^4$ which is way way off from observed value of $\rho_\Lambda \approx 10^{-47}\ GeV^4$. This is called the **fine-tuning problem**. Another important issue is that of the **Coincidence problem**. The observed values of dark energy density and matter density are both of similar order at the present epoch. In most of the models of dark energy, the ratio of these two is of order unity only at epochs close to $z = 0$. Hence it calls for an explanation of why it is

so at the present.
These and other various theoretical motivations ([30, 31, 32]), mostly motivated by a goal to find a unifying picture with standard particle physics, have led people to explore the reasons for accelerated expansion beyond Λ.

1.3 A Quick Introduction to Dark Energy

In the quest for seeking a cosmological theory that accounts for the acceleration of the expansion rate, there are two approaches that can be taken:

- **Modified Gravity Theories:** Cosmological evolution depends on the constituents of the Universe and the laws (e.g. GR) that connect space-time with these constituents. One can argue that late time acceleration is a consequence of deviations from GR. This is the paradigm of modified gravity theories[33, 34, 35, 36, 37, 38]. In this approach various modifications to Einstein's equations or Einstein-Hilbert action are proposed and tested.
- **Dark Energy:** The other way is to postulate the presence of a component with properties as required by observations of the expansion rate. To remain consistent with observations, this new component has to interact mainly through gravity. So it has to be minimally coupled through metric to other components or the direct coupling to other components[39] is extremely weak as constrained by observations. This new component postulated to solve the accelerated expansion problem is called "dark energy". There are many proposed forms: scalar fields like quintessence[40, 41, 42],tachyon fields[43, 44],etc., generalized scalar fields called k-essence[45, 46, 47], fluid descriptions[48], etc. Often there are phenomenological descriptions of dark energy with fluids characterized by parameters/parametric forms for w, effective speed of sound c_s^2 etc.[49]. In general, in these models, dark energy is dynamical in space-time i.e. its features can vary in both space and time, but often various approximations can be used in some models, where fluctuations/perturbations are ignored at some scales. One of the aims of this thesis work is to do self-consistent simulations of perturbations in scalar field models and check if these assumptions of small/insignificant dark energy clustering hold out or not.

These approaches are not "fundamentally" different as terms postulated in modified theories can be written as an effective stress-energy tensor with appropriate

couplings[50]. This statement is valid in the regime of classical theories.
In this work, we study the dynamics of perturbations in scalar field models, particularly quintessence and tachyonic dark energy. In the late part, we also consider fluid descriptions with effective w and c_s^2 that can be mapped from general scalar field models of k-essence.

1.4 Quintessence

Quintessence[51] refers to the canonical scalar field that is responsible for the late time acceleration of the Universe. A scalar field is one of the simplest components to include in the energy budget of the Universe. The use of scalar fields has already been well studied in the context of another era of accelerated expansion i.e. inflation ([52, 53, 54]). Even before the confirmation of late-time acceleration, people have studied cosmological implications of a scalar field [55]. The action for the quintessence is [42]:

$$I = \int d^4x\sqrt{-g}\left[\frac{1}{2}g^{\mu\nu}\partial_\mu\phi\partial_\nu\phi - V(\phi)\right] \tag{1.30}$$

Using FLRW metric with Einstein's equations, the equation of motion for the field in background cosmology is:

$$\ddot{\phi} + 3H\dot{\phi} + V_{,\phi} = 0 \tag{1.31}$$

where $V(\phi)$ is the potential for the quintessence and $V_{,\phi}$ denotes the derivative of potential with respect to the field. From variation of the full action (Einstein-Hilbert plus all components), we can obtain the stress-energy tensor for the field and the corresponding effective pressure (P_ϕ) and density (ρ_ϕ).

For FLRW geometry:

$$\rho_\phi = \frac{\dot{\phi}^2}{2} + V \tag{1.32}$$

$$P_\phi = \frac{\dot{\phi}^2}{2} - V \tag{1.33}$$

and the effective equation of state parameter (w_ϕ) is:

$$w_\phi = \frac{P_\phi}{\rho_\phi} = \frac{\dot{\phi}^2 - 2V}{\dot{\phi}^2 + 2V} \tag{1.34}$$

As mentioned in previous section 1.2 and obvious from eq. 1.5, we need $w < -1/3$ for accelerated expansion. Looking at eq.1.34, we notice that if kinetic part ($\dot{\phi}^2$) is small compared to potential part ($V(\phi)$), we get negative values of w. For slowly-rolling field $\dot{\phi}^2 \ll V(\phi)$, w is very close to Λ ($w = -1$). So with an appropriate potential and parameters we can obtain a background evolution which is very close to ΛCDM. In fact, for a number of choices for the functional form of $w(z)$, one can reconstruct the form of potential.
There can be different forms for potential motivated by various type of underlying mechanisms or phenomenology. Quintessence models are often classified according to the behaviour of $w(z)$. There are two broad classes[56, 57]: *freezing* and *thawing* models. In freezing potentials the field is initially rolling, and w is away from -1, with $\dot{w} < 0$. It approaches -1 at late times. Examples of freezing potentials are:

$$V(\phi) \propto \phi^{-n} \tag{1.35}$$

$$V(\phi) \propto \exp(\alpha\phi^2) \tag{1.36}$$

On the contrary, in thawing potentials, field is initially rolling very slowly, so that $w \sim -1$, but as we approach the present epoch, the field rolls and w moves away from -1 on higher side. Examples of thawing models are:

$$V(\phi) = V_0 + M^{4-n}\phi^n \tag{1.37}$$

$$V(\phi) = M^4 \cos^2(\phi/f) \tag{1.38}$$

There have been efforts to find quintessence models wherein the coincidence problem can be resolved. These efforts[56, 58, 59, 60], use dynamical systems approach to obtain solutions that have trajectories with attractors such that the field density tracks the other component for a wide range of initial conditions. Thus dark energy and matter-energy densities remain of the same order for an extended period. But these models do not completely alleviate the coincidence problem as often one coincidence is replaced by another[56].

1.5 Tachyonic models

The quintessence field is a canonical scalar field with a Lagrangian of the form "Kinetic Energy+Potential Energy" which is like the Lagrangian of a non-relativistic particle. Similarly, one can take the Lagrangian for a relativistic particle and write

a field theory version of it:

$$\mathcal{L} = -V(\phi)\sqrt{(1 - \partial^\mu\phi\partial_\mu\phi)} \tag{1.39}$$

This type of field is called tachyonic field[43] These models are effective low energy theories with an origin in string theory[61]. These models have also been investigated for the prospect of a unified dark sector[62]. Certain potentials in these models have nontrivial features which make them interesting for a detailed study. For example: exponential potential ($V \propto e^{-\phi}$) has an asymptotic future behavior that can avoid a future horizon[44] and $V \propto \phi^{-2}$ potentials can give scale dependent dark matter like behaviour[62].
In FLRW cosmology, the energy density and pressure for tachyonic field are:

$$\rho_\phi = \frac{V(\phi)}{\sqrt{1 - \partial^\mu\phi\partial_\mu\phi}} \tag{1.40}$$

$$P_\phi = -V(\phi)\sqrt{1 - \partial^\mu\phi\partial_\mu\phi} \tag{1.41}$$

Equation of state parameter is:

$$w = -1 + \dot{\phi}^2 \tag{1.42}$$

While the quintessence models are well studied, tachyonic models are not so. Background constraints on some tachyon models have been studied in [63] and a detailed study of perturbations has been done in [64].

1.6 Calculations of Dark Energy Cosmology

Once, we have decided on a dark energy model (like an action or phenomenological characteristics), simulations have to be done for comparison with observations. There are different phenomena that can be affected by the dynamics of dark energy and hence different types of calculations might be needed. Dark energy changes the average expansion rate of the Universe and hence any observation that depends on $a(t)$ or its derivatives is affected. This affects the distance-luminosity relations for any source of light, clustering of other components of the Universe, etc. For minimally coupled models, i.e. models in which dark energy interact only via gravity, dark energy affects other constituents only through metric.
This means simulations can be done at various levels of rigor/approximations depending upon which observations we want to explain. In this section, we look

at this "hierarchy of calculations". This structural study is important because different dark energy models might be sensitive to different types of observations. Sets of models that are "observationally degenerate" at one level of simulation/observations need another level for constraining the models. Different levels also set the phenomenological structure of dark energy theories.

1.6.1 Background

As discussed in previous sections the simplest cosmological calculations are done with assumptions of homogeneity and isotropy, using FLRW metric. This assumption means that all dependent variables of theory have only time dependence, e.g. the only degree of freedom in metric is $a(t)$, all densities are only time-dependent $\rho(t)$, dark energy Lagrangians are just functions of a time-dependent field and its time derivatives. With the assumption of minimal coupling, any dark energy model is completely specified, at the background level, by its equation of state $w(t)$. The energy density is given by the continuity equation 1.8 and we solve Friedmann equations for $a(t)$. Specification of $w(t)$ for each component lets us solve for evolution of all components and with Friedmann equations 1.41.5, the cosmological model is completely specified. Here the free parameters of theory are specifications of density parameters at present/initial time (Ω_0's for different components), current/initial value of Hubble factor H_0, and any parameters describing either a parametric form of $w_{de}(t)$ for dark energy or parameters of underlying dark energy model (like parameters of $V(\phi)$).

Almost all cosmological probes are affected by the average expansion of the Universe. So even if the calculations are being done at a more elaborate level (like including perturbations), changes in background cosmology are reflected in perturbations, non-linear structures, etc. So when we discuss the next levels of calculations, they encapsulate this background dynamics. An important task is to investigate if two models of dark energy give the same background expansion, how efficiently can they be distinguished by the next levels of calculations. For example, one can have two different types of scalar field models and reconstruct corresponding forms of the potential for these two fields such that they have the same effective $w(t)$. Then background expansion is same and we can ask if the linear perturbation theory based calculations/observations distinguish these. Work presented in this thesis attempts to address this question by working with different scalar field Lagrangians: quintessence and tachyonic field.

One important thing to note here is that **all observations which are only sensitive to background observations cannot distinguish two dark energy**

models with the same effective $w(t)$. However, this is fairly easy to do in a lot of models. ΛCDM gives an excellent fit to background cosmology and, hence most theories by construction have tunable parameters, which when adjusted, make the expansion very similar to ΛCDM, and hence satisfy background constraints.
Every cosmological observation is affected by the expansion rate, but observations that only depend on the luminosity-distance relationship, like supernovae observations, can only probe expansion history.

1.6.2 Linear Theory

The Universe has structures existing at different scales: e.g. planets, stars, galaxies, interstellar medium, clusters of galaxies, dark matter halos, etc. The origin and formation of these structures are entangled with the evolution of space-time. General Relativity (its modifications) are nonlinear theories and in most of the cases, we have to use approximations to solve equations. To study structure formation or perturbations in the Universe, we make certain assumptions (which can be tested against observations). The standard formalism is as follows: All the structures that we observe have originated from small fluctuations, seeded at early times in the history of the Universe. Standard cosmological models start from a singularity, called Big Bang ([11]) in past. The big bang was followed by a period of exponential expansion called inflation ([52, 53, 54]). At initial time, when the Universe was very tiny, primordial fluctuations were seeded by quantum fluctuations (though there are other theoretical possibilities, like topological defects[65]), which were then stretched out by inflation. These fluctuations were very small. This is validated by Cosmic Microwave Background (CMB) radiation ([66, 67, 68]), which was emitted much later than the end of inflation, which is almost uniform with anisotropies of order 10^{-5}. These primordial fluctuations evolved in the dynamic fabric of space-time, growing with time and forming nonlinear structures that we observe. Hence studies of the growth and formation of structures are very useful in investigating the theories of space-time dynamics. Once we assume primordial fluctuations to be small, we can study these at early times using linear perturbation theory (as discussed below)[69, 70, 71]. At linear order, in Fourier space, evolution for different lengthscales decouple and original partial differential equations can be approximated by ordinary differential equation for each Fourier mode (k). Furthermore, in Fourier space different length-scales evolve differently. After the end of inflation, modes above a certain length-scale are out of the comoving horizon, and hence these "super horizon" perturbations remain frozen until they come back into the horizon ([72, 73]). Given the initial

fluctuations were small and existence of an evolving horizon, we can effectively use linear approximations in two regimes: early time scales and large length scales.
Now we brifly discuss the formalism of (linear)cosmological perturbation theory. For comprehensive and detailed reviews, please see [69, 70, 71, 74].
Our starting point is assuming a background metric (FLRW like) and then perturbing it. All quantities are written as "background+perturbation", where the perturbation quantities are grouped or classified according to their transformation properties under 3-space transformations. This decomposition decouples different types of perturbations at linear order.
If $\bar{g}_{\mu\nu}$ is background metric and $g_{\mu\nu}$ is the metric with perturbations $\delta g_{\mu\nu}$, then

$$g_{\mu\nu} \approx \bar{g}_{\mu\nu} + \delta g_{\mu\nu} \tag{1.43}$$

$\delta g_{\mu\nu}$ can be decomposed into scalar, vector and tensor forms, then it can be shown that for symmetric and homogeneous Robertson-Walker spaces and linear perturbations on them, different components decouple and can be studied separately[69]. Further, tensor perturbations do not couple with energy densities or pressure inhomogeneities and vector perturbations decay in an expanding universe. Scalar perturbations can show instabilities and can significantly affect matter dynamics[69, 70]. Hence, in context of this work, we restrict ourselves to scalar perturbations:

$$g_{00} = a^2(1 + 2\psi) \tag{1.44}$$

$$g_{0i} = -aB_{,i} \tag{1.45}$$

$$g_{ij} = -a^2(\gamma_{ij}[1 - 2\phi] + 2E_{,ij}\,) \tag{1.46}$$

$$ds^2 = \; a^2(1 + 2\psi)d\eta^2 - aB_{,i}\,d\eta dx^i - a^2(\gamma_{ij}[1 - 2\phi] + 2E_{,ij}\,)dx^i dx^j \tag{1.47}$$

Here γ_{ij} is spatial symmetric metric, "," represents covariant derivative with respect to γ and $\{\psi, B, \phi, E\}$ are scalars (with respect to spatial transformations) that characterize the metric perturbations. This is a general form for perturbations. But these scalar functions are dependent on the choice of coordinates i.e. there is a "Gauge dependence". We discuss this next.

1.6.2.1 Gauge dependence

In General Relativity, space-time is a dynamical quantity and it is represented by a metric, a symmetric tensor of rank 4. So, $g_{\mu\nu}$ has 10 components/functions to be solved for. But, there is a freedom to choose coordinate systems and these 10

functions are coordinate dependent, so they take different forms for different coordinates. Given a solution, one can choose transformations to another coordinate system and hence get a different-looking solution. This is called "Gauge freedom". Transformations from one coordinate system to other (say from x^α to $\tilde{x}^\alpha$) are, in general, characterized by 4 functions:

$$\tilde{x}^\alpha = \xi^\alpha(x^0, x^1, x^2, x^3) \tag{1.48}$$

These functions are chosen by hand, to get a suitable coordinate system. Hence there are 4 more functions specified, hence the degree of freedom in unknown metric functions reduces to $10 - 4 = 6$. This is valid for any perturbative space-time dynamics.

But while doing linear perturbation theory, complications can potentially arise depending on the particular type of space-time.[69, 70]. A splitting is done on space-time between a "background space-time" and a "perturbed space-time", while in reality there is only one space-time, which is deformed compared to the background. A choice for a coordinate system on the background is made and then a coordinate system has to be established on perturbed space-time. Perturbations are defined as the differences of various functions on space-time, from corresponding functions on background space-time. Hence the definition of perturbations is dependent on the "correspondence of coordinate system on the background and perturbed space-time". As a manifestation of gauge freedom on perturbed space-time, this correspondence is not unique. While one can choose a particular gauge and work using it consistently, the physical meaning of perturbations in some gauges might be ill-defined. There is one particular gauge called the "synchronous gauge" where this confusion often arises[70].
When considering gauge transformations (1.48) in context of linear perturbations theory, we only consider small transformations i.e. functions ξ^α are only significant at first order. Further, when considering only scalar perturbations (as we are doing here), transformations 1.48 can be written in terms of two scalars:

$$\xi^0(x^\alpha) = \xi^0(x^\alpha) \tag{1.49}$$

$$\xi^i(x^\alpha) = \gamma^{ij}\xi(x^\alpha)_{,j} \tag{1.50}$$

Then perturbations in equations 1.47 transform as:

$$\tilde{\psi} = \psi - \frac{a'}{a}\xi^0 - \xi^{0\prime} \tag{1.51}$$

$$\tilde{\phi} = \phi + \frac{a'}{a}\xi^0 \tag{1.52}$$

$$\tilde{B} = B + \xi^0 - \xi' \tag{1.53}$$

$$\tilde{E} = E - \xi \tag{1.54}$$

In light of gauge-related complications, it is highly desirable that "gauge independent" approaches be studied. Bardeen [75] and Gerlach & Sengupta [76] built upon the previous works of other people to develop a gauge-invariant approach. The key point is to notice how various perturbations transform and find combinations of perturbations such that the resultant quantity is invariant under gauge transformations. Two such combinations were pointed out by Bardeen[75], which are called Bardeen potentials (Φ_A and Φ_H):

$$\Phi_A = \Psi = \psi + \frac{1}{a}[a(B-E)']' \tag{1.55}$$

$$-\Phi_B = \Phi = \phi - \frac{a'}{a}(B - E') \tag{1.56}$$

Gauge transformations for scalar perturbations involve two functions (ξ^0, ξ) and these can be chosen to reduce 4 scalar perturbations to 2. Two very common choices of gauge leverage this freedom to get equations that are suited for some particular applications. These are:

- **Synchronous Gauge:** This gauge is obtained by any such transformation which makes $\psi = 0$ and $B = 0$. These properties can be used to write transformations from any gauge to synchronous gauge. Synchronous gauge is popular for numerical codes as it shows better numerical suitability. However, transformations that are used to reach synchronous gauge still leave freedom for residual transformations which can sometimes lead to unphysical perturbations[70].

- **Conformal Newtonian Gauge:** This gauge is defined by conditions: $B = 0$ and $E = 0$. From the definition of Bardeen's potentials (1.56), it is obvious that the perturbations (ψ and ϕ) are themselves gauge-invariant. This is the most attractive feature of this gauge as many perturbations are naturally gauge invariant. Another useful feature is that of interpreting perturbations. If off-diagonal components of spatial part of stress-energy tensor vanish, then

$\phi = \psi$ which has correspondence with Newtonian potential. Metric in this gauge takes form:

$$ds^2 = a^2(1+2\psi)d\eta^2 - a^2(\gamma_{ij}[1-2\phi])dx^i dx^j \tag{1.57}$$

Because of the above-mentioned features, we use, for linear theory, Conformal Newtonian gauge. Now we discuss linear theory formalism in this gauge.

1.6.2.2 Basic Equations

Here we demonstrate the basic working procedure of linear theory with a simple example (assuming spatial curvature to be 0). All the equations are derived as in the usual GR formalism but all perturbations from respective background quantities are retained only at first order. Further going to Fourier space simplifies the calculations as different k- modes are de-coupled at first order and we are left with only ordinary differential equations to solve instead of partial ones. We start from metric 1.57 and use Einstein equations to obtain:

$$\begin{aligned} 6\frac{\psi}{a^2}\left[\frac{a'^2}{a^2} - 2\frac{a''}{a}\right] - 12\frac{a'}{a}\frac{\phi'}{a^2} - 6\frac{a'}{a}\frac{\psi'}{a^2} - 6\frac{\phi''}{a^2} + 2\frac{\Delta}{a^2}[\phi-\psi] \\ = 8\pi G(\delta T_1^1 + \delta T_2^2 + \delta T_3^3) \end{aligned} \tag{1.58}$$

$$\sum_{i=1}^{3}\left[\frac{a'}{a}\frac{\partial\psi}{\partial x^i} + \frac{\partial\phi'}{\partial x^i}\right] = 4\pi G a^2 \sum_{i=1}^{3}\delta T_i^0 \tag{1.59}$$

$$\left[\frac{\partial^2}{\partial x^1 \partial x^2} + \frac{\partial^2}{\partial x^2 \partial x^3} + \frac{\partial^2}{\partial x^3 \partial x^1}\right](\psi - \phi) = 8\pi G a^2(\delta T_2^1 + \delta T_3^2 + \delta T_1^3) \tag{1.60}$$

$$-3\frac{a'^2}{a^2}\psi - 3\frac{a'}{a}\phi' + \Delta\phi = 4\pi G a^2 \delta T_0^0 \tag{1.61}$$

Here δT represents first-order perturbations to stress-energy tensor and Δ is the Laplacian operator defined as:

$$\Delta \equiv \sum_{i=1}^{3}\frac{\partial^2}{\partial x^{i2}} \tag{1.62}$$

Here we consider a perfect fluid as source. Decomposing pressure and density in background+perturbation:

$$\rho(x,y,z,t) = \bar{\rho}(t)(1+\delta_m(x,y,z,t)) \tag{1.63}$$

$$p = \bar{p}+\delta p \tag{1.64}$$

and we have velocity perturbations (background/average velocity is 0) defined as:

$$v^i \equiv \frac{dx^i}{d\eta} \tag{1.65}$$

Then stress energy tensor for matter fluid is:

$$(\delta T^1_1 + \delta T^2_2 + \delta T^3_3) = -3\bar{\rho}c_s^2\delta_m \tag{1.66}$$

$$(\delta T^1_2 + \delta T^2_3 + \delta T^3_1) = 0 \tag{1.67}$$

$$\sum_{i=1}^{3}\delta T^0_i = \bar{\rho}\sum_{i=1}^{3} v_i \tag{1.68}$$

Defining Θ:

$$\Theta = \sum_{i=1}^{3}\frac{\partial v^i}{\partial x^i} = ik^j v_j \tag{1.69}$$

where the rhs of second equality is in Fourier space, i.e., v_i in rightmost term is Fourier coefficient of v_i. Now on, in this subsection we would work in Fourier space i.e. all variables are Fourier coefficient in following calculations. Using equations from time-space components:

$$\frac{k^2}{a^2}\left[\frac{a'}{a}\psi+\phi'\right] = -4\pi G\bar{\rho}(1+w)\Theta \tag{1.70}$$

To obtain the equations of motion for density and velocity, we can use continuity equations:

$$T^{\mu}_{\nu\ ;\mu} = 0 \tag{1.71}$$

We get

$$\delta'_m = -3\frac{a'}{a}(c_s^2-w)\delta_m + 3(1+w)\phi' - (1+w)\Theta \tag{1.72}$$

$$\Theta' = -\left[\frac{a'}{a}(1-3w)+\frac{w'}{1+w}\right]\Theta + k^2\left[\frac{c_s^2\delta_m}{1+w}+\psi\right] \tag{1.73}$$

The above two equations hold with off-diagonal terms of stress-energy tensor vanishing (as in eq.1.67), otherwise, there is an extra term proportional to anisotropic stress σ. Now we have all the equations that have to be solved for a

universe containing a single fluid. If there are multiple fluids then all perturbation sources (δT^{μ}_{ν}) have to be considered in Einstein equations 1.58-1.61. Also, the continuity/dynamics equation for each component has to be derived and solved simultaneously. For minimally coupled fluid, with vanishing anisotropic stress, continuity equations (1.72 and 1.73) should work. Looking at the continuity equation, we observe that such a fluid is characterized by two functions: equation of state for background ($w(\tau)$) and effective speed of sound c_s^2. In phenomenological investigations, these functions are often investigated. For example, if dark energy effectively behaves like a fluid, then what would be its equation of state or effective speed of sound. We will look at these investigations in greater detail in chapter 5. In practice, these equations are written considering different components (baryons, photons, neutrinos, dark matter, models of dark energy, etc) and solved on a computer. But it is worth looking into some simple observations from the above-mentioned equations:

- In case, off-diagonal components of spatial part of T^{μ}_{ν} vanish, then from eq.1.60, one can deduce that the two potentials are equal (i.e. $\psi = \phi$). In Newtonian approximation (i.e. small velocities) this turns out to be the Newtonian gravitational potential.

- In small scale limit ($k \gg aH$), one can show that (using the fact that potential changes are very small in this limit), matter fluctuations behave as per:

$$\delta_m'' + \frac{a'}{a}\delta' + k^2 c_s^2 \delta_m = 4\pi G \bar{\rho} \delta_m \tag{1.74}$$

  In a dark matter-dominated universe, this equation has a growing solution $\delta_m \propto a \propto t^{2/3}$.

1.6.3 Nonlinear Approximations

Linear theory works well at early times or at large length scales, it breaks down when perturbed quantities like δ approach 1. Then alternative methods need to be explored. Solving GR equations in their full nonlinear form is extremely hard for a general distribution of matter and energy. Hence, for nonlinear regimes, different types of approximations are employed. One is the N-body formalism which we discuss in the next subsection. Technically, one can do second-order linear theory ([77, 78]) and go on to higher-order as well. But even second-order turns out to be extremely cumbersome and this also fails as $\delta \to 1$.
There are other methods that remove the assumption of small perturbations but

make some other assumptions. For example, there are efforts exploiting some geometrical symmetry, like spherical, cylindrical, or ellipsoidal symmetry ([79, 80]). These calculations, although idealized, are very useful in giving physical insights. Combined with semi-analytical and partly numerical methods, these even give predictions for observables. In section 1.7, we will see how this can be done in an example with spherical symmetry.

1.6.4 N-body Simulations

Linear theory breaks down when perturbed quantities like δ_m become of order unity. N-body simulations try to simulate dynamics with an ensemble of particles and can have nonlinear matter structures in simulation. Most of (traditional) cosmological N-body simulations[81, 82, 83] use Newtonian approximations in an expanding universe. The particles are moved in a non-relativistic manner according to force calculated either from a potential or using some contribution scheme for force due to other particles. Even before the discovery of accelerated expansion using supernova observations, comparisons of results from N-body simulations with observations suggested the presence of cosmological constant[24, 25, 84]. Basic level implementation of dark energy in N-body simulations can be done by modifying the expansion background of the existing cosmological code. More advance implementations include dark energy perturbations/modified gravity effects as well (see [85] for a review). But most dark energy models are best described by relativistic fields and hence consistency would require simulating fields in General Relativity. There have been some recent efforts towards developing relativistic N-body cosmological simulations[86, 87, 88].

1.7 Spherical Collapse

General relativistic equations are in general too complicated to solve. But if we assume some symmetry, like spherical symmetry, equations not only become amenable to easy numerical implementation but may also have analytical closed-form solutions. Despite this strong symmetry assumption, this approach is very important because it allows us to probe strong perturbation regime. In absence of very general solutions, it is very useful to have solutions (corresponding to observables) in different regimes like linear assumptions without symmetry, symmetry assumptions without linearity constraints, etc.

Pioneering work in spherically symmetric models for cosmology was done by Lemaitre, Tolman, and Bondi ([89, 90, 91]). Gunn and Gott used the spherical collapse formalism to connect observational characteristics of galaxy clusters to cosmology[92]. Quantities calculated in spherical collapse formalism can be used to build semi-analytical models of halo-distributions[93, 94]. Here we review the basic formalism of spherical collapse. We will further review spherical collapse formalism in context of dark energy in chapter 2.

1.7.1 Newtonian Spherical Collapse

For an overdense or underdense sphere in otherwise homogeneous universe, dynamics of shell can be described using Newtonian mechanics (if there is only non-relativistic dark matter). For a shell that encloses mass M, dynamics is given by:

$$\frac{d^2R}{dt^2} = -\frac{GM}{R^2} \tag{1.75}$$

and an energy conservation equation can be written:

$$\frac{1}{2}\left(\frac{dR}{dt}\right)^2 - \frac{GM}{R} = \mathcal{E} \tag{1.76}$$

where $\mathcal{E}$ is energy averaged inside the shell. Dynamics depends on the sign of $\mathcal{E}$. For positive energy, the shell may go expanding forever. If the energy is negative, the system is bound, a shell initially expanding, expands to a finite radius, turns around, and collapses. For bound systems, the above equations have a parameterized analytical solution[95].

$$R = A(1 - \cos\theta) \qquad t = B(\theta - \sin\theta) \tag{1.77}$$

where A and B are constants obtained from initial conditions, and can be related to mass and energy:

$$A^3 = GMB^2 \qquad A = \frac{-GM}{2E} \tag{1.78}$$

These constants are determined by initial conditions. All collapsing halos have characteristic turn around and virial properties. Although analytical or numerical solutions eventually lead to singularity, in the real universe, it is assumed that the system goes through some stabilizing process and eventually leads to the formation of quasi-stable structures. The process of virialization[96], in dark matter collapse, is not well understood and is often implemented by hand in simulations.

This epoch of virialization, can be taken as the epoch at which overdensity tends to infinity or the time it takes to collapse to 0, or it can be imposed by other conditions, for example, virialization happens at a time which is twice the time turn around happens[95, 97]. A more physical way is to take the virial theorem of classical mechanics and use the kinetic-potential energy virial relation[98]. For a collapse with just dark matter, turn around overdensity δ_{ta} is independent of initial overdensity/size. It is:

$$\delta_{dm} = \frac{9\pi^2}{16} - 1 \tag{1.79}$$

while relation of radius at maximum (R_{ta}) to virial radius (R_v) can be very well approximated by $R_{ta} = 2R_v$.
In presence of simplest dark energy, that is in presence of cosmological constant, eq.1.76 is modified to:

$$\frac{1}{2}\dot{R}^2 - \frac{GM}{R} - \frac{1}{6}\Lambda R^2 = \mathcal{E} \tag{1.80}$$

This contains the previous case for $\Lambda = 0$. Expressions for virial and turn around radii can be obtained[97, 98]:

$$\begin{aligned} R_T &= \frac{3(1+\bar{\delta}_{in})}{\bar{\delta}_{in}} R_{in} \left(\frac{4\Omega_M(\bar{\delta}_{in}a_0)^3}{27\Omega_\Lambda(1+\bar{\delta}_{in})^2 a_{in}^3} \right)^{1/2} \\ &\quad \sin\left[\frac{1}{3} \arcsin\left\{ \left(\frac{27\Omega_\Lambda(1+\bar{\delta}_{in})^2 a_{in}^3}{4\Omega_M(\bar{\delta}_{in}a_0)^3} \right)^{1/2} \right\} \right] \end{aligned} \tag{1.81}$$

$$\begin{aligned} R_V = \left(\frac{2}{3}\right)^{1/2} & \left(\frac{\Omega_\Lambda R_T^3 + \Omega_M(\frac{a_0}{a_{in}})^3(1+\delta_{in})R_{in}^3}{\Omega_\Lambda R_T} \right)^{1/2} \\ & \sin\left[\frac{1}{3} \arcsin\left\{ \frac{\Omega_M a_0^3(1+\delta_{in})R_{in}^3}{a_{in}^3 R_T^3} \left(\frac{1.5}{1 + \frac{\Omega_M}{\Omega_\Lambda}(\frac{a_0 R_{in}}{a_{in} R_T})^3(1+\delta_{in})} \right)^{3/2} \right\} \right] \end{aligned} \tag{1.82}$$

The properties of collapsed objects depend on the cosmology in which they are formed. So, in principle, observations of characteristics of bound objects can shed some light on the nature of cosmological dynamics. But this requires a lot of approximations and a number of formalisms have been developed e.g. Press-Schechter mass function[93], excursion set approaches [94], semi-numerical approaches[99, 100], etc. Now we take a quick look at an example of how the properties of collapse can be related to observations: In linear theory, different k-modes evolve independently. Then, starting from a random density field, we can work with different smoothened versions of the field, i.e. fields at each point are replaced

by fields averaged over certain lengthscales. This is calculated at different times while the field is evolved using linear theory calculations. At any epoch, the points which go over some critical value, e.g. δ_v calculated using spherical collapse, are said to virialize. This can be used to guess the probability of the number of halos of various sizes formed at different redshifts. This is a simplified description of Press-Schechter formalism[93]. Similar approaches have been tried[100].

1.8 Spherical Collapse in General Relativity

Approaches described in the previous subsection are valid only in the case of non-relativistic (cold) dark matter and the cosmological constant. In General Relativity, one has to formally start from a metric and derive the equations. In this subsection, we look at how equations mentioned in the Newtonian case are obtained starting from metric and Einstein's field equations. This is necessary if we want to investigate dark energy models as these are best described in GR and might not have a Newtonian analog.
Starting from a very general form for spherically symmetric metric:

$$ds^2 = -e^{\lambda}dr^2 - e^{\omega}(d\theta^2 + sin^2\theta d\phi) + dt^2 \tag{1.83}$$

where λ and ω are, in general, functions of r and t. Putting this metric in Einstein's equations and using cold dark metter and cosmological constant as only sources, we can obtain dynamics equations. In this case first integrals or conserved quantities can be found:

$$\frac{e^{\frac{\omega}{2}}\omega'}{2e^{\frac{\lambda}{2}}} = f(r) \qquad \text{(is a first integral)}$$

$$e^{3\omega/2}\left(\frac{\dot{\omega}^2}{2} + \frac{2}{3}\Lambda\right) + 2e^{\omega/2}(1 - f^2) = F(r) \qquad \text{(another first integral)}$$

Defining

$$A(r,t) = e^{\omega/2} \tag{1.84}$$

We get following form:

$$ds^2 = -\frac{A'^2}{f^2(r)}dr^2 - A^2(d\theta^2 + sin^2\theta d\phi) + dt^2 \tag{1.85}$$

From Einstein's equations, we get:

$$\left(\frac{\dot{A}}{A}\right)^2 = \frac{F}{2A^3} + \frac{\Lambda}{3} - \frac{1 - f^2}{A^2} \tag{1.86}$$

which is equivalent to eq.1.80.
While working with dark energy models, we work in this GR based approach. We will review spherical collapse approaches with dark energy in next chapter 2.

1.9 Perturbations in Dark Energy

We have briefly looked at how perturbations are calculated in linear theory. The standard algorithm is similar for different models. One writes the Lagrangian densities for all components plus Einstein Hilbert action. Then using calculus of variations, equations are obtained at linear order in perturbations from the background. The presence of a dark energy component that is not Λ can, in general, affect the dynamics of perturbations beyond the effect coming from the change in background expansion. So, for consistency, one has to allow for dark energy perturbations also, as coming from equations. For example, if dark energy is a canonical scalar field (quintessence), then the total action is:

$$I = \int dx^4 \sqrt{-g} \left\{ \frac{1}{16\pi G} R + L_\phi + L_m \right\} \tag{1.87}$$

where L_ϕ is quintessence action (1.30) and L_m is for matter. In this section, ϕ represents quintessence field. For metric potentials we will just use ψ, using the fact that for scalar field and dark matter sources, two potentials are equal at linear order. If field is expanded into background plus perturbation ($\phi + \delta\phi$), upto first order (ϵ) stress-energy tensor corresponding to quintessence is (Newtonian gauge):

$$T^k_k = \left(V - \frac{\dot{\phi}^2}{2} \right) + \left((\delta\phi) V_{,\phi} + \psi\dot{\phi}^2 - \dot{\phi}\dot{(\delta\phi)} \right) \epsilon + O[\epsilon]^2 \tag{1.88}$$

$$T^t_t = \left(V + \frac{\dot{\phi}^2}{2} \right) + \left((\delta\phi) V_{,\phi} - \psi\dot{\phi}^2 + \dot{\phi}\dot{(\delta\phi)} \right) \epsilon + O[\epsilon]^2 \tag{1.89}$$

$$T^t_k = \left(\dot{\phi} \frac{\partial(\delta\phi)}{\partial x^k} \right) \epsilon + O[\epsilon]^2 \tag{1.90}$$

$$T^k_t = -\left(\frac{\dot{\phi}}{a^2} \frac{\partial(\delta\phi)}{\partial x^k} \right) \epsilon + O[\epsilon]^2 \tag{1.91}$$

$$T^j_k = O[\epsilon]^2 \tag{1.92}$$

Note: dot $(\dot{\cdot})$ represents a derivative wrt to time. Perturbations of field are governed by:

$$(\ddot{\delta\phi}) = -2\psi V_{,\phi} - (\delta\phi)V_{,\phi\phi} + 4\dot{\phi}\dot{\psi} - 3\frac{\dot{a}}{a}(\dot{\delta\phi}) + \frac{\Delta(\delta\phi)}{a^2} \tag{1.93}$$

Using this stress energy tensor along with that of matter, Einstein equations are solved for ψ along with field perturbation equations. Theoretically, this adds new degree of freedom in terms of perturbations of dark energy field. This is in addition to any effect that comes through background cosmology. As we can see from the case of Λ, the inclusion of a dark energy like component modifies the expansion and hence affects almost every aspect of cosmology. "How strong are the effects of dark energy perturbations, on top of background cosmology?"; this is a matter of investigation. A part of this thesis work tries to study this question, by separating the effects coming from different background cosmology from the effects coming from perturbations in dark energy. This brings us to the question of how to connect perturbations with observables.

Some of the ways in which perturbations can be related to observables are:

- **Matter/Large Scale Structure distribution:** Growth of matter perturbations can be related to the observed distribution of structures. Given the statistical nature of initial conditions and the assumptions of homogeneity and isotropy on average, cosmological fields (e.g. matter density) are characterized by statistical measures such as power spectrum. If a cosmological field $f(\vec{x}, z)$ is represented in Fourier space by its coefficients $\tilde{f}(z, k)$, then power spectrum $P_f(z)$ is given by:

$$f(\vec{x}, z) = \frac{V}{(2\pi)^3}\int \tilde{f}(z, k)e^{i\vec{k}.\vec{x}}d^3k \tag{1.94}$$

$$P_f(z, k) = \tilde{f}^*(k, z)\tilde{f}(k, z) \tag{1.95}$$

  We calculate the evolution of Fourier coefficients, in linear theory, for different quantities and then these are related to statistical measures like power spectrum. These are measurable quantities. Observations can measure the distributions of galaxies and other baryonic matter. These can be related to the distribution of dark matter using appropriate bias models ([101, 102]). Another statistics related to power spectrum of matter density contrast field

(δ_{dm}) is the correlation function $\xi(\vec{r})$:

$$\xi(\vec{r}) = \frac{1}{V}\int \delta_{dm}(\vec{x}+\vec{r})\delta_{dm}(\vec{x})d^3x \quad (1.96)$$

$$\xi(\vec{r}) = \frac{1}{(2\pi)^3}\int P(\vec{k})e^{i\vec{k}.\vec{r}}d^3k \quad (1.97)$$

Technically it is the inverse Fourier transform of the power spectrum. Physically, it indicates the deviation from the average distribution of galaxies at separation $\vec{r}$. Again this can be estimated from observations. Higher moments of fields can be calculated and compared with those estimated from observations. Large scale surveys of galaxies and other tracers of the mass distribution are done to estimate these.

The biggest effect of dark energy comes through the change in background expansion. Even before the discovery of accelerated expansion using SNIa, there were studies that indicated the presence of dark energy using the information from the amount of large-scale structures predicted from simulations [23, 24, 25, 26]. But if the dark energy model considered allows for perturbations, this has to be included and solved while simulating cosmological perturbations of space-time. Linear theory calculations are done as a primary tool to predict power spectrum, correlation functions, etc.

Velocities of observed structures can be related to linear theory and be used to match theoretical predictions with data[103]. Redshift distribution as measured from velocities is affected by both peculiar velocities as well as cosmological Hubble flow. But distribution or spectrum as measured by redshifts can be related to real space distribution using a number of approximations[103, 104]. Cosmological information such as the growth rate of perturbations can be obtained by measuring different multipoles of the spectrum[103].

- **Cosmic Microwave Background:** Interaction of photons with space-time: CMB photons emitted at the epoch of around $z \sim 1100$, travel through an evolving space-time to reach us at $z \sim 0$. Hence any dynamics that change the potential experienced by these photons, affect the CMB radiation. Since photons do not couple with dark energy and dark energy is a late time phenomenon (at least in minimally coupled models), the major contribution to the effects of dark energy on CMB comes through background cosmology. As photons travel through perturbed potentials, their energies change in accordance. Presence of dark energy makes these perturbations of metric potentials evolve in time and space. The photons passing through a perturbed space-time experience a potential that has evolved since the photon

entered that region and hence there may be an increment or decrement in photon energy/frequency. This is reflected in statistics of CMB anisotropy. This particular effect is called the Integrated Sachs Wolfe effect (ISW)[105]. Photons trajectories are curved by space-time and hence lead to lensing of sources. Statistical attributes of lensing are studied and can be related to theoretical models.

1.9.1 General Program to study Dark Energy perturbations

- Starting from a basic model (Lagrangian or phenomenological features), linear theory calculations are done to find how density contrasts (δ), peculiar velocities (v^i), metric perturbations, etc. evolve for different scales (k).
- Linear theory solutions are used to predict statistical quantities like power spectra. These are then compared with the observed distribution of "non-dark matter" as well as their velocities.
- Statistical indicators of distortions in photon propagation in evolving space-time are calculated and these are used to compare with observations e.g. weak lensing, ISW effect, etc.
- Non-linear, but simplified, simulations like spherical collapse or ellipsoidal collapse are done to get insights into properties of formation of nonlinear structures like virialization epoch, etc. These can be used to get an estimate of the abundances of halos.
- N-body simulations are done with various approximations. These simulations provide 3-d distribution of cosmic fields at different epochs. How to maximally utilize this information for model selection is a matter of active research.

1.10 About This Thesis

The work presented in this thesis aims at studying dynamics with dark energy perturbations (in scalar field models), in a fully consistent relativistic manner. We study non-linear spherically symmetric perturbations in quintessence and tachyonic dark energy models. We do not make any other assumption about dark energy perturbations apart from spherical symmetry.

We start in the next chapter with the study of spherically symmetric perturbations in quintessence dark energy. We find that metric perturbations induce perturbations in the dark energy field, which grow with time. But these are insignificant in comparison with nonlinear matter perturbations.
One important question that this work tries to investigate is: If two different Lagrangians for dark energy give the same background expansion, can they be distinguished by dynamics of perturbations? For this purpose, we consider two scalar field models with different Lagrangians: quintessence and tachyonic field. To address the above question, we need to reconstruct/find potentials in two models such that they give the same expansion history. The formalism for this reconstruction is presented in chapter 3 .
In chapter 4, we discuss the spherically symmetric perturbations in tachyonic models and how do they compare with quintessence models with the same background.

In chapter 5, we try to investigate if CMB observations can differentiate between the two. Here we stick to linear theory but rewrite equations in a manner, which helps illustrate why two models cannot be effectively distinguished using CMB observation in linear regime. We also constrain tachyon models with CMB data.
Finally, in chapter 6 we summarize the work in this Ph.D. project and provide outlook on future prospects.

Chapter 2

Nonlinear Spherical Perturbations in Quintessence Dark Energy

This chapter is based on following published article

Manvendra Pratap Rajvanshi and J.S. Bagla, Nonlinear spherical perturbations in quintessence models of dark energy, Journal of Cosmology and Astroparticle Physics, Volume 2018, June 2018 doi: 10.1088/1475-7516/2018/06/018 [arXiv:1802.05840]

In this chapter we study nonlinear perturbations in spherical symmetry, when dark energy is represented by quintessence. We start by looking into how dark energy perturbations are included in spherical collapse 2.1. We review some previous work on this topic and then go on to derive basic equations, for collapse in scalar field dark energy models, from first principles.
Main aims of this work are:

- Studying the effect of metric/matter perturbations on dark energy. We start with homogeneous dark energy field and let it evolve according to equations to see if perturbations are induced and how strong they are.
- Effect of dark energy perturbations on characteristics of dark matter perturbations is studied.

- Checking the validity of the assumptions of quintessence field remaining homogeneous on small scales.

Although we restrict ourselves to spherical symmetry, we do not make any assumptions about the clustering properties of quintessence.
In section 2.1, we review some previous work on spherical collapse in scalar field cosmology. In section 2.2, we derive the basic equations needed for our work and layout the formalism. This section also describes the initial conditions used and implementation of virialization. In section 2.3, we present the results. Results are further organized as dark matter perturbations results 2.3.1 and results concerning dark energy perturbations 2.3.2. We summarise in section 2.4.

2.1 Introduction

In chapter 1 (1.7), spherical collapse formalism was introduced. Here we briefly review the conceptual basis for inclusion of dark energy perturbations in spherical collapse. Most of such works ([106, 107, 108]), evolve spherical perturbed region as a separate universe with non-vanishing curvature. This can be justified rigorously in case of a spherical density embedded in otherwise empty region, using Birkhoff's theorem. In presence of various components, which can have perturbations, this justification loses its rigour.
Dark energy is itself modeled as an fluid with an effective equation of state and speed of sound. Then using continuity equation and Einstein's equations, equations of motion can be obtained for overdensity (δ) of spherical region or the radius of different shells. Equations simplify a bit, if form of perturbation is assumed to be top-hat.

There have been other works on spherical collapse in quintessence or other dark energy models [106, 109, 110, 111, 112, 113, 114, 115, 116, 117, 118, 119, 120, 121] But almost all of them either make assumptions about clustering of dark energy or use some kind of perturbation scheme. Some recent approaches [117], use methods from numerical relativity, to derive and solve equations from basic principles, similar in spirit to this work. But they do not do a thorough investigation of cosmological implications.
Most basic approach is to to assume that there are various kind of fluids and to derive the continuity equations for the fluids in spherically symmetric geometry[106]. There are also studies using Newtonian hydrodynamics for collapse[108]. An ex-

ample of continuity equation for dark energy[107]:

$$\dot{\rho} = -3\frac{\dot{R}}{R}(1+w)\rho + \Gamma \tag{2.1}$$

Here Γ is supposed to account for the clustering or the difference from background dynamics for the fluid and R corresponds to radius of spherical inhomogeneity. Different approximations for Γ lead to different clustering properties, see [107] for details. Another popular approach is to consider dark energy perturbations by phenomenological effective descriptions like fluids with effective speed of sound (c_s^2)[112, 122, 123].

In this work we try to work with minimal assumptions. We assume spherical symmetry and assume that the action for the dark energy component is that of a canonical scalar field. Equations follow from these assumptions and are solved using numerical methods.

2.2 Formalism

Here, we detail the formalism, derive basic equations, describe initial conditions and virialization. When the only content of the Universe is cold dark matter, Newtonian limit can be used to formulate spherical collapse. But when there are other components like scalar field, it is necessary that we derive the equations starting from GR, independent of Newtonian approximations. Here, we consider cold dark matter (i.e. pressure-less dust) and scalar field.

For modelling spatially isotropic perturbations, we start by considering a general spatially isotropic metric in comoving frame[90, 91]:

$$ds^2 \;=\; -e^{(2B)}dr^2 - R^2(d\theta^2 + sin^2\theta d\phi^2) + dt^2 \tag{2.2}$$

where $B(t,r)$ and $R(t,r)$ are arbitrary functions of r and t. Some of the characteristics of the metric in presence of pressure are discussed by Lynden-Bell, D. and Bičák, J.[124]. There are two functions representing space-time, $B(t,r)$ and $R(t,r)$, which we have to solve for, in addition to equations of dynamics for contents of the Universe. The full set of equations (Einstein's equations and continuity

equations):

$$\ddot{B} = -c^2 e^{-2B}\frac{R'^2}{R^2} + \frac{c^2}{R^2} + \frac{\dot{R}^2}{R^2} - \dot{B}^2 - 4\pi G\rho - \frac{8\pi G}{c}\left[\frac{\dot{\psi}^2}{2c^2} - e^{-2B}\frac{\psi'^2}{2}\right] \quad (2.3)$$

$$\frac{\ddot{R}}{R} = -\frac{4\pi G}{c}\left[\frac{\dot{\psi}^2}{2c^2} + \frac{e^{-2B}\psi'^2}{2} - V\right] - \frac{1}{2}\frac{\dot{R}^2}{R^2} + \frac{c^2}{2}\left[e^{-2B}\frac{R'^2}{R^2} - \frac{1}{R^2}\right] \quad (2.4)$$

$$\ddot{\psi} = c^2\left[-\frac{\partial V}{\partial \psi} + e^{-2B}\left\{\psi'' - \left(B' - \frac{2R'}{R}\right)\psi'\right\}\right] - \left(\dot{B} + \frac{2\dot{R}}{R}\right)\dot{\psi} \quad (2.5)$$

$$\dot{\rho_m} = -\left(\dot{B} + \frac{2\dot{R}}{R}\right)\rho_m \quad (2.6)$$

Here a dash/prime represents a partial derivative with respect to r and a dot represents a partial derivative with respect to t. In this problem, these are the two independent variables. Two potentials that are studied, are ($V \propto \psi^2$ and $V \propto \exp(-\psi)$). See Appendix (A.1 and A.2) for details of equations.

We set the initial conditions on a grid of r for B, R, $\dot{B}$, $\dot{R}$, ρ_m, ϕ and $\dot{\phi}$ and then evolve the system. An RK-4 based numerical scheme was used to solve these equations. See Appendix A.3 for details.

2.2.0.1 Initial conditions

To begin with, we look into solutions of derived equations, without any perturbations. Then, there is no dependence on r and the system reduces to a FLRW universe[11, 13, 125, 126]. In this limit $B(t,r) \to log(a(t))$ and $R(r,t) \to a(t)r$. We set initial conditions for this system so that the universe has $\sim$ 30% non-relativistic matter, and $\sim$ 70% dark energy at the present epoch. Dark Energy is represented by scalar field. To satisfy background cosmology constraints, we require that w (the effective equation of state) is close to -1. We set $\dot{\psi} = 0$ at the initial time. These requirements fix the initial conditions. Initial conditions were set at $z \sim 1000$.

We first solve for the background/homogeneous case i.e. equations for $a(t)$,H and average density parameters. The field is initiated with zero kinetic energy i.e. at initial time $w = -1$. For both the potentials, we can get solutions which remain fairly close to $w = -1$ till present epoch. We show the evolution of w and the density parameter for matter (Ω_{nr}) and field (Ω_ψ) in figure 2.1. This exercise allows us to set the parameters of the scalar field at the initial time for the case where we study non-linear evolution of perturbations.

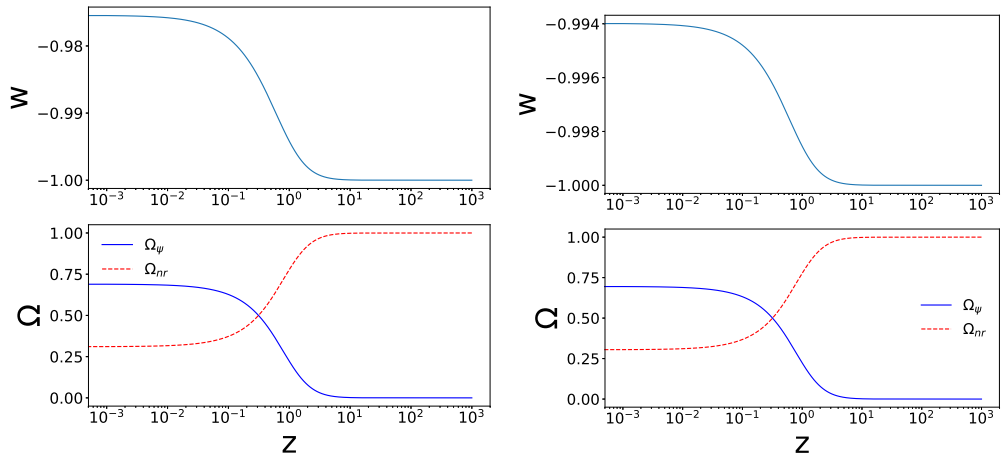

Figure 2.1: Evolution of the model without any perturbations. This is shown for the two potentials: $V \propto \psi^2$ (left column) and $V \propto \exp(-\psi)$ (right column). The top row shows the evolution of the equation of state parameter w as a function of redshift z. The lower row shows the evolution of the density parameter for non-relativistic matter and the dark energy components. We use initial conditions for the scalar field used here in all the simulations presented here unless mentioned otherwise. Initial conditions for dark matter at large r also fall back to this set.

At the initial time ($z \sim 10^3$), we assume that the scalar field (quintessence) is homogeneous. This has been shown to lead to the expected adiabatic mode for quintessence models [127]. This has also been noted by other authors who have studied attractors for dark energy perturbations [113]. Further we note that the evolution of metric is controlled by "net density" i.e. $\bar{\rho}(1+\delta)$, so even if the perturbations δ are of comparable order, it is the average or background density that plays the deciding role. So at earlier times, when dark energy contributions is very small to background energy budget, it is primarily the fluctuations of dominating constituent (dark matter here), that play central role in setting initial metric data.

We study results of our calculations at late times, $z \leq 10$ and hence there is adequate time for the solution to approach the attractor. From scalar field initial conditions assuming that there are no perturbations and $w = -1$:

$$\begin{aligned} \psi_i' &= 0 = \psi_i'' \\ \dot{\psi}_i &= 0 \\ \psi_i &= 1 \end{aligned} \tag{2.7}$$

Parameters of potentials, like amplitude of potential V_0 and λ in $V = V_0 \exp(-\lambda\psi)$ have to be decided. Choice of desired of background evolution fixes these.

At initial time, matter distribution has small perturbation. We use a compensated profile for perturbation, i.e, the central perturbation is offset by a perturbation of opposite sign so that at large r, the net perturbation integrated over volume goes to zero. We use the following functional form:

$$\delta_i(r) = \begin{cases} \alpha_0 \left[1 - \left(\frac{r}{\sigma_0}\right)^2\right]^2 - \alpha_1 \left[1 - \left(\frac{r}{\sigma_1}\right)^2\right]^2 & (r \leq \sigma_0) \\ -\alpha_1 \left[1 - \left(\frac{r}{\sigma_1}\right)^2\right]^2 & (\sigma_0 < r \leq \sigma_1) \\ 0 & (r > \sigma_1) \end{cases} \tag{2.8}$$

Here we require $\sigma_0 < \sigma_1$. The requirement of net perturbation after averaging over volume to $r = \sigma_1$ can be stated as:

$$\int_0^{\sigma_1} \delta_i(r) r^2 dr = 0 \tag{2.9}$$

Thus there is no net perturbation at scales larger than σ_1 and these regions should evolve as a smooth universe. This leads to the following relation between α_0 and α_1:

$$\alpha_1 = \alpha_0 \left(\frac{\sigma_0}{\sigma_1}\right)^3 \tag{2.10}$$

Initial velocity of each shell is set by assuming that these are comoving with the uniform Hubble expansion. This facilitates comparison as this assumption has been used in earlier studies [98] [92] as well. In comparison with linear theory it is important to recall that only 3/5 of the initial density perturbation in such a case is in the growing mode[1]. Using this with initial condition $R_i = a_i r$, we can obtain initial conditions for metric coefficients and their time derivative. For numerical convenience, we redefine the time variable as $t \to tH_i$ where H_i is initial value of the Hubble parameter.

$$B_i = \ln(a_i) - \frac{1}{2} \ln \left[1 - \frac{3}{r} \frac{\Omega_{im} a_i^2}{c^2} \int dr r^2 \delta(r)\right] \tag{2.11}$$

$$\dot{B}_i = 1 \tag{2.12}$$

$$R_i = a_i r \tag{2.13}$$

$$\dot{R}_i = R_i \tag{2.14}$$

$$R' = a_i \tag{2.15}$$

$$R'' = 0 \tag{2.16}$$

[1]While the number 3/5 is derived for the Einstein-deSitter model, it is a useful approximation as much of the evolution takes place in the matter dominated phase.

The subscript i refers to the initial value of the variable, a is the scale factor and H is the Hubble parameter. Ω_{im} is the initial value of density parameter for matter.

We note the presence of a logarithm in initial function for B. This means second term in expression for B_i, is constrained such that argument to log is positive. This restrict the amplitude and scale of overdense perturbations. In particular this affects the simulations of large scale over densities: comoving initial conditions for arbitrarily large perturbations are not allowed.

Overdense shells, initially comoving with hubble flow, expand initially, their expansion is slowed down by gravity of extra mass. If the initial density contrast is above a critical value, the shell eventually reaches a maximum radius (turn-around radius) and then collapses on to itself.

2.2.1 Virialisation

The solutions of system of equations, for spherical collapse, lead to a singularity. Each shell reaches turn around and collapses to origin. This is the "mathematical solution". In real world, perturbations collapse to form stable/pseudo-stable structures. Velocity dispersion and non-radial motions might come into play during late time dynamics. It is assumed that violent relaxation will drive the system to virial equilibrium. Dark matter can not radiate or exchange energy to other channels. Physics of virialisation of dark matter is very poorly understood. Further, inclusion of dark energy perturbations complicates the situation[96]. We start with a simplistic approach assuming that in-falling perturbation stabilizes at radius where kinetic energy and potential energy satisfy virial theorem (2.18).

In case of Einstein-deSitter universe, this leads to a simple expression for the virial radius: the radius of the virialised halo is exactly half of the maximum or the turn around radius for the shell [92]. Barrow and Saich[98] generalised this to the case when a non-zero cosmological constant is present besides non-relativistic matter.

$$R_V = \left(\frac{2}{3}\right)^{1/3} \left(\frac{\Omega_\Lambda R_T^3 + \Omega_M (\frac{a_0}{a_{in}})^3 (1+\delta_{in}) R_{in}^3}{\Omega_\Lambda R_T}\right)^{1/2} \sin\left[\frac{1}{3}\arcsin\left\{\frac{\Omega_M a_0^3 (1+\delta_{in}) R_{in}^3}{a_{in}^3 R_T^3}\left(\frac{1.5}{1+\frac{\Omega_M}{\Omega_\Lambda}(\frac{a_0 R_{in}}{a_{in} R_T})^3(1+\delta_{in})}\right)^{3/2}\right\}\right] \tag{2.17}$$

Here, R_{in} is the initial radius, R_T is the maximum or the turn around radius, δ_{in}

is the initial density contrast inside the shell, a_{in} is the initial value of the scale factor and a_0 is its present value, Ω_Λ is the density parameter corresponding to the cosmological constant at present and Ω_M is the density parameter for non-relativistic matter.

In case of dark energy perturbations, calculations are further involved. Maor and Lahav [96] summarize two limiting cases for a fluid model of dark energy. They point out that there are significant differences that arise depending upon whether or not dark energy participates in the virialisation process. The two limiting cases they consider are: only dark matter virialises and dark energy does not cluster, and, both dark matter and dark energy virialise. Maor and Lahav [96] show that if only dark matter virialises, then the ratio of virial radius to turn around radius is on lower side of Einstein-DeSitter value of 0.5, while if the two component system of dark energy plus dark matter virialises together, then this ratio is larger than half. It is relevant to note here that in the case of a cosmological constant, the expected ratio of virial radius to turn around radius is less than half.

As we shall see below, we find that in the case of scalar field, the ratio of virial radius to the turn around radius is less than half.

2.2.1.1 Evolution of dark energy beyond virialisation

We use the Virialisation condition:

$$< T > + \frac{1}{2} \langle R\, F_R \rangle = 0 \tag{2.18}$$

here T is the kinetic energy, R is the radius of the shell and F_R is the radial force on the shell. Angular brackets denote averaging over time.

$$T = \frac{1}{2}\dot{R}^2 \quad F_R = \ddot{R} \tag{2.19}$$

In case of cosmological constant one can use this relation to get an analytical form (2.17) for R_V is terms of R_T [98]. In case of quintessence being considered here, we track the value of the right hand side of Eqn.2.18 after turn around and declare the shell to have virialised when this value becomes zero for the first time.

It is important to note that in our implementation of virialisation, virialisation time is when the collapsing shell reaches the configuration where it satisfies the virial theorem. This implementation is different from approaches which assume the time of virialisation to be the time when shell collapses to singularity.

An implication of this is that the density contrast at the time of virialisation computed here is lower than that obtained with the usual method as the background density is higher.

For reference, note that in case of an Einstein-deSitter background, the density contrast at virialisation with this approach is 145, as compared to 168 that we obtain using the usual method.

After turn around, we check for condition (2.18) and at that particular $R(r)$ we freeze the metric terms $B(t,r)$ and $R(t,r)$, and we do so because $R(t,r)$ has physical meaning of physical radius which stabilizes at virialisation. In case of $B(t,r)$ we take a cue from ΛCDM where $B(t,r)$ is dependent on spatial derivatives of $R(t,r)$. Further, consistency requires that we set time derivatives of the two variables to zero.

As we freeze the metric coefficients, the set of equations we have can no longer be evolved self consistently. Therefore the solutions at later times, after virialisation of the innermost shells, are approximate solutions. As we shall see, dark matter dominates over dark energy in the virialised region and hence an approximate solution can be attempted without expecting a significant back reaction and an implied variation of metric coefficients. The scalar field equations need to be solved over the entire range of scales and it is not obvious whether any choices we make for the solution in the interior of the virialised region will have an impact on the evolution of the field at large scales.

We try three approaches to approximate solution for the scalar field in the virialised region.

1. The scalar field can be evolved as a test field in the space-time determined by the frozen metric coefficients in the virialised region.
2. The scalar field can also be frozen in the virialised region, i.e., we put $\dot{\psi} = 0 = \ddot{\psi}$ in this region.
3. We put $\ddot{\psi} = 0$ and freeze the value of $\dot{\psi}(r)$ inside the virial region.

We compare three approaches. We find that first approach is most numerically stable. Second and third approaches are more abrupt and they show numerical instabilities, particularly when simulating perturbations of physically relevant scales. All three approaches are numerically feasible at extreme lengthscale perturbations

Simulation	σ_0	σ_1	α_0	z_{vir}
OD1	3	18	0.0068	1.5
OD2	3	18	0.0136	4.0
OD3	6	18	0.0068	1.5
UD1	150	250	-0.0136	-
UD2	20	200	-0.0068	-
UD3	40	200	-0.0068	-
UD4	20	200	-0.0136	-
UD5	100	200	-0.0136	-

Table 2.1: Parameters used in simulations in this work. Note that for simplicity we have stated the approximate value of the redshift at which the first shell virialises in the case of simulations with over-densities. The simulations are referred to by the Simulation code in figure captions.

of order GigaParsecs. For these lengthscales, they show similar evolution at virial radius and are indistinguishable beyond turn around radius.

In the first approach given above, we solve for the scalar field inside the virial radius according to the following equation:

$$\ddot{\psi} = c^2 \left[-\frac{\partial V}{\partial \psi} + e^{-2B_{vir}} \left\{ \psi'' - \left(B'_{vir} - \frac{2R'_{vir}}{R_{vir}} \right) \psi' \right\} \right] \tag{2.20}$$

Here, R_{vir} and B_{vir} are the frozen values of metric coefficients inside the virial radius. We solve the full set of equations outside the virial radius.

A comparison of the three approaches is shown in Figure 2.2. We have plotted the density contrast δ_{de} for dark energy (top panel) and the equation of state parameter w (lower panel) as a function of scale r. The two columns are for two different potentials: the left column is for $V \propto \psi^2$ whereas the right column is for $V \propto \exp[-\psi]$. We have marked the turn around radius with a vertical line on these plots. We find that the qualitative trend is the same for the three approaches. The three approaches have differences at scales close to the virial radius, however the differences decrease rapidly beyond the turn around scale. Percentage difference among three approaches outside virial radius is less than 1% at all scales. The approach where we set $\dot{\psi} = 0$ deviates most from the other two approaches and the differences are most obvious in the plot of w as a function of scale r.

We use the first approach where the scalar field is evolved as a test field in the fixed background inside the virial radius in the following discussion.

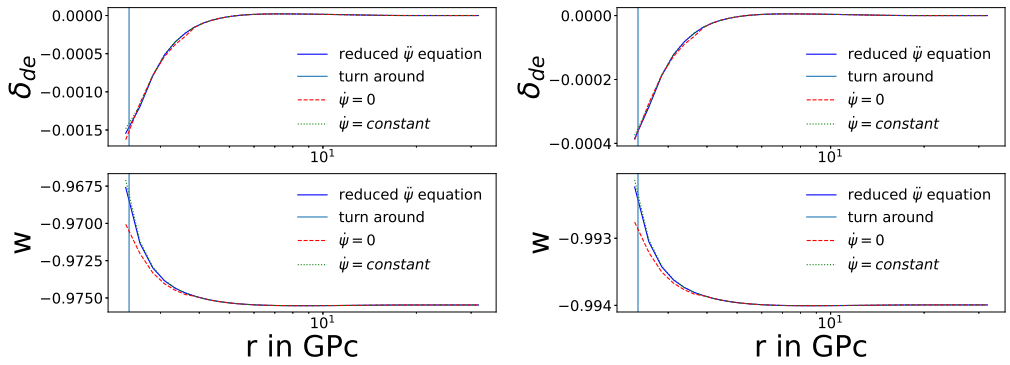

Figure 2.2: A comparison of the three approaches for evolving the scalar field in the virialised region. Here we show δ_{de} and w as a function of r at scales outside the virial radius at the present epoch. The left column is for $V \propto \psi^2$ and the right column is for $V \propto \exp(-\psi)$ The turn around radius is marked by the vertical line. The amplitude of perturbations is adjusted so that the innermost shells virialise at $z \simeq 1.5$. Simulation OD1 was used for these plots. We find that the three approaches match very well at all scales away from the virial radius. Differences between the three approaches are less than a few percent at all scales, and less than a percent at all scales larger than twice the virial radius.

2.3 Results

We present the results from our simulations in this section, showing the effects on dark matter and energy perturbations. The complete list of simulations with the relevant parameters is given in table 1. The section is divided into sub-sections where we separately study the effect of dark energy perturbations on collapse of dark matter, evolution of dark energy perturbations: both in the case of over density and an under density, analysis of variations with the scale as well as the amplitude of dark matter perturbations, and, a comparison of the evolution of dark energy perturbations with the linear perturbation theory.

2.3.1 Dark matter perturbations

We want to probe the question if presence of perturbations in dark energy field affects matter growth. For studying such effects, we run, in addition to quintessence simulations mentioned above, simulations with same initial conditions, but with dark energy modeled as a non-clustering fluid having same $w(z)$ for the background as the quintessence simulations. For this we first run a quintessence background for which we want to make comparisons, store the table for $w(z)$ and run simulation with dark energy as non-clustering fluid with this $w(z)$. A full-fledged quintessence simulation as governed by equations derived in previous sections is

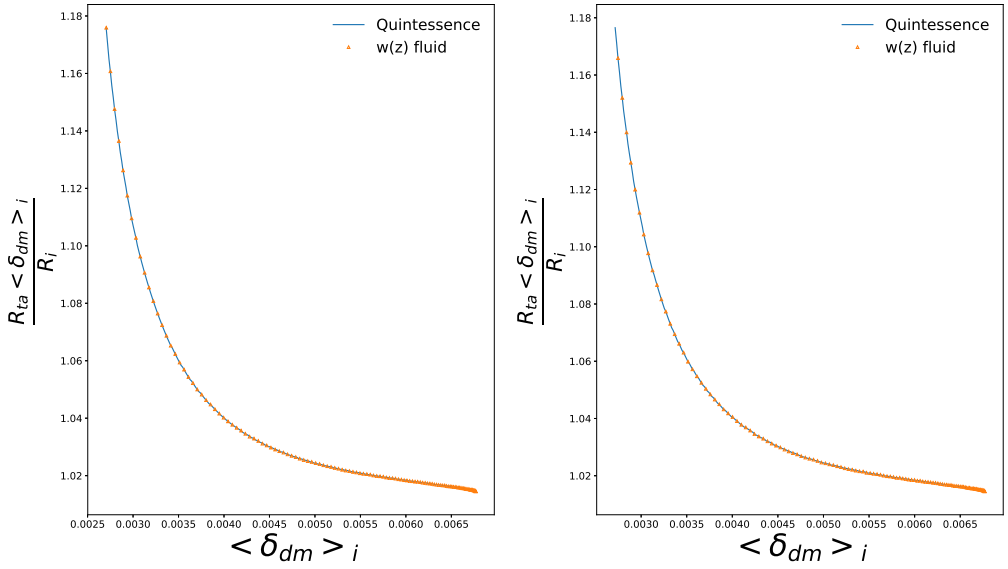

Figure 2.3: We have plotted the turn around radius in the combination $R_{ta}\langle\delta_{dm}\rangle_i/R_i$ as a function of the initial density contrast. The expected value of the combination is unity for the Einstein-deSitter model and we see that at large values of $\langle\delta_{dm}\rangle_i$ we indeed approach this value. The left panel is for $V \propto \psi^2$ while the right panel is for $V \propto \exp(-\psi)$. Simulation OD1 and the same initial conditions for the case without dark energy perturbations have been used for these plots. We plot values from our simulations with perturbations in dark energy as well as from a model where the dark energy does not have any perturbations. The two curves match to better than 0.03% at all scales, indicating that perturbations in dark energy do not influence collapse of dark matter perturbations.

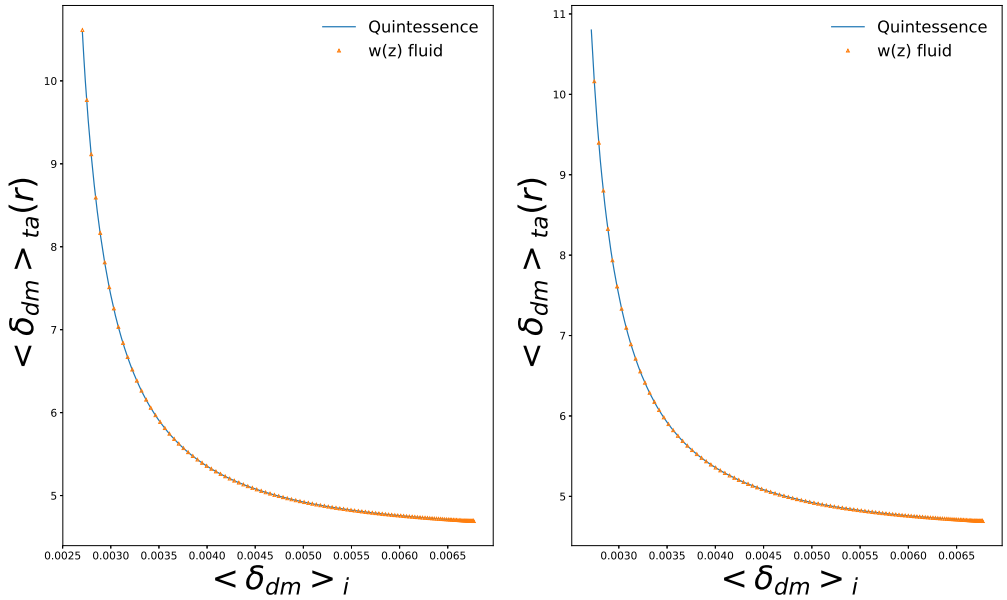

Figure 2.4: Density contrast at turn around is shown here as a function of the initial density contrast. The expected value of the combination is 4.55 for the Einstein-deSitter model and we see that at large values of $\langle\delta_{dm}\rangle_i$ we indeed approach this value. The left panel is for $V \propto \psi^2$ while the right panel is for $V \propto \exp(-\psi)$. We plot values from our simulations with perturbations in dark energy as well as from a model where the dark energy does not have any perturbations. Initial dark matter perturbations here correspond to simulation OD1. The two curves match to better than 0.06% at all scales, indicating that perturbations in dark energy do not influence collapse of dark matter perturbations.

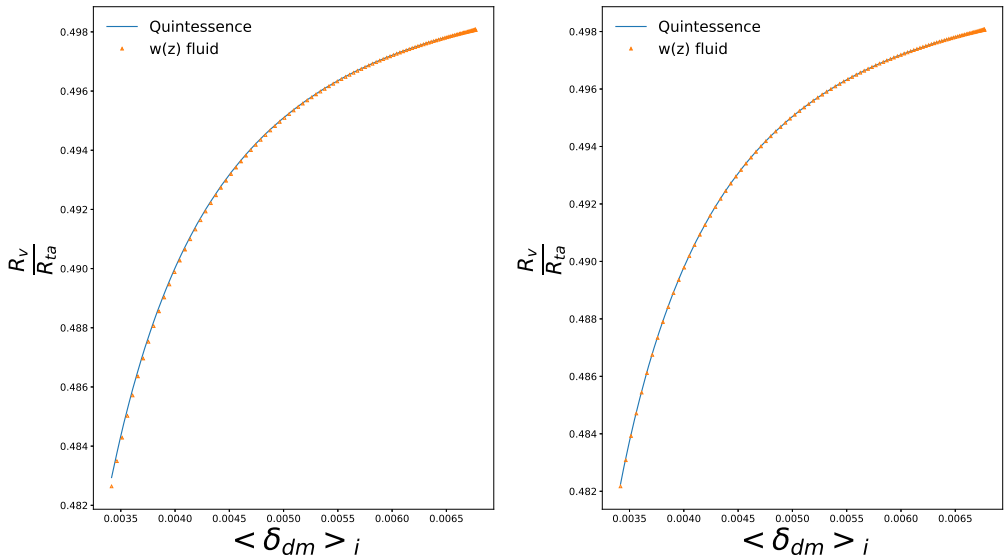

Figure 2.5: Ratio of virial radius to turn around radius is shown here as a function of the initial density contrast in dark matter. The expected value of the combination is 0.5 for the Einstein-deSitter model and we see that at large values of $\langle \delta_{dm} \rangle_i$ we indeed approach this value. A value lower than 0.5 signifies that dark energy does not cluster significantly [96]. The left panel is for $V \propto \psi^2$ while the right panel is for $V \propto \exp(-\psi)$. We plot values from our simulations (OD1) with perturbations in dark energy as well as from a model where the dark energy does not have any perturbations. The two curves match to better than 0.01% at all scales, indicating that perturbations in dark energy do not influence collapse of dark matter perturbations.

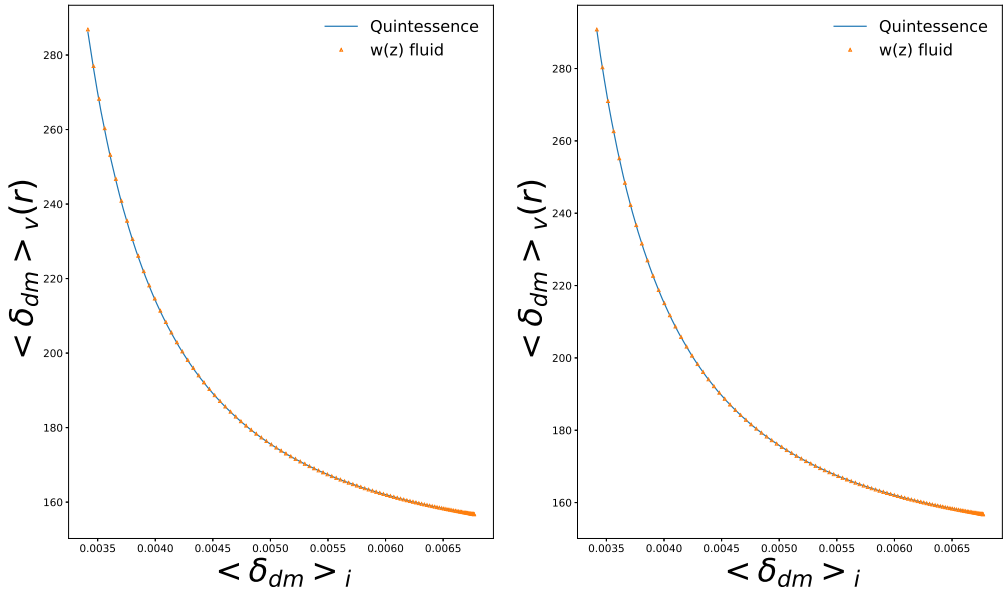

Figure 2.6: Density contrast at virialisation as a function of the initial density contrast in dark matter. The expected value in our approach for Einstein-deSitter universe is 145 (see text). We see that the curve is tending towards that value at large initial density contrast. The left panel is for $V \propto \psi^2$ while the right panel is for $V \propto \exp(-\psi)$. We plot values from our simulations (OD1) with perturbations in dark energy as well as from a model where the dark energy does not have any perturbations. The two curves match to better than 0.3% at all scales, indicating that perturbations in dark energy do not influence collapse of dark matter perturbations.

run and comparisons are made for collapse and virial properties of dark matter. So in following figures we have comparsions between a $w(z)$ fluid model, which does not have any dark energy perturbations and a quintessence simulation which allows for perturbations coming from the underlying equations. $w(z)$ fluid has following dynamics:

$$\frac{d\rho_{de}}{dt} = -3\frac{\dot{a}}{a}(1+w)\rho_{de} \tag{2.21}$$

Results of a comparative study of this fluid model with full-fledged spherical collapse in quintessence are presented here. We show the comparison for various quantities related to turn around and virialisation. We choose to plot these as a function of the initial density contrast δ_i. The choice is motivated by the emergence of a critical value for density contrast required for collapse in the case of the cosmological constant. We find that just like the cosmological constant model for dark energy, there is a critical value that emerges in the dynamical dark energy models. Perturbations with a lower initial density contrast do not enter a collapsing phase. Further, we find that various quantities of interest approach the values obtained in the Einstein-deSitter model as δ_i becomes much larger than the critical value. On the other hand, as we approach the critical initial density contrast from above, dark energy becomes more and more important, and hence it takes longer to begin collapse. Thus the universe expands by a significantly larger amount by the time such perturbations reach turn around or virialisation and hence the average density of matter in the universe is much lower.

Figure 2.3 shows the turn around radius as a function of δ_i. Instead of the turn around radius, we choose to plot the combination $R_{ta}\langle\delta_i\rangle/R_i$. Here R_i is the initial radius of the shell and $\langle\delta_i\rangle$ is the average density contrast inside this shell at the initial time. This combination is unity for spherical collapse in the Einstein-deSitter model. The left panel is for the ψ^2 potential whereas the right panel is for the exponential potential. Curve for the model with dark energy perturbations and points for the corresponding model without dark energy perturbations are plotted in the same panels. The difference between the two cases is too small to be seen from these panels. In both models, and for the cases with and without dark energy perturbations, the qualitative trend is the same: the turn around radius is larger for smaller δ_i. At large δ_i, we approach the turn around radius approaches the expected value in the Einstein-deSitter model. Bottom panels show the percentage difference between the turn around radius in the two models (with and without dark energy perturbations) as a function of δ_i. We find that the percentage difference is well below one percent for the turn around radius.

Figure 2.4 shows the turn around density contrast for different shells in the same format as Figure 2.3. We find that the density contrast at turn around for shells with large δ_i approaches the expected value for the Einstein-deSitter model. As we approach lower δ_i, we find that the density contrast at turn around increases rapidly. This is largely because it takes longer to reach turn around for shells with a smaller initial density contrast, and in this time the density of matter in the universe decreases significantly, leading to a larger density contrast within the perturbation. In this case too, the difference between the model with dark energy clustering and without dark energy clustering is smaller than a percent at all scales for the two potentials studied here.

Figure 2.5 and Figure 2.6 show the virial radius (in units of the turn around radius) and the density contrast at the time of virialisation, respectively. We find that the two quantities approach the values expected for the Einstein-deSitter model at large δ_i. For shells with smaller δ_i, the virial radius is less than half the turn around radius with the ratio decreasing as we get to shells with a smaller initial δ_i. The density contrast at virialisation increases rapidly for smaller initial δ_i, whereas for larger δ_i, we get the value expected in the Einstein-deSitter model (145).

2.3.2 Dark Energy Perturbations

In this subsection, we present dark energy perturbation results. As mentioned before, at initial time, there is no perturbation in dark energy field. As the system evolves, perturbations in dark matter drive the perturbations in metric, which in turn induce perturbations in dark energy. We study both, initially underdense dark matter and initialy overdense dark matter regions.

As stated in initial condition discussion, we cannot simulate arbitrary large overdensities, but we can simulate very large voids. One imporatant feature that we notice from our simulations is that dark perturbations are stronger for bigger scales. Hence large voids offer better prospects of probing dark energy perturbations. We start by looking into overdense cases.

2.3.2.1 Over dense Profile

In a region with an initial over density in matter, gravitational instability ensures that the density of dark matter in the region increases monotonically when com-

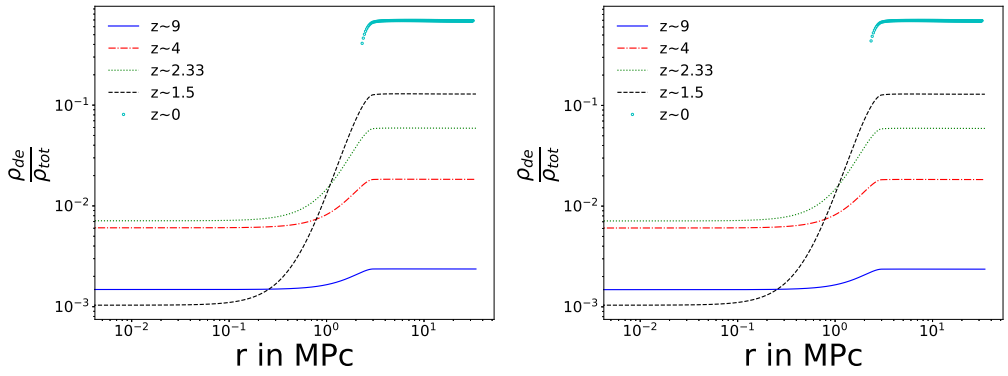

Figure 2.7: Contribution of Dark Energy to total energy density for over dense case (simulation OD1). We see that at large r, the relative contribution of dark energy increases monotonically. However, within the over dense region the contribution of dark energy reaches a maximum of ~ 0.007 and then drops to lower values. The left panel is for $V \propto \psi^2$ while the right panel is for $V \propto \exp(-\psi)$. We have shown curves outside the virial radius while omitting the values inside the virial radius as we do not have a self-consistent evolution inside the virialised halo. This omission of data within the virial radius impacts only one of the curves shown here.

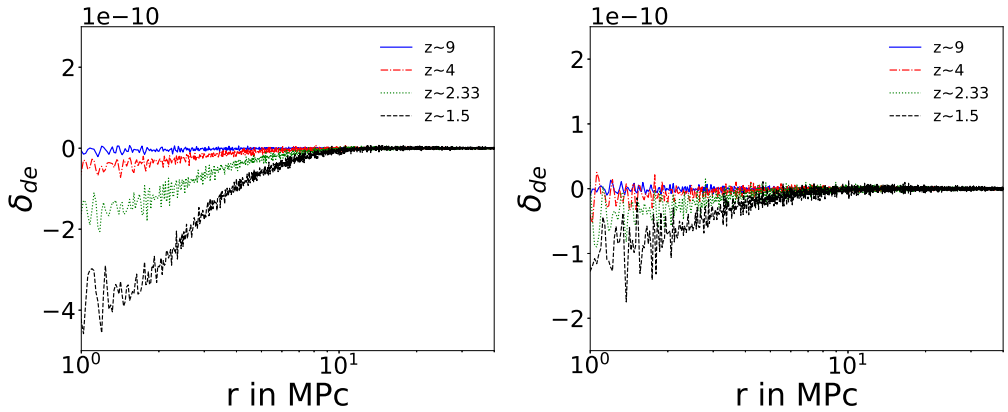

Figure 2.8: Density contrast for dark energy as a function of scale at different epochs. We see that the amplitude of perturbations in dark energy remains small at all scales and at all times. We have plotted values only at scales outside the virial radius for simulation OD1. The left panel is for $V \propto \psi^2$ while the right panel is for $V \propto \exp(-\psi)$.

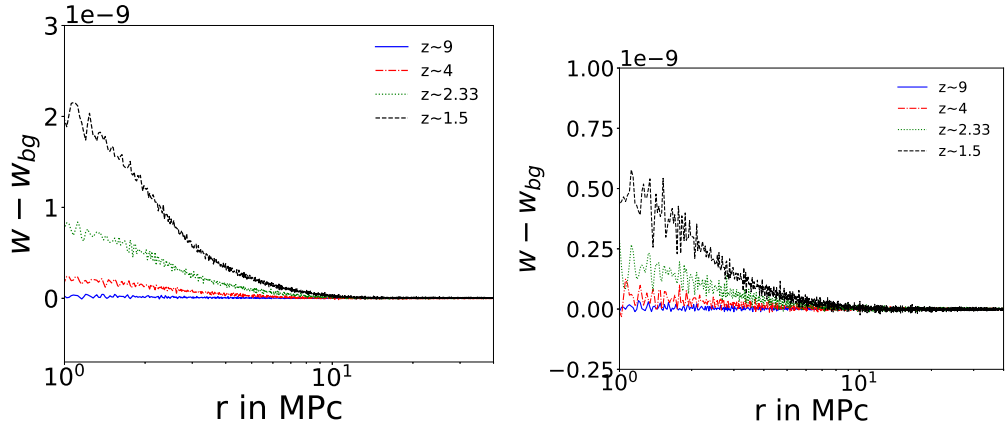

Figure 2.9: The equation of state parameter for dark energy as a function of scale at different epochs from simulation OD1. We see that the variation in w with scale is fairly significant, particularly at late times. The lower row of plots shows the variation of w with respect to the value in the background model, or the asymptotic value at large scales. We have plotted values only at scales outside the virial radius. The left panel is for $V \propto \psi^2$ while the right panel is for $V \propto \exp(-\psi)$.

pared with the average density of matter in the universe. If the initial density contrast is sufficiently high, we find that gravitational instability leads to local collapse and a sharp increase in the density of matter within the collapsed region. It is important to assess the evolution of dark energy density in the region. We show the relative contribution of energy density of dark energy as compared to dark matter drops significantly in the region where dark matter collapses. We show this for a model with $\sigma_0 = 3$ Mpc, $\sigma_1 = 18$ Mpc and the redshift of virialisation $z \sim 1.5$. This is shown in Figure 2.7. Each curve refers to a specific epoch as marked in the legend. We find that at very large scales dark energy becomes more and more dominant with time, as is expected for the background model that is dominated by dark energy at present. However, within the collapsed region, the relative role of dark energy diminishes strongly at late times. We see that even before virialisation, the energy density of dark energy drops to less than a few percent of its background value near the centre of the perturbation. Thus in terms of the local contribution to the energy budget, dark energy plays a negligible role inside the perturbation.

We plot the density contrast for dark energy as a function of scale for the same model used above 2.8. We find that the density contrast for dark energy grows in response to the dark matter perturbation, however its amplitude remains small as compared to unity through the non-linear evolution of dark matter perturbations. Thus we do not expect any significant impact of dark energy density contrast and its variations on observables at small scales.

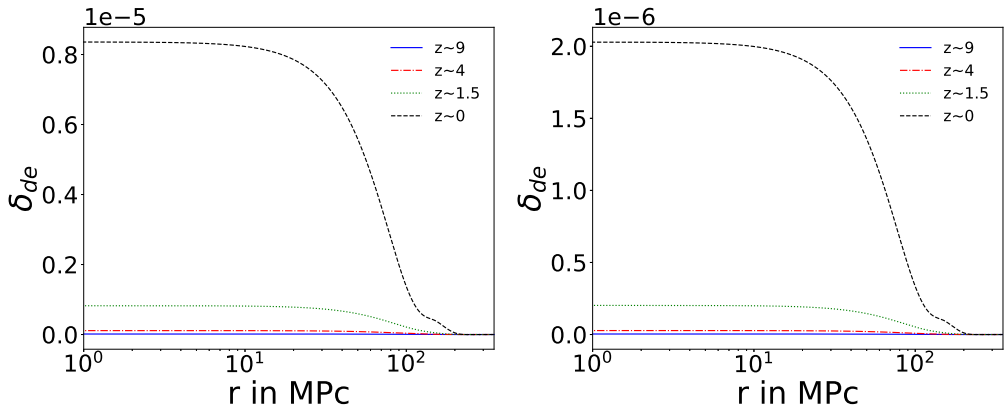

Figure 2.10: Density contrast for dark energy as a function of scale r for a void, i.e., a matter under-density from simulation UD1. This is plotted at multiple epochs. We find that dark energy perturbations grow but the amplitude remains small in absolute terms. The left panel is for $V \propto \psi^2$ while the right panel is for $V \propto \exp(-\psi)$.

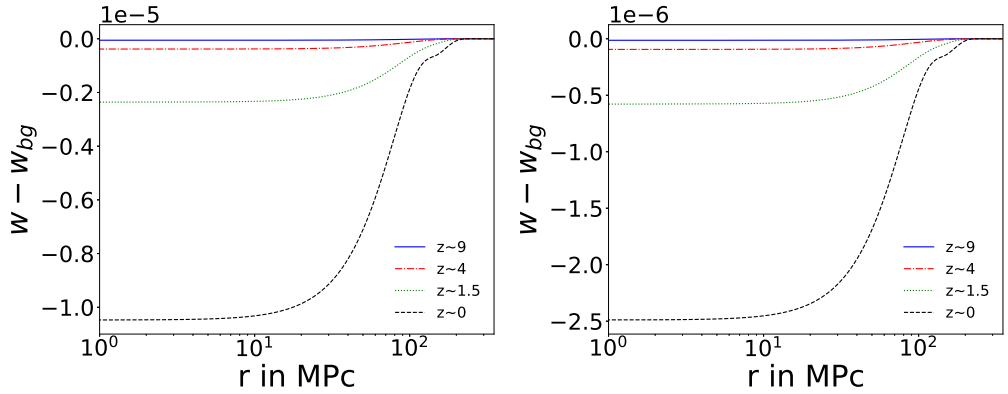

Figure 2.11: Equation of state parameter w as a function of scale r for a void, i.e., a matter under-density for simulation UD1. This is plotted at multiple epochs. We find that w inside the void is smaller than at large scales. The left panel is for $V \propto \psi^2$ while the right panel is for $V \propto \exp(-\psi)$.

A surprising feature that may have implications for observations and hence work as a diagnostic for dynamical dark energy models is the spatial variation in the equation of state parameter w. We already know from background evolution and our choice of initial conditions that $w = -1$ at early times and it increases slowly with time. We show variation of w as a function of r in Figure 2.9. This is shown for four epochs leading up to the epoch of virialisation. We find that w increases more rapidly in regions around the collapsing dark matter perturbations.

2.3.2.2 Under dense Profile

So far we have discussed the evolution of matter over densities. We now turn our attention to the evolution of under densities, or voids. The large scale of voids coupled with the fact that the magnitude of the spatial variation of w is larger for perturbations at large scales makes these a potential test bed for observing the effects of dynamical dark energy.

We show results for a model with $\sigma_0 = 150$ and $\sigma_1 = 250$, thus the characteristic length scale of the perturbation is 250. We find that the dark energy contributes a very significant fraction to the total energy budget mainly due to depletion of matter. This becomes clear in figure 2.10 that shows the density contrast in dark energy as a function of scale r. We find that the amplitude of density contrast is very small compared to unity at all scales and at all times.

We have plotted the variation of w, the equation of state parameter, as a function of scale at different epochs in figure 2.11. We find that the increase in w with time slows down in under dense regions. This is mainly due to the faster than average expansion rate in the voids. We find that the differential in w is larger for larger voids. The variation with the initial density contrast for matter is less significant, but a larger initial under density leads to a larger differential in w.

Voids may be the optimal sites for testing changes in w. This is primarily because dark energy dominates in terms of the overall energy budget.

2.3.2.3 Comparison with Linear Perturbation Theory

We have seen that the density contrast in dark energy remains much smaller than unity in all cases considered here. This makes it possible to consider density fluctuations in dark energy at a perturbative level. We compare the rate of growth of dark energy perturbations in our simulations with the rate of growth expected in linear perturbation theory. Such a comparison is useful as it allows us to assess the significance of non-linear dark matter perturbations that our model takes into account.

Before carrying out the comparison, we note that the growth of dark energy perturbations has been studied and it has been found that the growth of perturbations is stunted at small scales. It has been shown that at very large scales

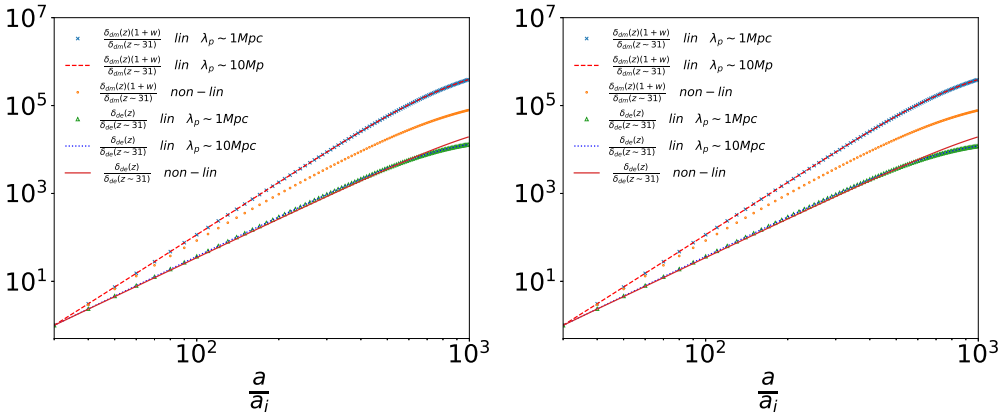

Figure 2.12: A comparison of the evolution of dark energy perturbations. Left panels are for $V \propto \psi^2$ while right one are for $V \propto \exp(-\psi)$. At very large scales the linear theory prediction for the magnitude of dark energy perturbations scales as $(1 + w)\delta_{dm}$. We have plotted this combination for linearly evolved δ_{dm} for two scales: 1 Mpc (cross) and 10 Mpc (dashed line). Linear evolution of dark energy density contrast for the two scales is also shown here as triangles (1 Mpc) and dotted line (10 Mpc). We find that the linear evolution for dark energy perturbations is slower at small scales as compared to the expected variation at large scales. All points pertaining to linear evolution are normalised to unity at the left corner.

$\delta_{DE} \propto (1+w)\delta_{DM}$, which is the expected relation for adiabatic perturbations. For thawing models, $w \simeq -1$ at early times and increases slowly over time. Thus the rate of growth of dark energy perturbations in such models can be much larger than the rate of growth of perturbations of dark matter perturbations. However, same studies indicate that the rate of growth of dark energy perturbations at small scales is slower than the rate at large scales. Specifically, it has been shown that at scales much smaller than the Hubble radius, the linear growth rate is independent of scale.

In figure 2.12, we show the growth in density contrast for a particular co-moving radius for non-linear spherical case and the corresponding Fourier space amplitude (δ_k) for two length scales 1 Mpc and 10 Mpc. We show results from simulation UD1. The curves are normalised at the left corner to avoid crowding and facilitate comparison. This also subsumes an offset required due to different initial conditions (growing mode vs. comoving initial conditions for the two calculations) used in the two different calculations. We find that the rate of growth in the two calculations differs. In particular, at late times, the growth rate of density perturbations in dark energy in the simulation increases and the final amplification factor is higher than expected in the linear perturbation theory. Also, we find that the linear evolution for dark energy perturbations is slower at small

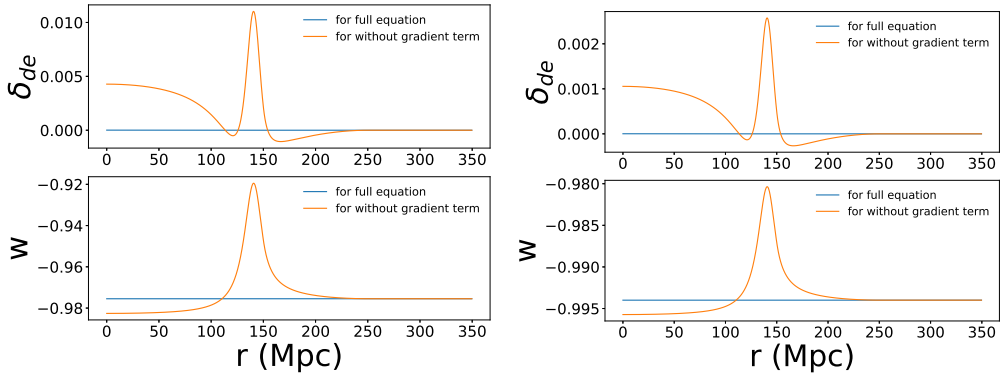

Figure 2.13: In this figure we explore the leading cause of variation of equation of state parameter w for simulation UD1. We show the variation computed by retaining only the local Hubble expansion terms in the equation of motion and compare it with the full simulation. In the former case, we ignore the gradient term. We find that the variation of w is fairly strong and has some localised features when the gradient terms are ignored. The localised features are not present in the full simulation indicating that the gradients of the scalar field are suppressed in the evolution, and the local Hubble expansion is not the only determining factor.

scales as compared to the expected variation at large scales. Thus the non-linear evolution of density fluctuations in dark matter leads to a more rapid growth of perturbations in dark energy.

2.3.2.4 Exploring dark energy perturbations

The variation in w around a dark matter over density is caused mainly by the slower expansion rate that leads to a more rapid rolling down of the scalar field. In case of under dense regions, the faster expansion slows down the rolling of the field further. We test this conjecture by running a simulation with only the local Hubble flow terms retained. The field equation in this case reduces to:

$$\ddot{\psi} = -c^2 \frac{\partial V}{\partial \psi} - \left(\dot{B} + \frac{2\dot{R}}{R} \right) \dot{\psi} \tag{2.22}$$

where we have dropped the terms related to ψ' and ψ''. We find that evolving the system with this equation gives rise to sharp features that are not seen in the full simulation as shown in Figure 2.13. We surmise that in addition to the variation in expansion rate, there is also a suppression of gradient of the scalar field.

The variation of w around matter perturbations is interesting and we investigate it further. This is important in order to ascertain the possibility of constraining models using observations. Specifically, we explore the magnitude of variation

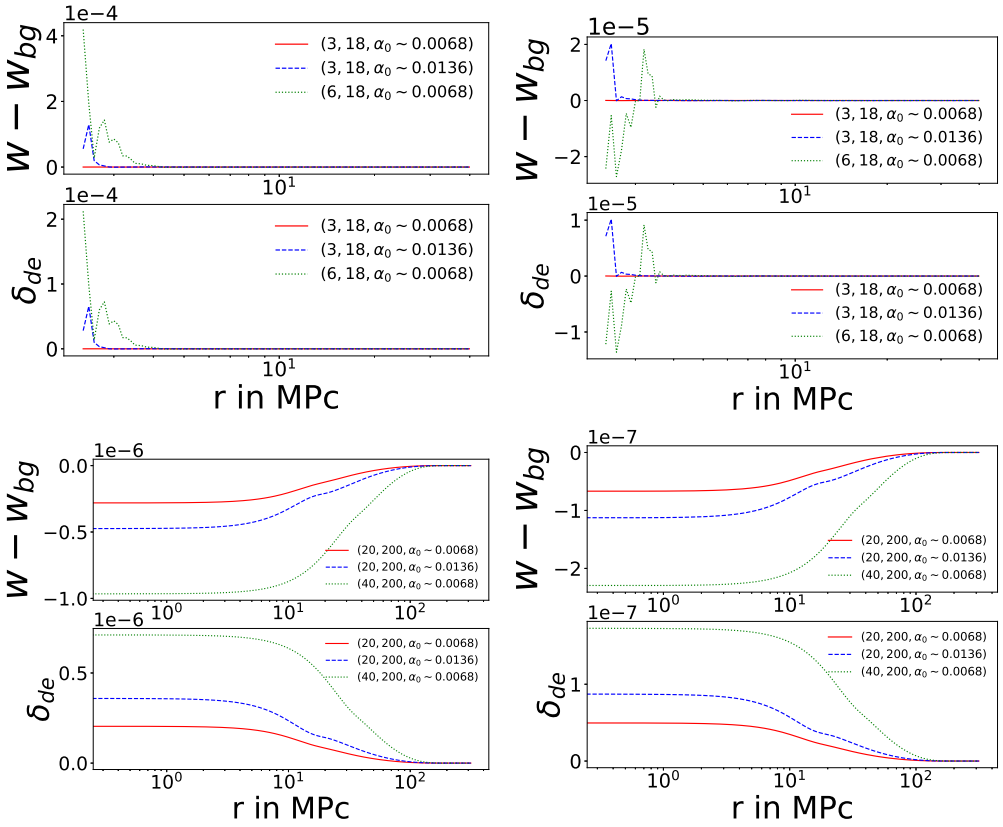

Figure 2.14: In this figure we explore the dependence of the variation of w on the scale of perturbations in dark matter and also on the amplitude of initial density contrast for dark matter. We plot the variation of w with scale for three overdense (upper panel) models (OD1, OD2 and OD3) and underdense cases (UD2, UD3 and UD4) in lower panel. Two of the models are for the same initial density contrast in matter but for different scales of perturbation. The third model has the same scale of perturbation as our fiducial model, but has a significantly higher amplitude of the initial matter perturbation. We find that the variation of w is strongest in the model with the larger scale but same amplitude as the fiducial model. The variation with the change in amplitude of perturbation is much smaller. This is evident from bigger void simulations (lower panel). The left panel is for $V \propto \psi^2$ while the right panel is for $V \propto \exp(-\psi)$.

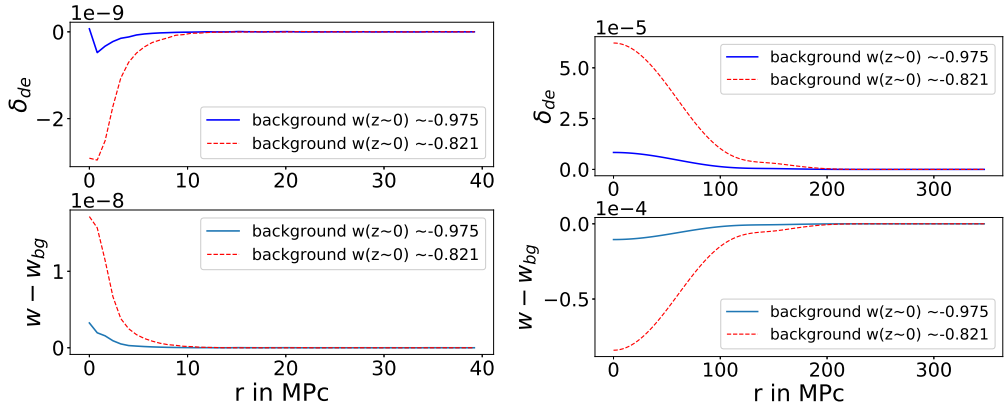

Figure 2.15: In this figure we study the impact of the equation of state parameter w for the background on the growth of dark energy perturbations and the radial variation of the equation of state parameter. Here we show perturbation growth in two different background models for $V \propto \psi^2$. Curves are labeled by present day values of w for the background model. We see that the perturbations have a larger amplitude and w has a larger variation for a larger $1 + w_0$. The left panel here is for an over-density (OD1) and the right panel is for a void (UD5). We see that the effect is strongly pronounced for under density partly because larger scales are involved. The curves for over density are plotted for $z = 1.5$, before virialisation of the innermost shells. Curves for UD5 are plotted at $z = 0$.

as a function of the amplitude of perturbation, i.e., δ_i, and also as a function of the scale of perturbation.

We find that the effect of the scale of perturbation is much more important than the effect of the amplitude of initial perturbation in matter. In Figure 2.14, we see that for two perturbations with the same amplitude, variation of the scale of perturbation has more pronounced effect than variation of amplitude of perturbation for same scale of perturbation.

We note that we have explored the parameter space for models in the vicinity of the cosmological constant by requiring $w \sim -1$ through the evolution. In models that deviate strongly from the cosmological constant, the perturbations in dark energy become more significant. Example in figure 2.15 illustrates this where we compare perturbations in models with different present values of the equation of state parameter $w(z = 0)$. The amplitude of density contrast in dark energy as well as the radial variation in w is much stronger in the model with the larger $1 + w$. We also see that the spatial variation of w for the void is very significant when the present day value for the background deviates strongly from -1.

2.4 Discussion

We have presented results of our analysis of spherical collapse of dark matter and dark energy for a canonical scalar field model. Now we summarize and discuss few implications.

We find that the turn around & virial characteristics and evolution of dark matter density contrast is not significantly affected by dark energy perturbations. This is demonstrated by comparing the evolution in our model with an equivalent model with the same background evolution and no perturbations in dark energy. This result provides justification for ignoring the role of dark energy perturbations while studying collapse of dark matter perturbations. This also implies that there is no significant effect of dark energy perturbations on structure formation. Such effects have been studied earlier in effective models, e.g., [128].

We have shown that the evolution of dark energy perturbations outside the virial radius is insensitive to the scheme used to evolve dark energy perturbations within the virial radius. We have used the approximation of treating the scalar field as a test field inside the virial radius, patching up with the self consistent evolution outside the virial radius. In all plots we have either restricted ourselves to epochs prior to virialisation, or we have plotted functions at scales larger than the virial radius.

We find that the dark energy perturbations remain small, i.e., $|\delta_{DE}| \ll 1$ at all scales and times. This is not to say that there is no effect of non-linear evolution of dark matter perturbations. We show, by comparing with the expected linear growth rate for dark energy perturbations, that the rate of growth of dark energy perturbations is strongly enhanced in the vicinity of non-linear dark matter perturbations. This is encouraging and we plan to study collapse in other dark energy models to explore if dark energy perturbations grow to a significant amplitude in some cases.

This finding encourages us to explore approximations between linear perturbation theory and full non-linear collapse, where we may consider the dark energy to have small perturbations but dark matter may be allowed to have large over densities. It may be possible to relax the restriction of spherical collapse in a suitable approximation scheme.

The most remarkable finding of our work is that the equation of state parameter w becomes a function of space. This has been reported for fluid based models

where the equation of state parameter and the effect speed of sound for dark energy perturbations are not the same [129].

The evolution of w in the models being studied here shows a steady increase from the initial value that is close to -1 for the background. In the vicinity of over dense regions, this value increases at a faster rate as the local Hubble expansion is slowed down and halted. In voids, the local Hubble expansion is faster than the background and the change in w away from $w = -1$ is slowed down. As a result, w takes on larger values around collapsed halos and it takes on smaller values in voids. Thus w becomes a weak function of over density and we get an interesting coupling between the non-relativistic matter and dark energy sectors even though we are working with a model with minimal coupling.

We find that the effects of dark energy clustering and spatial variation of w are strongest for large scale perturbations. Thus the largest over-densities and voids may be appropriate places to look for observational evidence.

We have considered two thawing models here but we expect that the variation of w will have an opposite trend for freezing models, i.e., it will take on values closer to -1 around collapsed halos and values away from this in voids. This expectation follows from the evolution of the field towards the asymptotic value of -1, which is slowed down or hastened by the variations in local Hubble flow.

We may model the relation of equation of state parameter as:

$$w\left(\mathbf{r}, t\right) = \bar{w}(t) + \epsilon f\left(\delta_{DM}, \ldots\right) \tag{2.23}$$

where $\bar{w}$ is the value for the background model, ϵ is a small number, and f is a suitable function of density contrast and possibly other quantities such as the velocity field. Such models can be used to explore the impact of spatial variation in w on weak lensing and other physical quantities of interest. It may also be possible to test for such variations by stacking over many objects/voids. We are studying potential avenues for testing the variation of w in space. We study spherical collapse for other models of dark energy in next chapters.

For any given form of the Lagrangian, we can tune the potential to produce a suitable expansion history in the form of an $a(t)$, where a is the scale factor. However, if we fix $a(t)$ then we have precisely one model for each form of Lagrangian. A comparison of perturbations in models with the same expansion history will allow us to explore the information that we may extract from observational probes

of perturbations in dark energy.

We will continue along these lines in next chapters. Looking into methods of reconstruction in next chapter, followed by simulations and comparisons of perturbations in tachyonic dark energy models.

Chapter 3

Reconstruction of Dynamical Dark Energy Potentials: Quintessence, Tachyon and interacting models.

This chapter is based on following published article

Manvendra Pratap Rajvanshi, J. S. Bagla, Reconstruction of dynamical dark energy potentials: Quintessence, tachyon and interacting models J Astrophys Astron (2019) 40: 44.[arXiv:1905.01103]

3.1 Introduction

As we have seen from previous chapters, in many dark energy models, dark energy is dynamical in the sense that its properties are a function of space and time. In order to study the theoretical and observational implications for these theories, we have to solve the equations describing the dark energy. Analysis of some observations only requires the variation of scale factor with time, however other observations can have a dependence on spatial variations in dark energy and thus details of the model become relevant.

It is well known that if two models have the same evolution of the scale factor, tests relying only on distance measurements cannot distinguish between such models. Therefore it is important to study growth of perturbations in matter for

different models of dark energy with the same evolution of the scale factor. This opens up comparison based on CMB anisotropies ([130, 131, 132]), weak lensing ([133, 134, 135]), and growth of perturbations ([136, 137]). In this context, it is useful to have a formalism for constructing potentials for different models of dark energy that lead to the same expansion history. In this chapter, we compute the corresponding potentials in quintessence and tachyon models which can give same background evolution. We reconstruct potential $V(\phi)$ assuming a particular equation of state $w(z)$. We give analytical expressions wherever possible, in other cases we reduce the problem to quadrature for numerical reconstruction of $V(\phi)$.

There has been a lot of interest in recovering dark energy potential from the observed expansion history ([138, 139, 140]). For example Huterer and Turner ([141]), provide an early work on constructing potential from simulated data and inspired further research. Li et.al ([142]) construct potential by approximating luminosity distances and also do a comparison for reconstruction using parameterization of equation of state $w(z)$. A number of other attempts for reconstruction using a parametric or a non-parametric approach have been made. See ([143, 144, 145]) for a review. We approach this problem by attempting to construct potential for a given redshift dependence of the equation of state parameter $w(z)$ for the dark energy component. We do this for both quintessence and tachyon models: while a number of solutions exist for quintessence models ([146, 147]), few solutions are available for tachyon models. In Scherrer ([146]), a mapping between CPL parameters and potentials is explored while an analytic approximation for various scalar field models is obtained by Battye & Pace ([147]).

In §3.2, we set up equations for tachyon and quintessence models. In §3.2.2 and §3.2.3, we do reconstruction of potential for $w(z) = constant$. In §3.3, we outline the numerical recipe for reconstruction for any general $w(z)$ and illustrate it with results for some simple cases.

3.2 Basic Equations

We are interested in late time evolution of the Universe. Given observations that indicate that the spatial curvature is consistent with zero, and that radiation does not contribute to the expansion history at $z \leq 100$, we choose to work with only matter and dark energy. The method we outline can be generalized without any modifications to include other cases. For illustration of the method, we work with the CPL parameterization (Chevallier & Polarski [148]; Linder 2002[149]). The

functional form for $w(z)$ is defined in terms of two constants, which we call p and q:

$$w = p + q(a - a_i) \tag{3.1}$$

p is the value of w at some $t = t_i$ while q gives rate of change of w with scale factor. Symbols w_0 (for p) and w_1 (for q) are often used while using this parameterization, if t_i is taken to be the present time t_0. Continuity equation for dark energy density ρ_{de} is:

$$\frac{d\rho_{de}}{dt} = -3(1 + p + q(a - a_i))\frac{\dot{a}}{a}\rho_{de} \tag{3.2}$$

Using this equation, we get:

$$\rho_{de} = \rho^i_{de}\left(\frac{a_i}{a}\right)^{3(1+p-qa_i)} \exp[-3q(a - a_i)] \tag{3.3}$$

where ρ^i_{de} is density at some initial time. From now on we use a scaled dimensionless variable for time: $t = tH_i$. Friedmann equation then takes the form:

$$\frac{\dot{a}^2}{a^2} = \frac{\alpha}{a^3} + \frac{\beta}{a^{3(1+p-qa_i)}e^{3qa}} \tag{3.4}$$

where α and β are constants defined as:

$$\alpha = \Omega_{m\,i} \quad \beta = (1 - \Omega_{m\,i})a_i^{3(1+p-qa_i)}e^{3qa_i} \tag{3.5}$$

These are related to the density parameter for matter and dark energy at the initial time.

3.2.1 Tachyon field

Tachyon models for dark energy have an action of the following form:

$$I = \int d^4x\sqrt{-g}\left[-V(\phi)\sqrt{1 - \partial^\mu\phi\partial_\mu\phi}\right] \tag{3.6}$$

In these models the energy density and pressure can be written as:

$$\begin{aligned} \rho_\phi &= \frac{V(\phi)}{\sqrt{1 - \partial^\mu\phi\partial_\mu\phi}} \\ P_\phi &= -V(\phi)\sqrt{1 - \partial^\mu\phi\partial_\mu\phi} \end{aligned}$$

For these models the equation of state parameter is related to the time derivative

of the field as $w = -1 + \dot{\phi}^2$ for a homogeneous field. Thus we have:

$$\frac{d\phi}{dt} = \sqrt{1 + p + q(a - a_i)} \tag{3.7}$$

Combining eq.(3.4) and eq.(3.7)

$$\phi(a) = \int \frac{\sqrt{a(1 + p + q(a - a_i))}}{\sqrt{\alpha + \frac{\beta}{a^{3p - qa_i} e^{3qa}}}} da \tag{3.8}$$

Using the relation between the energy density and the potential, we can write:

$$V(\phi) = \sqrt{-w}\rho_{de} \tag{3.9}$$

Since we know ρ_{de} as a function of a from eq.(3.3), we can compute $V(a)$. The combination of Eqn.3.8 and Eqn.3.9 gives a parametric solution for the potential as a function of the field ϕ, with the scale factor a playing the role of the intermediate parameter.

3.2.2 Tachyon field: Constant w

We start by considering the special case of $w =$ constant, i.e., $q = 0$. The integral in equation (3.8) takes following form for constant w:

$$\phi(a) = \int \frac{\sqrt{a(1 + w)}}{\sqrt{\alpha + \frac{\beta}{a^{3w}}}} da \tag{3.10}$$

Defining:

$$x^2 = \alpha + \frac{\beta}{a^{3w}} \tag{3.11}$$

reduces the integral to form:

$$\phi(x) = \int \frac{\sigma}{(x^2 - \alpha)^k} dx \tag{3.12}$$

where σ and k are:

$$\sigma = -\frac{2\sqrt{1 + w}}{3w\beta} \beta^k, \qquad k = \frac{w + \frac{1}{2}}{w} \tag{3.13}$$

Integral in eq.(3.12) is trivial for $w = -\frac{1}{2}$ where we get:

$$\phi(a) = \sigma\sqrt{\alpha + \beta a^{3/2}} \tag{3.14}$$

Potential $V(a)$ for constant w case is:

$$\frac{V(a)}{H_i^2} = \frac{3\sqrt{-w}\beta}{8\pi G a^{3(1+w)}} \tag{3.15}$$

When $w = -\frac{1}{2}$, we get:

$$\frac{V(\phi)}{H_i^2} = \frac{3\beta}{8\pi G\sqrt{2}\left[\frac{\phi^2}{\beta\sigma^2} - \frac{\alpha}{\beta}\right]} \tag{3.16}$$

For other values of w, integral in equation (3.10) does not have a closed form solution. The result can be expressed in the form of hypergeometric functions:

$$\begin{aligned}\phi(a) =& \frac{2a}{3}\left[\frac{a\,(1+w)\,(\beta a^{-3w}+\alpha)}{\alpha\,(\beta a^{-3w}+\alpha)}\right]^{1/2} \\ & \times\ {}_2F_1\left[\frac{1}{2}, -\frac{1}{2w}; 1-\frac{1}{2w}; -\frac{a^{-3w}\beta}{\alpha}\right]\end{aligned} \tag{3.17}$$

From eq.(3.15), we have $V(a)$, we need to invert eq.(3.17) to get $a(\phi)$ and substitute it in equation (3.15) to get $V(\phi)$. Please note that for background calculations one does not really need $V(\phi)$, $V(a)$ contains the relevant information. However for a study of spatial perturbations we require $V(\phi)$ as ϕ can take on different values at different points at a given time. A number of numerical libraries provide routines for calculation of ${}_2F_1(a,b,c,g)$. GNU Scientific library has function `gsl_sf_hyperg_2F1`, which computes ${}_2F_1(a,b,c,g)$ for $|g| < 1$. In case of eq.(3.17), $g < 0$ and for extending to $g < -1$, there are standard transformations available in literature (see Pearson's thesis (2009) for a detailed account of computation of hypergeometric functions, we use transformations mentioned in section 4.6 of Pearson's thesis ([150]2009)). For $g = -\frac{a^{-3w}\beta}{\alpha} < -1$, we use following formulae for computing ${}_2F_1(a,b,c,g)$:

$$\begin{aligned}{}_2F_1(a,b,c,g) =& \frac{1}{(1-g)^a}\frac{\Gamma(c)\Gamma(b-a)}{\Gamma(b)\Gamma(c-a)} \\ & {}_2F_1(a, c-b, a-b+1, \frac{1}{(1-g)}) \\ & + \frac{1}{(1-g)^b}\frac{\Gamma(c)\Gamma(a-b)}{\Gamma(a)\Gamma(c-b)} \\ & {}_2F_1(b, c-a, b-a+1, \frac{1}{(1-g)})\end{aligned} \tag{3.18}$$

Equation (3.10) can be written in the form of a differential equation which makes its relationship with other functions clear. Let

$$g = -\frac{a^{-3w}\beta}{\alpha} \tag{3.19}$$

Then eq.(3.10) can be differentiated to obtain:

$$g(1-g)\frac{d^2\phi}{dg^2} + \left[\left(\frac{1}{2w}+1\right) - \left(\frac{3}{2}+\frac{1}{2w}\right)g\right]\frac{d\phi}{dg} = 0 \tag{3.20}$$

It can be integrated twice to obtain $\phi(g)$ in terms of incomplete beta functions $B(g;a,b)$, which are related to ${}_2F_1(a,b,c,g)$:

$$\phi(g) = C_1 B(g; 1-u, 1+u+v) + C_2 \tag{3.21}$$

where C_1, C_2 are constants of integration and

$$\begin{aligned} u &= \left(\frac{1}{2w}+1\right) \\ v &= -\left(\frac{3}{2}+\frac{1}{2w}\right) \end{aligned} \tag{3.22}$$

$B(g;a,b)$ is related to ${}_2F_1(a,b,c,g)$ (Weisstein webpage 2018[151]) as follows:

$$B(g;a,b) = \frac{g^a}{a}{}_2F_1(a, 1-b, a+1, g) \tag{3.23}$$

We can invert either eq.(3.17) or eq.(3.23) to obtain $a(\phi)$ and then us eq.(3.15) to obtain $V(\phi)$. We have used the Newton-Raphson method for inversion from $\phi(a)$ to $a(\phi)$ and then on to $V(\phi)$. This is useful in dynamically calculating $V(\phi)$ and the derivative $V_\phi(\phi)$ when ϕ has spatial variations in presence of perturbations.

3.2.2.1 Form of the potential for constant w

Here we plot (figure 3.1) the potential $V(\phi)$ for different values of w. We can see from the plot that the dependence of $V(\phi)$ is close to a power law. To get insight into this behaviour, we plot derivatives of log of potential with respect to log of field in figure 3.2. We see that in central part there is approximate flat curve indicating that in this region the potential can be approximated by power laws.

We can approximate potential in this flat region with form:

$$V(\phi) = c\phi^b \tag{3.24}$$

For this form we have done fitting for different values of constant w and then we find the relationship between constant w and b which is linear as shown in 3.3 . These fittings are crude given that evolution of w and other quantities is very sensitive to form of potential.

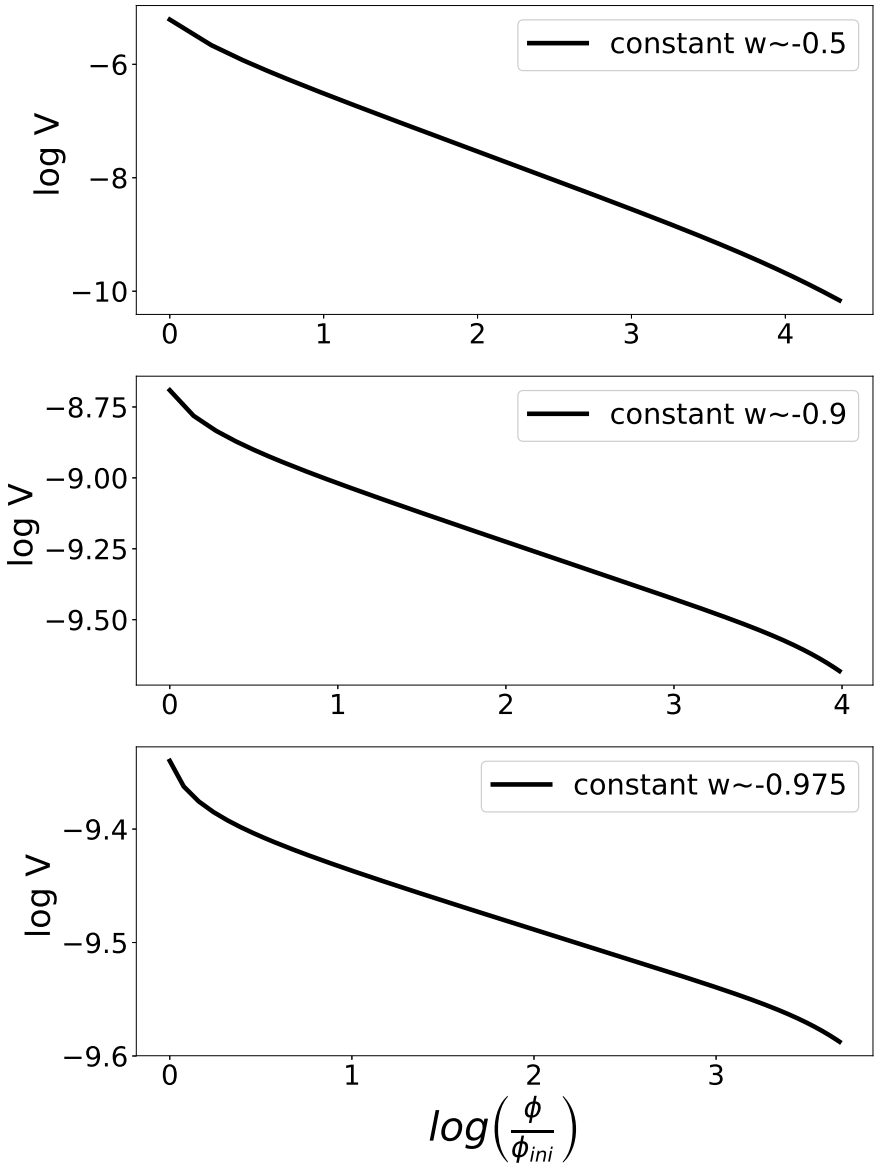

Figure 3.1: We plot tachyon potentials simulated, for constant w, using methods described in previous section. Different panels are for different constant w values.

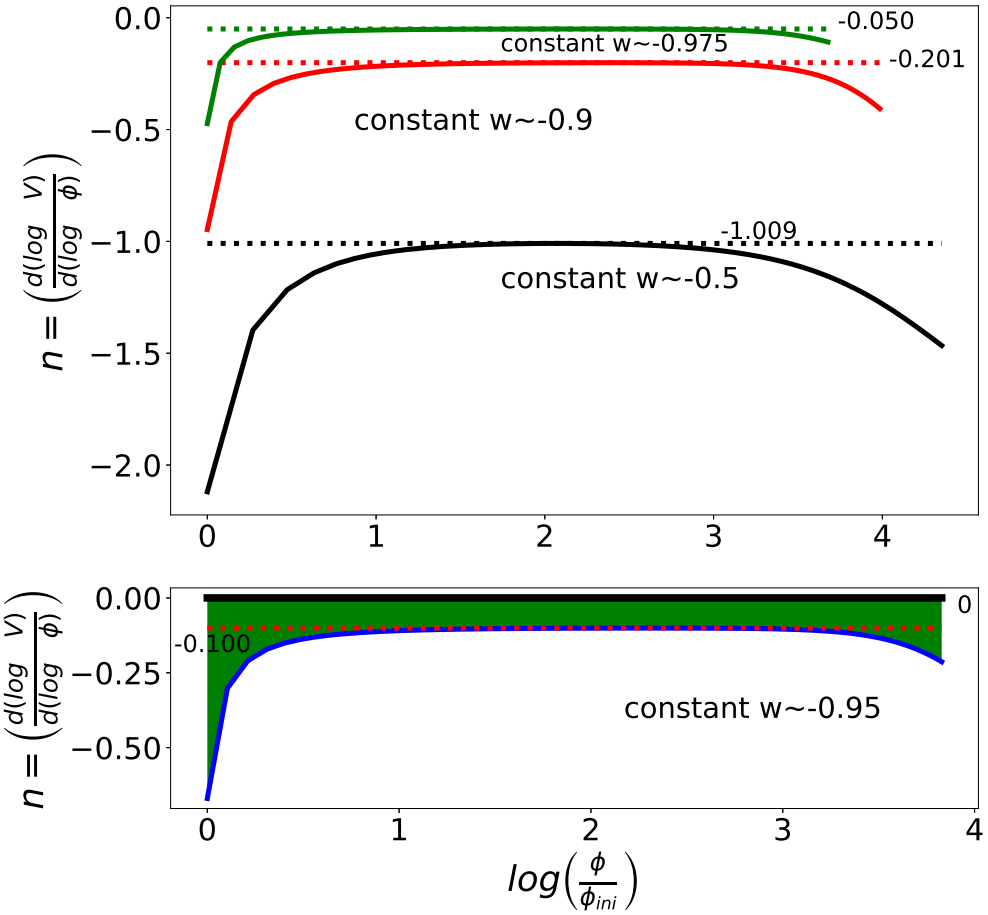

Figure 3.2: We plot the slope of the potential as a function of the field. From this log-log plot we can see that there is a almost flat plateau with deviations at two ends. Thus the potential is close to a power law. In upper panel we plot three cases of constant w. Lower panel is for 3-σ constrained boundaries (-1.0,-0.95) as described in text. The shaded region is allowed set of potentials as per the constraints found in Tripathi *et al.* (2017). The value of constant central part changes with value of constant w.

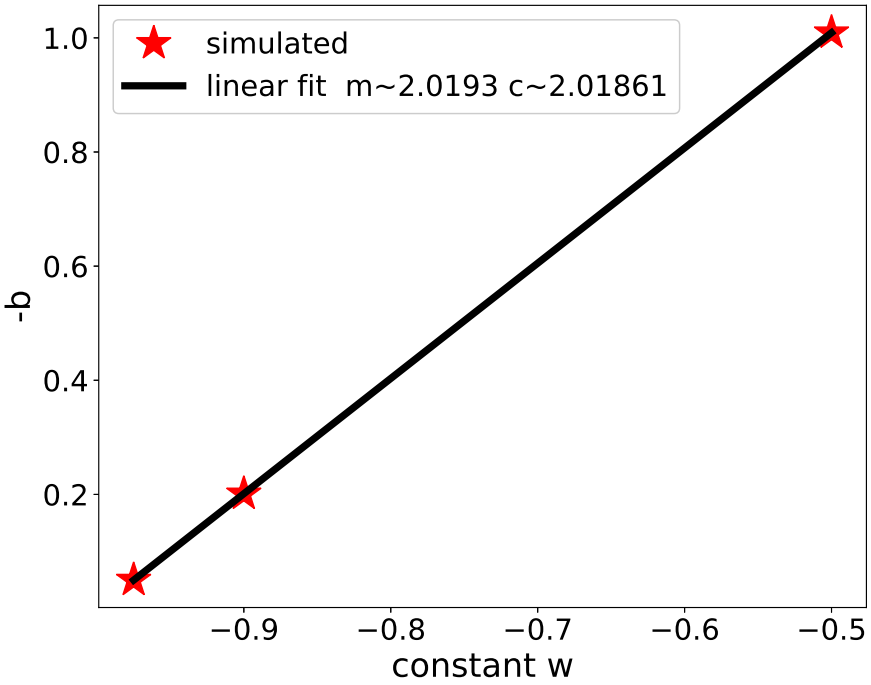

Figure 3.3: For different $w = constant$ values, we obtain the approximate b for central linear part (as marked in figure3.2). As shown here, b values follow a linear relation with w. the fitted line has slope $m = 2.3163$ and intercept $c = 2.30258$.

This can potentially be used to constrain the potential for tachyon fields if one already has observational constraints on w. We are working on a detailed analysis of observational constraints to be presented in a forthcoming publication, here we present an example of such an exercise. We make use of existing studies of observational constrains on $wCDM$ models. In one such study, Tripathi *et al.* (2017) combined the results from 3 different data sets to obtain 3σ confidence intervals for constant w and CPL $w(z)$ models. We use confidence intervals for the constant w while working in the regime $w \geq -1$, i.e., we use the confidence interval $(-1.0, -0.95)$ and reconstruct corresponding potential slope in lower panel of 3.2. This is shown as a shaded region and marks the allowed slope for the potential. This is a simplistic approach and we are working on a detailed analysis while accounting for possible variations of other cosmological parameters.

3.2.3 Quintessence

The action for quintessence field is:

$$I = \int d^4x\sqrt{-g}\left[\frac{1}{2}g^{\mu\nu}\partial_\mu\phi\partial_\nu\phi - V(\phi)\right] \tag{3.25}$$

with effective pressure and density:

$$\rho_\phi = \frac{\dot{\phi}^2}{2} + V(\phi) \tag{3.26}$$

$$P_\phi = \frac{\dot{\phi}^2}{2} - V(\phi) \tag{3.27}$$

$$w_\phi = \frac{P_\phi}{\rho_\phi} = \frac{\dot{\phi}^2 - 2V}{\dot{\phi}^2 + 2V} \tag{3.28}$$

For Quintessence models of dark energy, w is related to time derivative of the field and the potential, and we have:

$$\frac{d\phi}{dt} = \sqrt{(1+w)\rho_\phi} = \sqrt{(1+p+q(a-a_i))\rho_\phi} \tag{3.29}$$

where

$$V(\phi) = \frac{1}{2}(1-w)\rho_\phi = \frac{1}{2}(1-p-q(a-a_i))\rho_\phi \tag{3.30}$$

From equations (3.3) and (3.29), we obtain:

$$\frac{d\phi}{dt} = \sqrt{(1+p+q(a-a_i))\frac{3}{8\pi G}\frac{\beta}{a^{3(1+p-qa_i)}}e^{-3q(a-a_i)}} \tag{3.31}$$

Equation (3.31) can be combined with eq.(3.4) to obtain $\frac{d\phi}{da}$. For potential we have from (3.30) and (3.3):

$$\frac{V}{H_i^2} = \frac{3}{2}\frac{(1-w)}{8\pi G}\frac{\beta}{a^{3(1+p-qa_i)}}e^{-3q(a-a_i)} \tag{3.32}$$

This system of equations specifies the solution.

3.2.4 Quintessence field: Constant w

For $w(a) = constant$, we obtain a closed formula for $V(\phi)$ (see Sangwan *et al.* (2018) and references within for previous work on this). In this case, eq.(3.31) reduces to:

$$\frac{d\phi}{dt} = \sqrt{(1+w)\frac{3}{8\pi G}\frac{\beta}{a^{3(1+w)}}} \tag{3.33}$$

and

$$\frac{d\phi}{da} = \sqrt{\frac{3(1+w)}{8\pi G}}\sqrt{\left[\frac{1}{\frac{\alpha a^{3w}}{\beta}+1}\right]}\left(\frac{1}{a}\right) \tag{3.34}$$

Defining:

$$\lambda = \sqrt{\frac{3(1+w)}{8\pi G}} \tag{3.35}$$

and

$$x^2 = \frac{\alpha a^{3w}}{\beta} + 1 \tag{3.36}$$

We have,

$$\phi(x) = C_1 + \frac{2\lambda}{3w}\int \frac{dx}{x^2-1} \tag{3.37}$$

here C_1 is a constant of integration. The solution is :

$$\phi(x) = -\frac{\lambda}{3w}[\log(1+x) - \log(x-1)] \tag{3.38}$$

Inverting this we get:

$$x = \frac{e^{-3w\phi/\lambda}+1}{e^{-3w\phi/\lambda}-1} \tag{3.39}$$

Defining:

$$m = -\frac{3w\phi}{2\lambda} \tag{3.40}$$

We rewrite eq.(3.39):

$$x = \coth m \tag{3.41}$$

And we get

$$a^{3w} = \frac{\beta}{\alpha}\left[(\coth m)^2 - 1\right] \tag{3.42}$$

Substituting this in eq.(3.32),

$$\frac{V(\phi)}{H_i^2} = \frac{3(1-w)\beta}{16\pi G}\left[\frac{\beta}{\alpha}((\coth m)^2-1)\right]^{-\frac{(1+w)}{w}} \tag{3.43}$$

Equivalently,

$$\frac{V(\phi)}{H_i^2} = \frac{3(1-w)\beta}{16\pi G}\left[\frac{\alpha}{\beta}\sinh^2\left(-\frac{3w\phi\sqrt{8\pi G}}{2\sqrt{3(1+w)}}\right)\right]^{\frac{(1+w)}{w}} \tag{3.44}$$

Derivations for constants w case for quintessence and phantom models were done by Sangwan *et al.* (2018[152]) and they obtain the same form for quintessence models as in eq.(3.44). The reconstruction approach can be used to constrain potentials from observations, as was done in Sangwan *et al.* (2018[152]). They used the constrained ranges from Tripathi *et al.* (2017[153]), to constrain the quintessence potentials for constant w. They also constrain the potentials for CPL and logarithmic $w(z)$ using some approximations. Their work can be numerically generalized, using formalism developed in this article, to various $w(z)$ for both

tachyonic as well as quintessence models.

3.3 General case

For an arbitrary function $w(a)$, continuity equation for that component is:

$$\frac{d\rho_\phi}{\rho} = -\frac{3(1+w)}{a}da \tag{3.45}$$

giving

$$\rho_\phi = \rho_{\phi_i} \exp\left[-3\int \frac{1+w}{a}da\right] \tag{3.46}$$

Equivalently

$$\Omega_\phi := \frac{8\pi G\rho_\phi}{3H_i^2} = \Omega_{\phi_i} e^{-3\int \frac{1+w}{a}da} \tag{3.47}$$

Subscript i represent values at some initial time.

Using this evolution equation for energy density we can write differential equations for tachyon and quintessence fields:

$$\frac{d\phi_{tach}}{da} = \frac{\sqrt{1+w}}{\sqrt{\frac{\alpha}{a} + a^2\Omega_{\phi tach}}} \tag{3.48}$$

$$\frac{d\phi_q}{da} = \frac{\sqrt{3(1+w)\Omega_{\phi q}}}{\sqrt{8\pi G}\sqrt{\frac{\alpha}{a} + a^2\Omega_{\phi q}}} \tag{3.49}$$

where $\Omega_{\phi q}$ and $\Omega_{\phi tach}$ are quintessence and tachyon field density parameters scaled as shown in eq.(3.47) respectively. The potentials for two fields are:

$$\frac{V(a)}{H_i^2} = \frac{3(1-w)\Omega_{\phi q}}{16\pi G} \tag{3.50}$$

$$\frac{V(a)}{H_i^2} = \frac{3\sqrt{-w}\Omega_{\phi tach}}{8\pi G} \tag{3.51}$$

One can numerically integrate equations (3.47) and (3.48)/(3.49) to get $\phi(a)$ and alongside use (3.50)/(3.51) to obtain $V(a)$. Hence one can obtain a numerical table of $V(\phi)$ vs ϕ in desired range. This table can be used for numerical fitting or interpolation functions. For example, cubic splines (see book by Antia (2012[154])) can be used for fitting to obtain spline coefficients which can be used for calculating $V(\phi)$ and its gradients given a value of ϕ. Once we have spline coefficients and ϕ, task is to find the interval in which the value of ϕ lies so that we can use coefficients

corresponding to that interval. Evaluation of the function can be time consuming, but the fact, that for background values ϕ there is a correspondence between ϕ and a, comes to our rescue. Typically perturbations have a small amplitude and hence deviation from background in a particular simulation domain is small, and this can be used to guess spline interval in that region. For example, one might be simulating a spherical collapse in real space and perturbations may be really strong towards centre but they merge into background as one moves away from centre. In this case for large radii, interval can be guessed from background and then one can move toward smaller radii. In this way for each new inner point one has to only search in the adjacent intervals for interpolation if the field is continuous. As an example we show here CPL potentials for quintessence and tachyon field in 3.4. The form obtained is similar to that obtained by Scherrer (2015).

3.4 Coupled Quintessence mimicking ΛCDM

Minimally coupled quintessence models ([155, 156]) can exactly mimic ΛCDM only with a completely flat potential, that is no field dynamics is involved and equations just reduce to that in case of Λ. However if energy exchange is allowed between quintessence field and dark matter, a Λ like evolution is possible even with field dynamics and a time varying w. In this section we consider a quintessence model with following type of coupling (Barros *et al.* 2018[157]):

$$ {}^{\phi}T^{\mu}_{\nu}{}_{,\mu} = Q\sqrt{8\pi G}\phi_{,\nu}\,\rho_{cdm} \tag{3.52} $$

$$ {}^{c}T^{\mu}_{\nu}{}_{,\mu} = -Q\sqrt{8\pi G}\phi_{,\nu}\,\rho_{cdm} \tag{3.53} $$

Please note a bit different notation in this section as described below. Q is the coupling constant between matter and Quintessence. Subscript *lcdm* denotes quantity corresponding to ΛCDM and *cdm* subscript is for corresponding quantities for cold dark matter in model with field, e.g. ρ_{cdm} is density for cold dark matter in model with an interacting dark energy field while ρ_{lcdm} is cold dark matter density as evolved within ΛCDM. Also Ω_c^i is density parameter for dark matter at initial time and Ω_Λ^i is Λ counterpart. Basic equations for this type of coupled model mimicking ΛCDM were derived in Barros *et al.* (2018[157]). They write the potential $V(\phi)$ in terms of other variables, and do not specify exact formula for $V(\phi)$. Here we start from the equations derived in Barros *et al.* (2018[157]) and then reconstruct the formula for potential that gives the required Λ like behaviour.

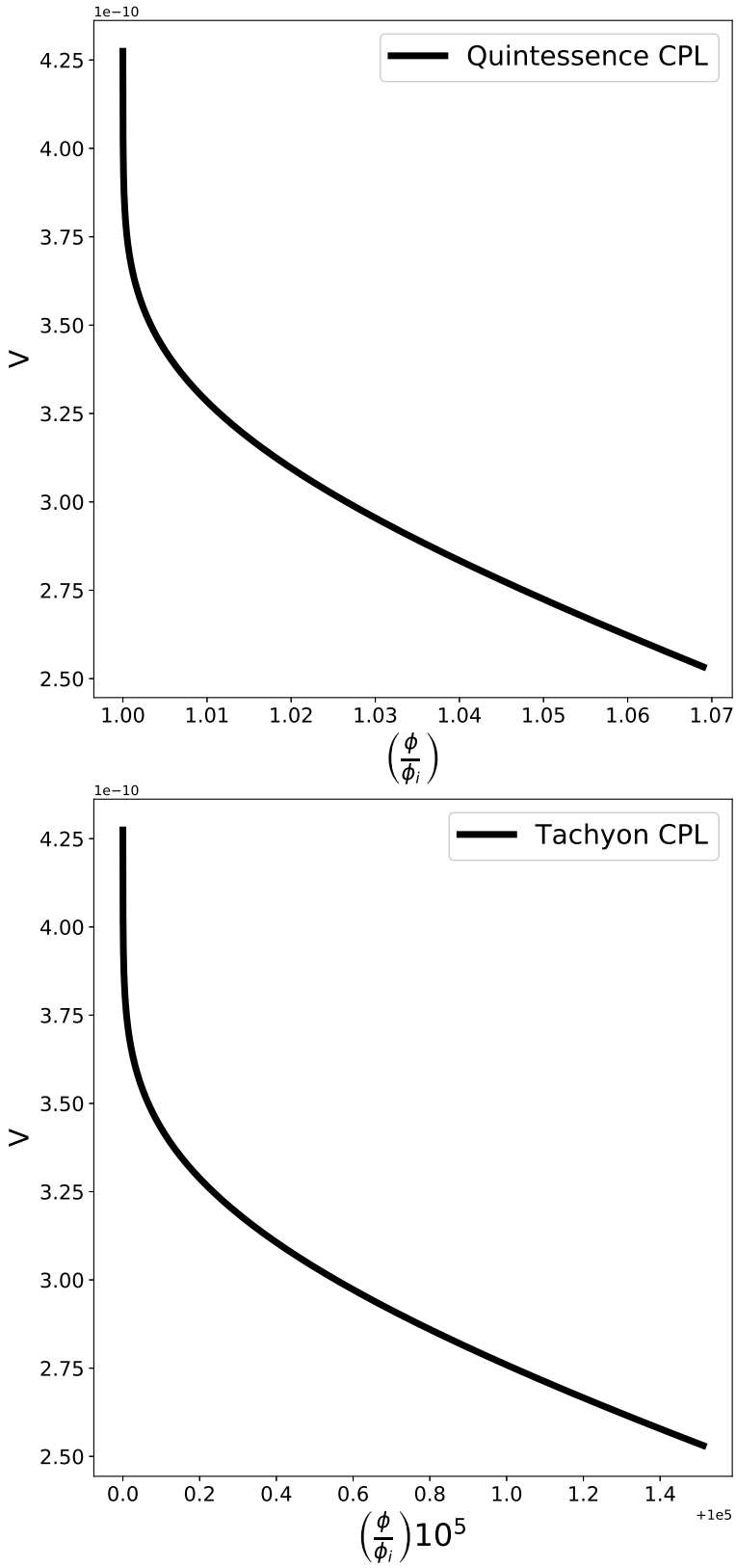

Figure 3.4: $V(\phi)$ simulated for CPL parameterization for quintessence and tachyon models. The shape of curve is same for quintessence and tachyon field but the rate of evolution of field very different. Field traverses longer distances in field space for quintessence case. This might have interesting implications in context of Swampland criteria of String theory.

For a field model giving same $a(t)$ as that of ΛCDM, we have:

$$\left(\frac{\dot{a}}{a}\right) = \left(\frac{\dot{a}}{a}\right)_{\Lambda CDM} \tag{3.54}$$

Ignoring baryons and radiation we have:

$$\rho_{cdm} + \rho_{\phi} = \rho_{lcdm} + \rho_{\Lambda} \tag{3.55}$$

and

$$p_{\phi} = p_{\Lambda} = -\rho_{\Lambda} \tag{3.56}$$

Combining the two, we have:

$$\dot{\phi}^2 = \rho_{lcdm} - \rho_{cdm} \tag{3.57}$$

Continuity equation for matter is:

$$\dot{\rho_{cdm}} + 3H\rho_{cdm} = -Q\sqrt{8\pi G}\dot{\phi}\rho_{cdm} \tag{3.58}$$

giving:

$$\rho_{cdm} = \rho^i_{cdm}\frac{a_i^3}{a^3}e^{-Q\sqrt{8\pi G}\phi} \tag{3.59}$$

Using (3.57) and (3.59) along with standard Friedmann equation for ΛCDM, we get:

$$\frac{d\phi}{da} = \sqrt{\left(\frac{3}{8\pi G}\right)}\left(\frac{1}{a}\right)\frac{\sqrt{1 - e^{-Q\sqrt{8\pi G}\phi}}}{\sqrt{1 + \frac{\Omega^i_{\Lambda}a^3}{\Omega^i_c a_i^3}}} \tag{3.60}$$

Arranging and integrating equation we obtain:

$$\begin{aligned} \omega \quad & \log\left[\sqrt{e^{Q\sqrt{8\pi G}\phi} - 1} + e^{Q\sqrt{8\pi G}\phi/2}\right] = \\ & \log\left[\frac{\sqrt{1 + \frac{\Omega^i_{\Lambda}a^3}{\Omega^i_c a_i^3}} - 1}{\sqrt{1 + \frac{\Omega^i_{\Lambda}a^3}{\Omega^i_c a_i^3}} + 1}\right] \end{aligned} \tag{3.61}$$

where $\omega = \pm\frac{2\sqrt{3}}{Q}$ (- for negative Q)
Writing $a(\phi)$ as a function of ϕ:

$$a^3(\phi) = \frac{4C_1\Omega^i_c a_i^3}{\Omega^i_{\Lambda}}\left[\frac{f(\phi)^{\omega}}{(1 - C_1 f(\phi)^{\omega})^2}\right] \tag{3.62}$$

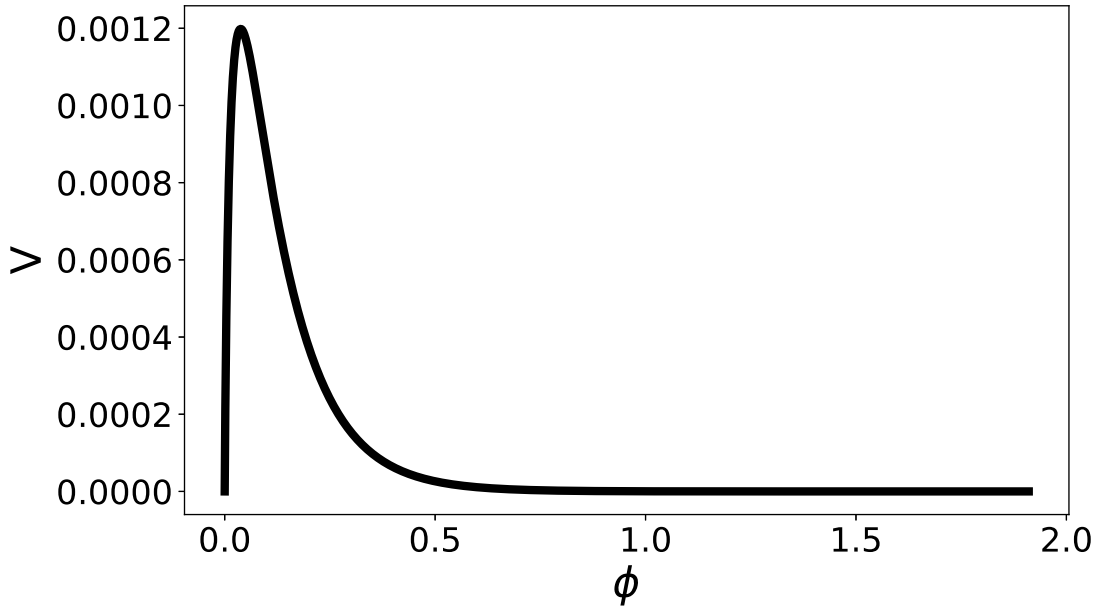

Figure 3.5: $V(\phi)$ for coupled quintessence mimicking ΛCDM in background kinematics.

with C_1 taking care of any constant of integration and

$$f(\phi) = \sqrt{e^{Q\sqrt{8\pi G}\phi} - 1} + e^{Q\sqrt{8\pi G}\phi/2} \tag{3.63}$$

Potential V can be obtained from equations (3.56), (3.57) and (3.59):

$$\frac{V(\phi)}{H_i^2} = \frac{3\Omega_c^i}{8\pi G}\left[\frac{a_i^3}{2(a^3(\phi))}(1 - e^{-Q\sqrt{8\pi G}\phi}) + \frac{\Omega_\Lambda^i}{\Omega_c^i}\right] \tag{3.64}$$

Where $a^3(\phi)$ has a functional form as mentioned in (3.62). Form of potential is illustrated in 3.5.

$$\begin{aligned} V_{,\phi} = & \frac{3\Omega_c^i}{8\pi G} \\ & \left[\frac{Q\sqrt{8\pi G}e^{-Q\sqrt{8\pi G}\phi}a_i^3}{2a^3} - \frac{a_i^3}{2a^6}\frac{d(a^3)}{df}\frac{df}{d\phi}(1 - e^{-Q\sqrt{8\pi G}\phi})\right] \end{aligned} \tag{3.65}$$

Studies of perturbations in the coupled quintessence models can play an important role in distinguishing these from ΛCDM models. Our analysis of such models will be reported elsewhere.

3.5 Summary

In this chapter, we have described basic equations for reconstructing potentials for quintessence and tachyon field. We have given results for $w = constant$ case. We show that analytical closed formulas are possible for quintessence potentials in these cases while for tachyon fields such formulae are obtained only for $w = -0.5$ case. For other values of constant w, we provide formulae for numerical reconstruction. We also find a rough approximation to these constant w potentials for tachyon dark energy. We describe numerical methods for numerical construction of tachyon and quintessence potentials for arbitrary $w(a)$. From numerical calculation of potentials for CPL cases for quintessence and tachyon we show that the shape of potential is same for both of these, but the field rolls much more in quintessence case than in tachyon case. This could motivate further investigations in context of String Swampland (Heisenberg *et al.* 2018[158]; Agrawal *et al.* 2018[159]; Akrami *et al.* 2018[160]). We have also studied coupled quintessence models.

The results of this study can be used for analysis of perturbations in such models. In particular we can compare growth of perturbations in models of different types that have the same expansion history. We use formalism developed in this chapter to perform simulations of quintessence and tachyonic perturbations with similar background. These are presented in next chapter.

Chapter 4

Non-linear spherical collapse in tachyon models and a comparison of collapse in tachyon and quintessence models of dark energy.

This chapter is based on following published article

Manvendra Pratap Rajvanshi, J. S. Bagla, Non-linear spherical collapse in tachyon models and a comparison of collapse in tachyon and quintessence models of dark energy. Classical and Quantum Gravity, Volume 37, Number 23 doi:10.1088/1361-6382/abbb63 [arXiv:2003.07647]

4.1 Introduction

In most of the models, well constrained by data, the dynamics of the Universe approximates the cosmological constant in order to reproduce accelerated expansion. Present observations allow for small deviations from the cosmological constant model. Thus, there are qualitative and quantitative differences in the dynamics, though each model can be tuned to produce the expansion history required by observations within some reasonable constraints.

A fundamental difference between the cosmological constant and other models is that the cosmological constant does not vary with time or location, whereas other dark energy models allow for such variations. In all other models the dark energy component is allowed to vary and respond to variations in the gravitational field. A number of studies have been carried out to study dynamics and perturbations in various dark energy models [43, 44, 63, 64, 127, 161, 162, 163, 164]. The key result of these studies, obtained using linear perturbation theory or other approximations, is that the perturbations in dark energy remain very small. However, perturbation theory is valid only at early times or at very large scales at late times. Thus it cannot be used to study dark energy perturbations and their interplay with highly non-linear dark matter perturbations at small scales.

In previous chapters, we have studied fully non-linear evolution of spherically symmetric perturbations in quintessence models of dark energy [136, 137]. We found that the amplitude of dark energy perturbations remains small in all cases. We also found that the effective equation of state parameter of dark energy becomes a function of coordinates and this variation is correlated with the density contrast of dark matter.

Here we use the same methodology and study tachyon models for dark energy. There are low energy effective theories that arise from string theory that contain tachyon fields [165] with Lagrangian:

$$\mathcal{L} = -V(\psi)\sqrt{(1 - \partial^{\mu}\psi\partial_{\mu}\psi)} \tag{4.1}$$

Here ψ is tachyon field and $V(\psi)$ is potential. As an analogy, if one sees quintessence a field form of classical particle Lagrangian (kinetic term+ potential part), then tachyon Lagrangian is field form of Lagrangian for relativistic particle. Tachyon models and their characteristics have been studied in detail[43, 44]. As shown in [44], some potentials (particularly exponential potential $V \propto e^{-\psi}$) have interesting asymptotic future behavior with the possibility to avoid future horizon. There have also been some attempts to unify dark matter and dark energy in terms of a single tachyon field [62]. Here, inverse square potential ($V \propto \psi^{-2}$) as a function of field ψ averaged over some scale gives a dark matter like behaviour at certain scales. While quintessence models have been extensively studied in context of various types of perturbations, tachyonic models have not been studied in as much detail (see [64] for study of linear perturbations in tachyon models). Different theoretical motivations/insights might lead to different class of models, but there has to be framework that can be used to distinguish different type of models. It is

in this context, that we carry on from our previous work[136] where we simulated spherical collapse for quintessence, modify the formalism for tachyonic field and do a systematic comparison. We study two potentials ($V \propto \psi^{-2}$ and $V \propto e^{-\psi}$) that have been proposed and studied for tachyon models because of their interesting features as discussed above (see [43, 44]). Further, in order to explore the dependence of the growth of perturbations on the class of models, we compare the evolution of perturbations in quintessence models and tachyon models *for the same expansion history.*

We describe the formalism and equations in §4.2. Details of the expansion history in models to be studied is discussed in §4.3 for two potentials studied here for tachyon models. Evolution of perturbations for dark matter and dark energy in these cases is described in §4.4. We then proceed to compare quintessence and tachyon models by working with potentials that give us the same expansion history. These are discussed in §4.5. Results are summarised in §4.5.1 and §4.5.2, dealing with dark matter properties and dark energy properties respectively.

4.2 Equations and Formalism

We follow the scheme set out in Rajvanshi and Bagla [136, 137] (and chapter 2 in this thesis) and refer the reader to the paper for more details.

We assume spherical symmetry and treat dark matter as a pressure-less fluid. Tachyon models are described by the following Lagrangian density:

$$\mathcal{L} = -V(\psi)\sqrt{(1 - \partial^{\mu}\psi\partial_{\mu}\psi)} \tag{4.2}$$

Space-time is described by the following metric:

$$ds^2 \; = \; -e^{(2B)}dr^2 - R^2(d\theta^2 + sin^2\theta d\phi^2) + dt^2 \tag{4.3}$$

where $B(r,t)$ and $R(r,t)$ are unknown functions of comoving radial coordinate r and time t.

These allow us to obtain dynamical equations for all the variables in the system.

Note: We work in units where speed of light c and gravitational constant G, both are unity. V denotes potential as a function of ψ and $V_{,\psi}$ represents gradient of this potential with respect to ψ. The full set of equations along with Einstein's

equations is:

$$\ddot{B} = -e^{-2B}\frac{R'^2}{R^2} + \frac{1}{R^2} + \frac{\dot{R}^2}{R^2} - \dot{B}^2 - 4\pi\rho_{dm} + 4\pi V\left[\frac{e^{-2B}\psi'^2 - \dot{\psi}^2}{\sqrt{1-u^2}}\right] \quad (4.4)$$

$$\frac{\ddot{R}}{R} = \frac{4\pi V}{\sqrt{1-u^2}}\left[1-u^2-e^{-2B}\psi'^2\right] - \frac{1}{2}\frac{\dot{R}^2}{R^2} + \frac{1}{2}\left[e^{-2B}\frac{R'^2}{R^2} - \frac{1}{R^2}\right] \quad (4.5)$$

$$\begin{aligned}\ddot{\psi}RV(e^{2B}+\psi'^2) = {} & 2e^{-2B}VR'\psi'^3 - 2V\dot{R}\dot{\psi}\psi'^2 + 2VR'\psi'(1-\dot{\psi}^2) - RV_{,\psi}\psi'^2 \\ & -RVB'\psi'(1-\dot{\psi}^2) + RV\psi''(1-\dot{\psi}^2) - 2RV\dot{\psi}\dot{B}\psi'^2 \\ & +2RV\dot{\psi}\psi'\dot{\psi}' - RV_{,\psi}e^{2B}(1-\dot{\psi}^2) \\ & -V\dot{\psi}(1-\dot{\psi}^2)(R\dot{B}+2\dot{R})e^{2B} \end{aligned} \quad (4.6)$$

$$\dot{\rho_{dm}} = -\left(\dot{B} + \frac{2\dot{R}}{R}\right)\rho_{dm} \quad (4.7)$$

where $u^2 = \partial^\mu\psi\partial_\mu\psi$ and ρ_{dm} represents dark matter density.
Here a prime represents a partial derivative with respect to r and a dot represents a partial derivative with respect to t.

We study evolution of perturbations for two potentials with tachyon models, details of the potentials are given in the following discussion.

In order to compare evolution of perturbations in tachyon models with quintessence models, we work with potentials that lead to the same expansion history. Methods for computing the potential given an expansion history have been developed for a variety of models [148, 149]. This process is often called reconstruction of potentials. We have done these calculations for w = constant and Chevallier-Polarski-Linder (abbreviated as "CPL" from here on, see equation 4.9) parametrization for quintessence and tachyon models, details of the approach are given in [166].

4.2.1 Computational Methods

We consider a 1-d discrete grid in radial variable r, and the dependent variables (fields and their first time derivatives) are simulated on this grid as a function of r which are evolved in time using fourth order Runge-Kutta scheme (RK-4). At each time instant t_i we calculate all spatial derivatives using finite difference schemes, this allows us to write all first order time derivatives (including derivatives of 1st time derivatives i.e. accelerations) of dependent variables as functions of quantities at t_i. These functions allow us to get prediction for 1st sub-step of RK-4 scheme

and temporary values of all dependent variables which are used for calculations of further sub-steps. This process is repeated until the time for the final intended output is reached. We check for numerical stability and convergence by running for different time steps. The computational methodology is described in detail in paper I[136] (see appendix A).

4.3 Results: Background Evolution

We use two potentials for tachyon models that have been studied extensively. We study the background evolution for potentials $V \propto \psi^{-2}$ and $e^{-\psi}$. Figure 4.1 shows the evolution of density parameters for the tachyon field and dark matter, and the equation of state parameter (w). Although each of these potentials has a unique asymptotic behaviour[44], here we have tuned the parameters such that they satisfy observational constraints [63]. Both the models shown here have a thawing behaviour. These plots illustrate the generic behaviour in tachyon models that is consistent with observations. More details for background evolution and comparison with observations can be found in the detailed study by Singh et. al [63].

4.4 Evolution of perturbations

We study perturbations in dark matter and dark energy for two potentials: the exponential potential and the inverse square potential. The initial conditions are set such that the dark matter does not have any peculiar velocities at the initial time. Dark matter has an initial density perturbation. This initial density perturbation has a compensated profile i.e. δ_{dm} integrated from center to outermost radius comes out to be zero, so that average density contrast is 0. Please see [136] for details of initial profile. Dark energy is set to have no perturbations at the initial time. We find that such an initial condition quickly leads to the expected adiabatic mode at early times. We start at $z_{ini} = 10^3$ and evolve the system towards lower redshifts. We first study the evolution of an over-density. A note for figures: In figures we often use scientific notation for quoting numbers i.e. format a x 10^b with exponent part quoted on top of figure, so any no. that is quoted on top left of figure has to be multiplied to y-axis values to get actual values. Exponents are in powers of 10. For example, in figure 4.3, one has to multiply 10^{-9} to y values. Figure 4.2 is a plot of dark matter density contrast at the time

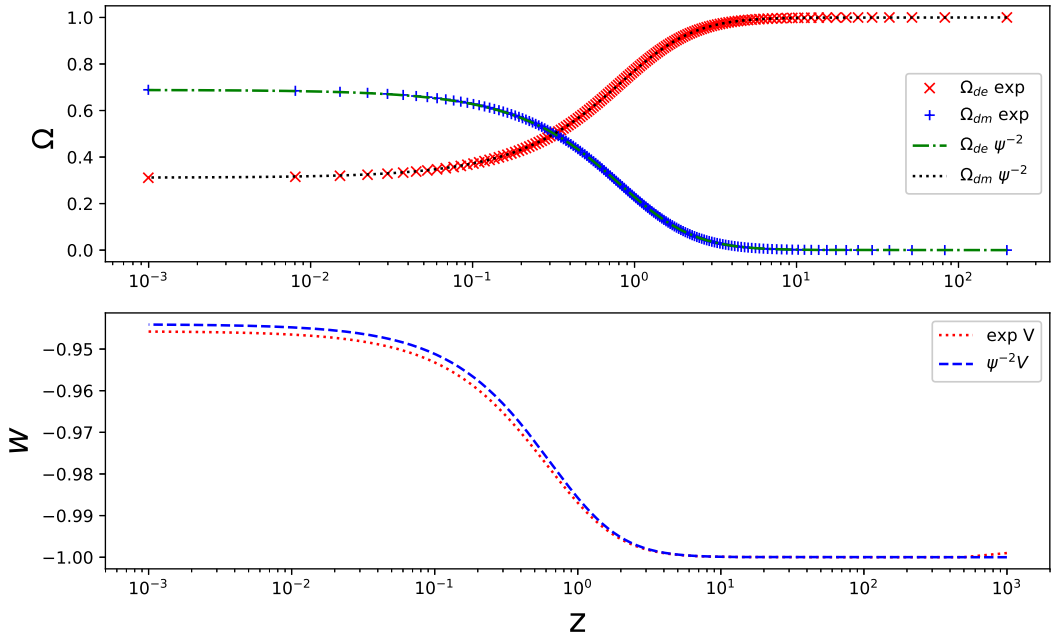

Figure 4.1: Energy densities (Upper Panel) contribution of dark matter and dark energy as a function of redshift (z). Bottom panel show the evolution of equation of state (w) of tachyon field. Both backgrounds are very similar in terms of observations with slight difference in effective equation of state parameter (w).

when the inner regions begin to virialize at $z \simeq 1.5$.

The overdensity has been evolved from $z \sim 1000$. This is for an initially overdense (OD) system. This is shown for the two potentials we are studying and it can be seen that the dark matter density contrast in these two cases is indistinguishable. This similarity results from an almost identical expansion history.

Corresponding plots for density contrast in dark energy are shown in Figure 4.3. This is for initially overdense (OD) system. At the start of simulation ($z \sim 1000$) there was no perturbation in dark energy field, but metric perturbations induce perturbations in dark energy sector which grow with time. We see that the perturbation in dark energy is very small for the two cases, but there are apparent differences in the two curves.

The dark matter perturbation reaches maximum radius, called the turn around radius, before collapsing back and eventually reaching dynamical or virial equilibrium. The ratio of virial to turn around radius is plotted in Figure 4.4. It is apparent from this plot that there is no discernable difference in the values for the two potentials mainly because of a similar expansion history.

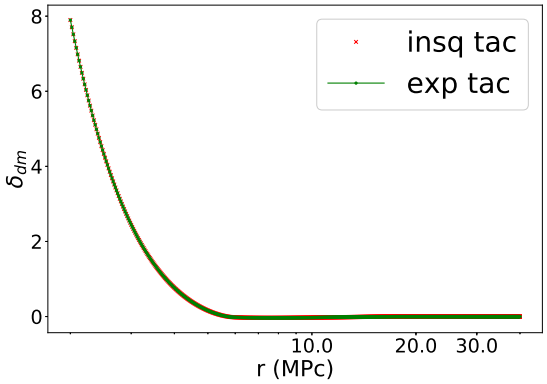

Figure 4.2: Dark matter density contrast as a function of comoving radius at $z \sim 1.5$. The two curves correspond to two different dark energy potentials. Label 'insq' refers to $V \propto \phi^{-2}$ and 'exp' refers to $V \propto$ exp.

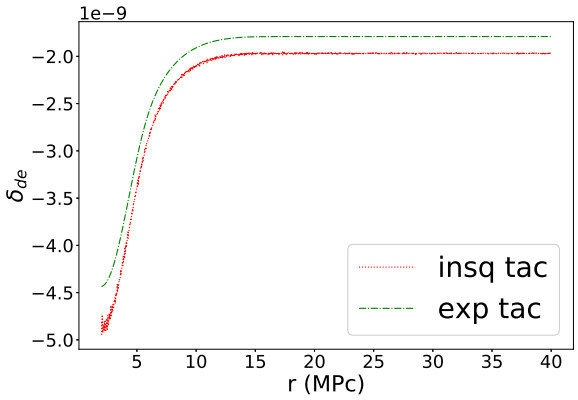

Figure 4.3: Dark energy density contrast as a function of comoving radius at $z \sim 1.5$. Label 'insq' refers to $V \propto \phi^{-2}$ and 'exp' refers to $V \propto$ exp.

We now turn our attention to evolution of an under-dense region. While an under-dense region is limited to $\delta_{dm} \geq -1$, whereas the density contrast for an over-dense region can be very large. On the other hand, a realistic over-dense region with a large density contrast cannot be arbitrarily large in size, whereas underdense regions can easily be tens of Mpc across. In terms of analysis, we also avoid loosing information inside the virialized region as the equations cannot be solved self consistently in this region [136, 137].

The dark energy perturbations are shown in Figure 4.5. The density contrast is significant over the scale of the under-dense region. We also observe a rapid growth of dark energy perturbations at late times, even though the amplitude of perturbations remains small at all times. We see some variation between the two potentials but it remains at a few percent level and this can be attributed to the difference in expansion history.

We note that the qualitative behaviour of perturbations in dark matter and dark energy closely follows that seen for quintessence models studied earlier [136, 137]. In the following discussion we focus on a comparison of quintessence and tachyon models for the same expansion history.

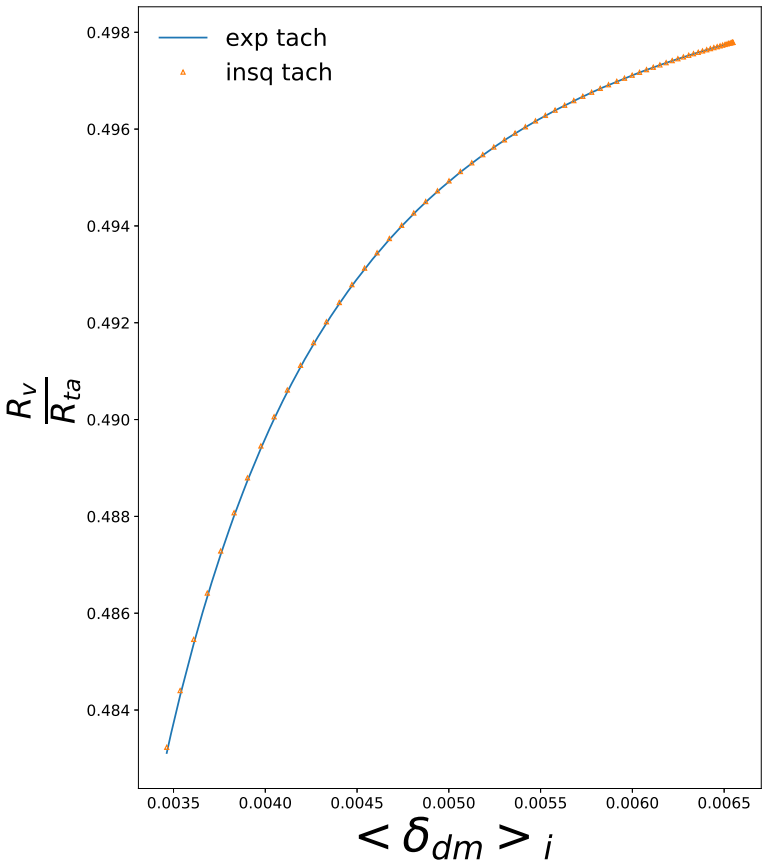

Figure 4.4: Ratio of virial radius to turn around (maximum) radius as a function of initial matter overdensity averaged over interior r till that particular r. The ratio tends toward Einstein-DiSitter value of 0.5 as the initial overdensity tends to infinity i.e. dark energy effects on perturbation become less significant as dark matter perturbation become stronger.

4.5 Results: Evolution of Perturbations in Quintessence vs Tachyon Models

In order to compare perturbations in tachyon vs quintessence models of dark energy, we reconstruct potentials in both models that correspond to the same expansion history. We codify the expansion history by the variation of the equation of state parameter for dark energy with the scale factor $w(a)$. Details of the procedure adopted for computing the potential are given in [166]. We work with two different forms for w for this comparison: $w = constant$ and CPL [148, 149]. We choose three values of constant w for comparison and numerically reconstruct the corresponding potentials for quintessence and tachyonic fields,

$$w = -0.5, \quad w = -0.9 \quad and \quad w = -0.975 \tag{4.8}$$

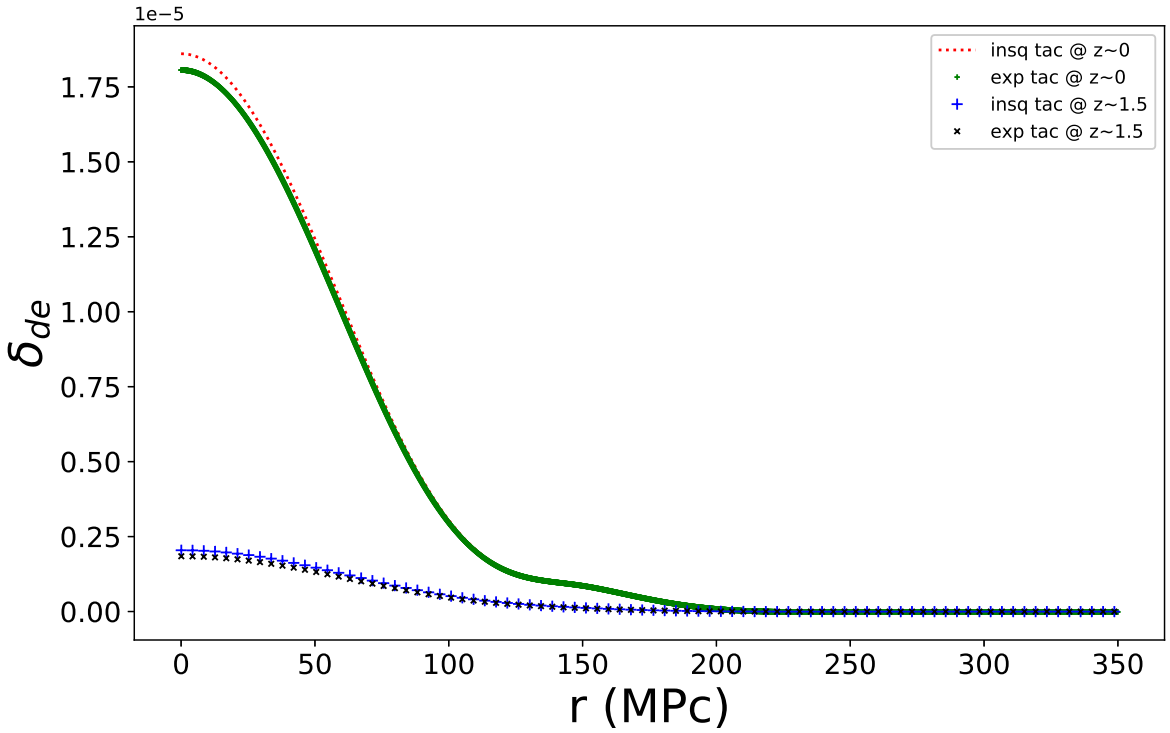

Figure 4.5: Dark energy (DE) density contrast as a function of comoving radius at two different redshifts. Here the initial matter perturbation was underdense. There was no perturbation in DE at initial time, but metric perturbations induce perturbation in DE field. This perturbation grows stronger with time as can be seen from curves at 2 different redshifts.

and for CPL parametrization[148, 149] with form $w(a)$:

$$w = w_0 + w_a(1 - \frac{a}{a_0}) \tag{4.9}$$

we have $w_0 = -0.9$ and $w_a = \pm 0.09$. That is, the present day equation of state parameter is -0.9 in both the cases but in one case it decreases as we go to earlier epochs, and in the other it increases as we go to earlier epochs. In figures we represent cases with $w_a = +0.09$ with notation "cpl+" and $w_a = -0.09$ model with "cpl-". We investigate turn around and virialization characteristics for overdense regions for these cases.

4.5.1 Dark Matter Perturbations

We have run our simulations setting initial conditions in the early universe (at $z \sim 1000$) for underdense and overdense dark matter perturbations. We start with an unperturbed dark energy (see [136, 137] for details of initial conditions). The

density contrast at present time is shown in figure 4.6 for constant w for underdense initial condition. We see that the density contrast for different expansion histories differs from each other but *there is no difference in the profile for quintessence and tachyon models.* This clearly implies that the choice of dark energy model (tachyon or quintessence) has no discernable impact on dark matter density profiles in an underdense region as long as the expansion history is the same. Next we proceed to study the same in the two cases for the CPL parameterization. We refer to models by the sign of the term w_a and w_0 is same in the two cases ($w_0 = -0.9$). The two cases differ as we have $w_a = \pm 0.09$. We show the dark matter density profile for the same initial condition as above in Figure 4.7. Again, we find that there are distinctions between the two cases with a different expansion history but there is no discernable difference in the dark matter density profile for the two different models of dark energy. This is remarkable. Note that bump in contrast around 150 Mpc is because of the compensating overdense region at edge of void to ensure that we go over to an FLRW universe at large r.

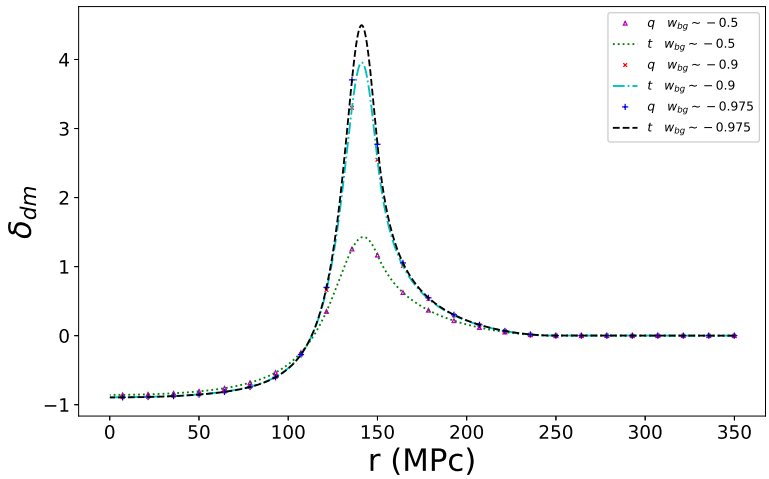

Figure 4.6: Underdense cases constant w comparison: Dark matter density contrast evolved to $z \sim 0$. "q" refers to quintessence models while "t" for tachyonic models. "w_{bg}" is constant value of background w. Curves are clustered by background histories with quintessence and tachyonic models with same background having indistinguishable matter perturbation dynamics.

We now turn our attention to growth of overdensities in dark matter. In these cases the perturbations collapse to form virialized halos if the initial density is higher than a critical value as in the case for ΛCDM [98]. Results for the two CPL parameterizations are shown here. We show the characteristics of perturbations at turn around in Figure 4.8. Variation of the turn around radius as compared to the expected value in the Einstein-deSitter model as a function of the initial overdensity is shown in the left panel. The right panel shows the density contrast

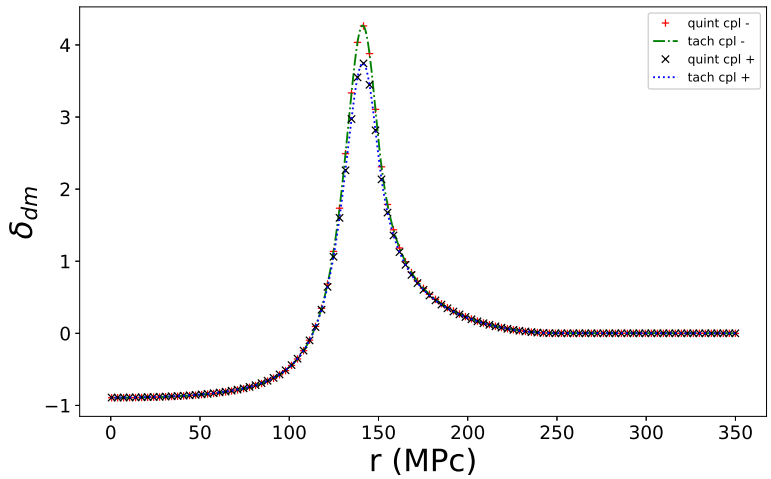

Figure 4.7: Underdense cases CPL:Dark matter density contrast evolved to $z \sim 0$. cpl+ denotes $w_a = +0.09$ case and cpl- represents $w_a = -0.09$. "quint" stands for quintessence and "tach" stands for tachyonic. As with constant w cases, it is background evolution that is distinguishing the models rather than field dynamics Lagrangian being quintessence or tachyonic type.

at turn around as a function of the initial dark matter overdensity. Note that the overdensities are always volume averaged, so as to facilitate comparison with the Einstein-deSitter and the ΛCDM models. The qualitative behaviour seen in the two panels is very similar to what is known for the ΛCDM model in that the turn around radius becomes very large as we approach the critical initial overdensity from above. The density contrast also increases in this limit as the time taken to reach turn around increases and the background also increases and the average density of the universe decreases to give us an enhanced density contrast. The two CPL models representing two different expansion histories lead to different curves. However, there is no obvious difference between the tachyon and quintessence models for a given expansion history.

We present the characteristics of virialization in Figure 4.9. We have plotted the ratio of the virial radius to the turn around radius in the left panel as a function of the initial density contrast. The expected value for this ratio is 0.5 in the Einstein-deSitter model. In case dark energy clusters significantly and also participates in the virialization process, the expected value is above 0.5, and if dark energy clustering is not relevant to the virialization process then the expected value is below 0.5 [96]. In the right panel we have plotted the density contrast at the time of virialization. Here, virialization is defined by the epoch at which

$$< T > + \frac{1}{2} \langle R\, F_R \rangle = 0 \tag{4.10}$$

here T is the kinetic energy, R is the radius of the shell and F_R is the radial force on the shell, see [136] for details. Thus the volume averaged overdensity within a virialized shell is expected to be around 145 in Einstein-deSitter model. In the ΛCDM model, the expected value is higher as perturbations take a longer time to collapse. Further, as we approach the critical density contrast for collapse from above, the density contrast at virialization shoots up. Similar behaviour is observed for quintessence models [136, 137]. We see that the qualitative behaviour for the two CPL cases is similar to that for ΛCDM and that seen for some quintessence models. The ratio of virial radius to the turn around radius varies almost in the same manner for the two CPL models with small differences for large initial density contrast. There are no systematic differences between tachyon and quintessence models for a given CPL prescription for the equation of state parameter. Curves for the two CPL models differ clearly from each other in the right panel but again, there are no differences between tachyon and quintessence models for a given set of CPL parameters.

These results are remarkable in that it appears that we can ignore the precise choice of dark energy model and use any convenient prescription as long as we get the same expansion history. This can be done if our interest is restricted to perturbations in dark matter.

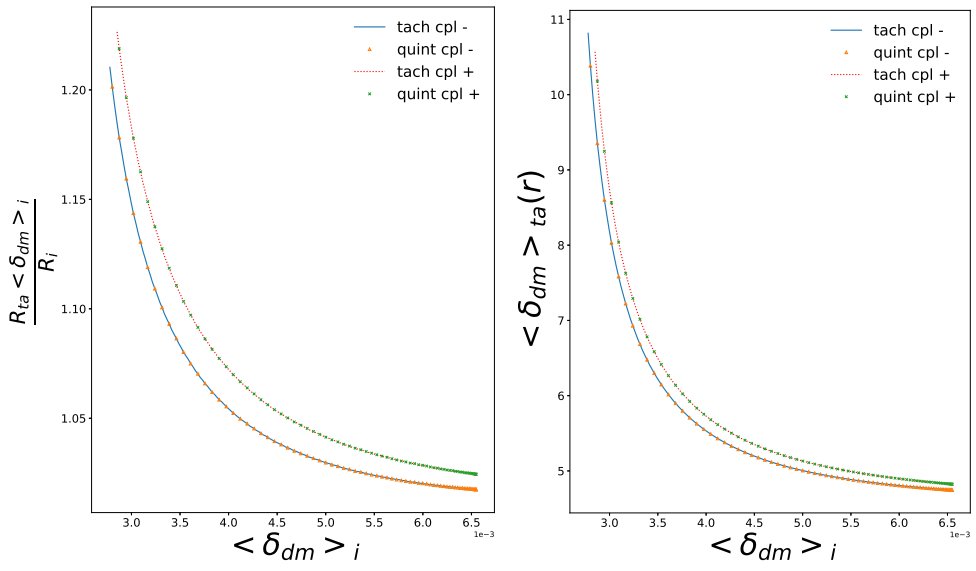

Figure 4.8: Turn around characteristics for CPL case. Left panel shows turn around radius in the combination $R_{ta}\langle\delta_{dm}\rangle_i/R_i$ as a function of the initial density contrast. Right panel shows density contrast at turn around as a function of the initial density contrast. quint denotes quintessence and tach represents tachyonic field. cpl+ denotes $w_a = +0.09$ and cpl- represents $w_a = -0.09$.

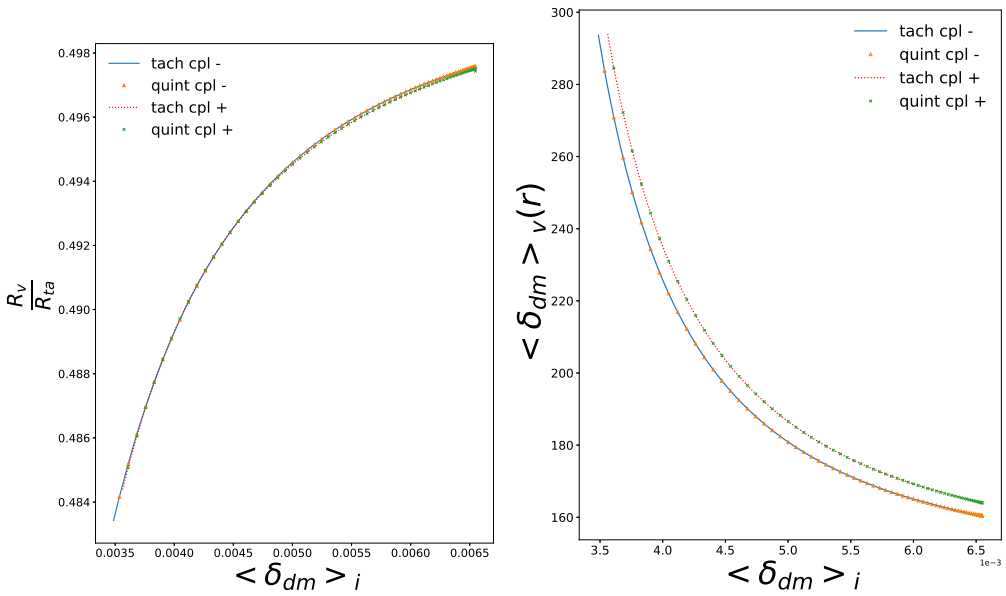

Figure 4.9: Virial characteristics for CPL case. Left panel shows ratio of virial radius to turn around radius as a function of the initial density contrast in dark matter. Right panel shows Density contrast at virialisation as a function of the initial density contrast in dark matter. "quint" denotes quintessence and "tach" represents tachyonic field. cpl+ denotes $w_a = +0.09$ and cpl- represents $w_a = -0.09$.

4.5.2 Perturbations in Dark Energy

We now turn our attention to perturbations in dark energy. We study two physical quantities, density contrast for dark energy δ_{de} and the equation of state parameter w. These are shown as a function of radius for an initially underdense matter perturbation. We have plotted δ_{de} as a function of r for constant w cosmologies in Figure 4.10 (upper panel). Curves are plotted at $z = 0$ and refer to the simulations used in Figure 6. We see that density contrast in dark energy remains small at all scales. The amplitude of dark energy perturbations is higher when the model deviates significantly from ΛCDM: we see that the amplitude is highest for the model with $w = -0.5$ and decreases for models with a smaller w. We see that the curves for each w are distinct. We also note that the tachyon models and quintessence models differ from each other and this difference is larger for models with a larger w. We have shown in earlier work that w becomes a function of space for dynamical dark energy models. Variations from the expected value in the background for constant w models is shown in Figure 4.10 (lower panel) as a function of r.

We see that for an underdensity in matter, w is smaller than the value in the background model. Deviations are larger for models that deviate significantly

from the ΛCDM models. Differences between tachyon models and quintessence models can be seen and these are larger for the models with a larger w.

Plots for CPL models are given in Figure 4.11. Both the models here are consistent with most low redshift observations [153]. We keep $w_0 = -0.9$ and $w_a = \pm 0.09$, we refer to these models as *cpl+* or *cpl−* depending on the sign of w_a. These figures refer to the simulations used for Figure 7. Quantities are plotted at $z = 0$. We see that there are differences between the tachyon and quintessence models for each CPL model but the differences remain small at all scales.

Unlike dark matter, we find that dark energy perturbations do carry an imprint of the model. Differences between tachyon and quintessence models for the same expansion history become larger for models with large deviations from the ΛCDM model. Differences are small for constant w models allowed by observations.

4.6 Summary

We have presented results of our study of evolution of perturbations in dark matter and tachyon models of dark energy. We find that differences across models arising from different potentials are small. As different potentials correspond to different expansion history, it is difficult to delineate the dependencies.

In order to study the dependence of evolution of perturbations on the class of models, we construct potentials in quintessence and tachyon models corresponding to constant equation of state w for dark energy and CPL parameterization. This allows us to address the question of the dependence of evolution of perturbations on the class of models.

We study spherically symmetric perturbations using a self-consistent relativistic code. We study evolution of regions where dark matter is underdense/overdense.

We find that evolution of dark matter perturbations depends only on the expansion history. There is no discernible imprint of the dark energy model on the evolution of dark matter perturbations.

Dark energy perturbations remain small in all cases studied here. The amplitude of dark energy perturbations depends on the expansion history as well as the dark energy model (tachyon/quintessence). *Thus in principle there is an observable signature of the class of dark energy models, though the differences are*

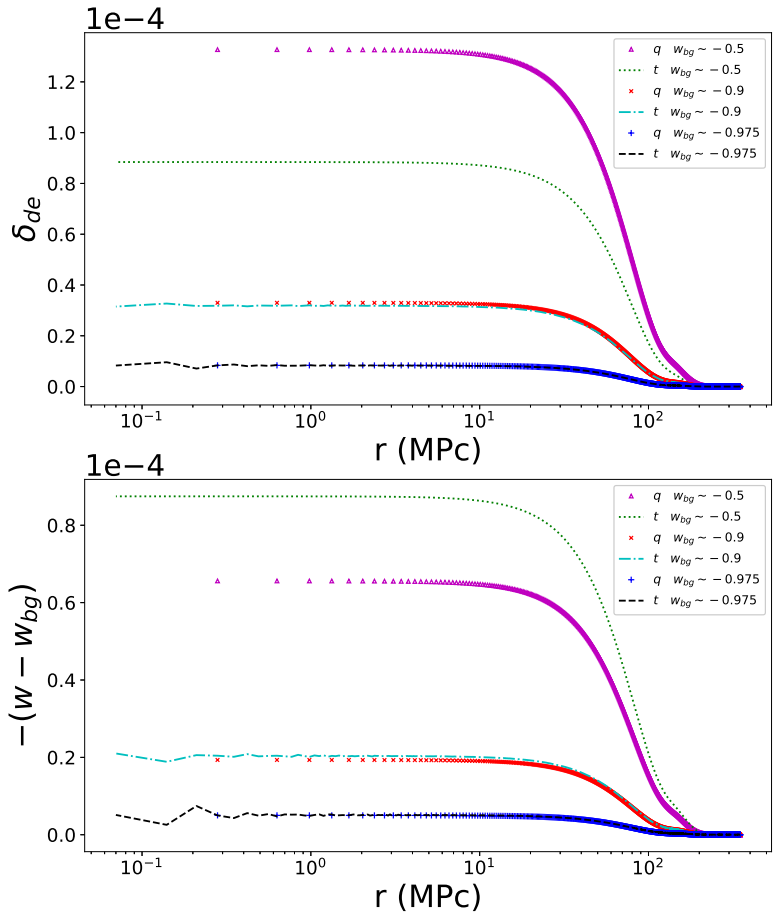

Figure 4.10: Underdense case: (Upper panel) Dark energy density contrast evolved to $z \sim 0$. q denotes quintessence and t represent tachyonic field. w_{bg} for constant value of background equation of state for dark energy field. This is for initially underdense case (UD1). Lower panel: Equation of state comparison for three constant equation of state cases.

very small. These differences are larger for models that deviate significantly from the ΛCDM model in terms of the expansion history.

While the results follow from well defined theoretical models and numerical calculations, it is useful to have some physical insight. One can argue from continuity that as one goes towards the ΛCDM limit of $w = -1$, all models should converge to Λ like behaviour. One crucial point to check here is for the deviations of w from -1, that are allowed by observations, can different models be distinguished by perturbations? In this chapter, we have done nonlinear calculations to probe this question. One of the key takeaways from our work is that the two classes of models considered here are indistinguishable not only for cases very close to Λ

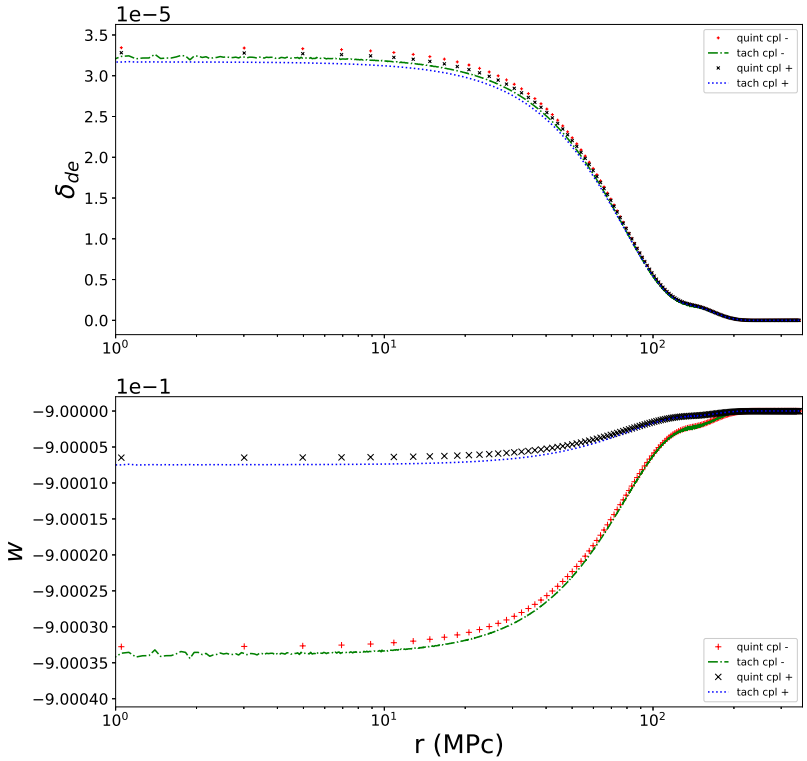

Figure 4.11: Underdense CPL case: (Upper Panel) Dark energy density contrast evolved to $z \sim 0$. q denotes quintessence and t represent tachyonic field. cpl+ denotes $w_a = +0.09$ and cpl- represents $w_a = -0.09$. This for initially underdense case (UD1cpl). Lower Panel: Equation of state (w) evolved to $z \sim 0$. This is for initially underdense case (UD1cpl).

limit, but are so even for scenarios which are significantly different from Λ limit. The above statement applies to characteristics of dark matter perturbations. We believe that this is due to matter being the dominant component for much of the expansion history and matter dominating over dark energy in regions with high overdensity of matter. While this has been pointed out in studies based on linear theory or heuristic arguments, we believe that the calculations presented here establish this for the first time with self consistent and relativistic calculations in the non-linear regime.

The useful conclusion that we can draw from this study is that we may choose any dark energy model to reproduce the appropriate expansion history as the evolution of dark matter perturbations is insensitive to the specifics of the dark energy model other than the expansion history.

At the same time, the very small magnitude of differences of dark energy

perturbations indicate that it will be almost impossible for us to discover the true dark energy model from measurements of distances or characteristics of dark matter perturbations.

Chapter 5

Tachyonic vs Quintessence dark energy: prospects of distinguishing them using linear perturbations and CMB data

This chapter is based on following article

Manvendra Pratap Rajvanshi, Avinash Singh, H.K. Jassal, and J.S. Bagla, Tachyonic vs Quintessence dark energy: linear perturbations and CMB data.

arXiv:2104.00982

5.1 Introduction

Previous chapters looked at the evolution and comparisons of perturbations in scalar field dark energy models in nonlinear, but spherically symmetric spacetimes. Although the nonlinear treatment offered by spherically symmetric case is useful in exploring deviations from linear growth, spherical symmetry is very restrictive assumption. It can be shown that small deviations from spherical sym-

metry lead to quick divergence from symmetry[98]. Linear theory calculations do not assume any symmetry, but are valid for small perturbations only. Dark energy models, in general, have a scale-dependent response to perturbations in the matter. Linear theory of cosmological perturbations [69, 70, 71] is used for studying the evolution of fluctuations in dark energy. These can be used to compute transfer functions, cosmic microwave radiations anisotropies [68], and other observables.

Dark Energy perturbations have been studied in detail for quintessence [127, 130, 164, 167, 168]. Perturbation theory employs a split between background and perturbations over that background. Comparisons of dynamical dark energy models with standard ΛCDM show deviations in expansion history. Dark energy perturbations also induce differences in the power spectrum, CMB anisotropies, and other observables. For models allowing perturbations, the evolution is parameterized by a combination of background evolution (or expansion history) and characteristics of the model. This point needs careful consideration when comparing dark energy models. Their potentials often have tunable parameters that can be adjusted to get the same expansion history so that any observation based on background cosmology (e.g. supernova data) cannot be used to distinguish these. In that case, a question that can be asked is if perturbations-based observations show any difference between such models? We address this question from the perspective of linear theory. Further, we constrain tachyonic models with CMB data. Tachyonic models have been constrained with low redshift observations by Singh et. al [63, 64]. Here we use data from Planck 2018 data in addition to other observational datasets to constrain tachyonic models.

We present the results for quintessence and tachyonic models where we compare the growth of perturbations in linear theory. In the next two sections, we describe the formalism for writing perturbation equations that demonstrate explicitly that the difference between these two models diminish as we go towards $w = -1$. Specifically, it depends on factor $(1+w)$, where w is the equation of state parameter. We demonstrate that differences between the two classes of models are suppressed by the factor $(1+w)$ and hence diminish rapidly as we approach closer to the cosmological constant. We also relate our formalism with earlier work as well as the fluid description. In section 5.4, we present the numerical results. In section 5.5, we use an approximate parametric representation for quintessence and tachyonic models to use CMB data to see if these can be distinguished by current data. We find that if the respective potentials for tachyonic and quintessence

models are chosen such that the background evolution is identical then it is not possible to distinguish these with present observations. Finally, in section 5.6, we constrain two tachyonic models with CMB data. We summarize in the last section 5.7.

5.2 Perturbation Theory

We consider scalar metric perturbations in the Newtonian gauge with the following form of the metric:

$$ds^2 = (1+2\psi)dt^2 - (1-2\xi)a^2(dx^2+dy^2+dz^2) \tag{5.1}$$

The problem of dark energy perturbations and its relevance for observables has been studied by many authors [64, 127, 130, 164, 167, 168, 169, 170, 171, 172]. Often, a fluid form for dark energy is assumed. This fluid at the background level is characterized by the equation of state parameter ($\bar{w}(z)$). For properly treating perturbations in fluid, one needs to know how energy density perturbations as well as pressure perturbations evolve. One can obtain dynamical equations for density perturbations and velocity perturbation either directly from Lagrangian density or from continuity equations (see Kodama & Sasaki [69], Bean & Dore [170] or Mukhanov [70], Ma & Bertschinger [71]). The set of equations derived in this manner is complete if additional information is provided for term $\delta p/\delta\rho$. In Newtonian gauge, ignoring anisotropic stress, we have [71]:

$$\dot{\delta} = -3H\left[\left(\frac{\delta p}{\delta\rho}\right) - \bar{w}\right]\delta + 3(1+\bar{w})\dot{\psi} - \frac{1+\bar{w}}{a}\theta \tag{5.2}$$

$$\dot{\theta} = -(1-3\bar{w})H\theta - \frac{\dot{\bar{w}}}{1+\bar{w}} + \frac{k^2\psi}{a} + \frac{k^2\delta}{(1+\bar{w})a}\left(\frac{\delta p}{\delta\rho}\right) \tag{5.3}$$

where δ is the fluid energy density contrast, θ is defined as:

$$\theta\bar{\rho}(1+\bar{w}) = -ik^j(\delta T)^0_j \tag{5.4}$$

For adiabatic perturbations in fluids, there exists a relation between pressure perturbations and density perturbations. Using this relation we can eliminate pressure perturbations and solve for density perturbations. In general, one has to solve for both perturbations. In cases where density and pressure are effective quantities, e.g., scalar fields, the underlying system of equations has to be solved.

A common approach is to quantify the variation of pressure perturbations using a gauge-invariant quantity called the effective speed of sound c_s^2. In an arbitrary gauge, pressure perturbations are written as [170, 173]:

$$(\delta p) = c_s^2(\delta\rho) + 3\dot{a}(1+\bar{w})(c_s^2 - c_a^2)\bar{\rho}\frac{\theta}{k^2} \tag{5.5}$$

There are a few subtle points that need to be considered while using this definition:

- In order to ensure gauge invariance, c_s^2 is defined in terms of $\delta p/\delta\rho$ in a frame comoving with fluid, i.e., frame in which θ is zero. Then from eq.(5.5), c_s^2 is just $\delta p/\delta\rho$ but in the frame comoving with fluid.

- In general, there are entropy perturbations as well. The gauge invariant amplitude of entropy perturbation is [69, 170]:

  $$\bar{w}\Gamma = (c_s^2 - c_a^2)\delta \tag{5.6}$$

  where c_a^2 is a quantity determined by quantities related to evolution of the model background:

  $$c_a^2 = \bar{w} - \frac{\dot{\bar{w}}}{3H(1+\bar{w})} \tag{5.7}$$

  For adiabatic perturbations, Γ vanishes, and $c_a = c_s$.

- Equation (5.5) can be derived [170] starting from eq.(5.6). δ in general is not gauge invariant, but δ in the frame comoving with the fluid is a gauge invariant quantity. δ and θ can be combined to form a gauge invariant quantity:

  $$\delta_{rf} = \delta + 3\dot{a}(1+\bar{w})\frac{\theta}{k^2} \tag{5.8}$$

  In eq.(5.6), the left hand side is gauge invariant implying that combination on the right-hand side is gauge invariant too. Now we define c_s^2 as $\delta p/\delta\rho$ in the rest frame of fluid meaning each term on the right-hand side is individually gauge-invariant in the context of this definition. Then in any frame we can substitute for rest frame δ using the quantity in eq.(5.8) in eq.(5.6) and then obtain eq.(5.5). For multicomponent systems, there can be an additional entropy perturbation besides intrinsic entropy perturbations [69]. This can be due to difference in dynamics (different c_a^2) or due to non-minimal coupling. In such cases, working in terms of field variables is simpler and less prone to ambiguities.

- For scalar fields [49], let $L(X,\phi)$ be the Lagrangian density, where $X =$

$\frac{1}{2}\partial_\mu\phi\partial^\mu\phi$ is the kinetic term while ϕ is the field. Rest frame for field is defined as the one in which $(\delta\phi)$ vanishes. In an arbitrary frame:

$$(\delta p) = \frac{\partial p}{\partial X}(\delta X) + \frac{\partial p}{\partial \phi}(\delta\phi) \tag{5.9}$$

with similar equation for $(\delta\rho)$. In rest frame:

$$(\delta p) = \frac{\partial p}{\partial X}(\delta X) \tag{5.10}$$

Combining equations for (δp) and $(\delta\rho)$ in rest frame, we get

$$c_s^2 = \frac{(\delta p)}{(\delta\rho)} = \frac{p_{,X}}{\rho_{,X}} \tag{5.11}$$

where $p_{,X}$ is partial derivative wrt X.

Earlier work [49, 169, 170, 171, 172, 174] along these lines has assumed some form for c_s^2 and then constrained c_s^2 and other parameters. These forms are assumed independent of $\bar{w}(z)$, thus the model is described by two functions. One general result from these studies is that the effects of different c_s^2 but same $\bar{w}(z)$ on observables are significant only in cases where dark energy has some significant contribution (at least a few percent) at time of recombination [49, 171]. But this itself means that $\bar{w}(z)$ should be of such a form that dark energy has a significant contribution at early times. For scalar fields, given the form for Lagrangian density, there is no need of using any ad-hoc approximate form for c_s^2. Equations for systems with scalar field perturbations can be written entirely in terms of field perturbations (gauge-invariant) and perturbations in other constituents. But studies with effective parametrization of c_s^2 are useful because they provide a general framework to compare different type of Lagrangian densities. Different Lagrangian densities may have different effective speeds of sound. For example, canonical scalar field Lagrangian of form:

$$L = X - V(\phi) \tag{5.12}$$

always have $c_s^2 = 1$, while k-essence ones with the form:

$$L = V(\phi)F(X) \tag{5.13}$$

can have a time-dependent c_s^2.

In this work, we consider the question whether two different scalar field La-

grangians (tachyonic and quintessence) with the same background evolution can be distinguished at the level of linear perturbations. Instead of working with an assumed form of c_s^2 and using fluid equations, we directly work with scalar fields and their perturbations. Our model space is limited as we choose two specific Lagrangians, but our calculations are concrete with few assumptions. Our choice of formalism is well motivated by the question: all observations sensitive to background cosmology (only) give us a certain evolution of background quantities, then that can be explained by both quintessence and tachyonic models with corresponding reconstructed potentials. We explore if these models can be distinguished by observations sensitive to linear perturbations?

5.3 Basic equations for scalar fields with effective fluid approach

In this section, we derive equations for quintessence and tachyonic fields. For establishing correspondence between field description and the effective fluid description we define a new perturbation quantity: u which is the deviation in the equation of state from background homogeneous fluid. The fluid description we employ is slightly different from the standard approach but is useful in highlighting differences in quintessence and tachyonic models. We also give relations between standard fluid variables and the variables used here.

Let Φ be the field for a scalar field representing dark energy. Then its stress energy tensor can be written as:

$$T_{\mu\nu} = (\rho + P)v_\mu v_\nu - P g_{\mu\nu} \tag{5.14}$$

where

$$v_\nu = \frac{\partial_\nu \Phi}{\sqrt{\partial^\alpha \Phi \partial_\alpha \Phi}} \tag{5.15}$$

We define first order quantities, density contrast and the corresponding variation in the equation of state parameter.

$$\rho = \bar{\rho}(1+\delta) \qquad W = \bar{w}(1+u) \tag{5.16}$$

where variables with a bar are background quantities dependent on time only,

while the first order variations (δ & u) can vary in space-time. We also define

$$\omega = 1 + \bar{w} \tag{5.17}$$

Effective pressure (P) for a scalar field theory (with identification of P as per equation eq.(5.14)) is the Lagrangian (L_Φ) of field while the effective density ρ is:

$$\rho = 2g^{\mu\nu}\frac{\partial L_\Phi}{\partial g^{\mu\nu}} - L_\Phi \tag{5.18}$$

Writing the field as the sum of background and perturbation:

$$\Phi = \phi + (\delta\phi) \tag{5.19}$$

and substituting it in equation eq.(5.14), retaining only the first order terms, we get the first order stress energy tensor using metric eq.(5.1):

$$\begin{aligned} T_0^0 &= \bar{\rho}\delta \\ T_j^i &= \bar{\rho}(u+\delta)(1-\omega) \qquad for \quad i=j \\ T_j^0 &= \frac{\bar{\rho}\omega}{\dot{\phi}}\frac{\partial(\delta\phi)}{\partial x^j} \end{aligned} \tag{5.20}$$

Off-diagonal spatial components of stress-energy tensor of both dark matter and field vanish at this order, hence the two metric potentials can be taken to be equal. We choose to work with ψ. The first order Einstein equation

$$G_1^1 = 8\pi G T_1^1 \tag{5.21}$$

can be used to obtain

$$\ddot{\psi} + 4\frac{\dot{a}}{a}\dot{\psi} + \psi\left[\frac{2\ddot{a}}{a} + \frac{\dot{a}^2}{a^2}\right] = -4\pi G\bar{\rho}(u+\delta)(-\bar{w}) \tag{5.22}$$

We obtain the dynamical equations for δ and u by requiring that the four divergence of stress energy tensor vanishes, i.e.

$$T^\mu_{\nu;\mu} = 0 \tag{5.23}$$

$$\dot{\delta} = 3u(1-\omega)\frac{\dot{a}}{a} + \omega\left[3\dot{\psi} + \frac{\nabla^2(\delta\phi)}{a^2\dot{\phi}}\right] \tag{5.24}$$

Making use of the following off-diagonal Einstein equation:

$$\frac{\dot{a}}{a}\frac{\partial\psi}{\partial x^j}+\frac{\partial\dot{\psi}}{\partial x^j}=\frac{4\pi G\bar{\rho}\omega}{\dot{\phi}}\frac{\partial(\delta\phi)}{\partial x^j}+4\pi G\quad {}^{dm}T^0_j \tag{5.25}$$

with dark matter stress energy contribution as

$${}^{dm}T^0_j=-a^2\bar{\rho}_{dm}\frac{\partial U}{\partial x^j} \tag{5.26}$$

where U is dark matter velocity potential, we rewrite equation (5.24) as:

$$\dot{\delta}=3u\frac{\dot{a}}{a}(1-\omega)+3\dot{\psi}\omega+\frac{1}{4\pi G\bar{\rho}a^2}\nabla^2\left[\frac{\dot{a}}{a}\psi+\dot{\psi}\right]+\frac{\bar{\rho}_{dm}}{\bar{\rho}}\nabla^2U \tag{5.27}$$

We also get a constraint equation for u

$$(-1+\omega)\frac{\partial u}{\partial x^j}=(1-\omega)\frac{\partial\delta}{\partial x^j}+\frac{\omega}{\dot{\phi}}\frac{\partial(\delta\phi)}{\partial x^j}\left[3\frac{\dot{a}}{a}+\frac{\dot{\bar{\rho}}}{\bar{\rho}}+\frac{\dot{\omega}}{\omega}\right]+\frac{\omega}{\dot{\phi}}\left[-\frac{\ddot{\phi}}{\dot{\phi}}\frac{\partial(\delta\phi)}{\partial x^j}+\frac{\partial(\dot{\delta\phi})}{\partial x^j}\right]-\omega\frac{\partial\psi}{\partial x^j} \tag{5.28}$$

We observe that equations (5.22) and (5.27) do not have explicit dependence on particular details of scalar field (whether it is quintessence or tachyonic), but equation 5.28 does have such a dependence. Therefore any differences between models will arise from this equation. We rewrite these equations in a less "field-specific" form and find that the equations in one of the theories have more terms. For tachyonic field, equation (5.28) can be written as:

$$\begin{aligned}\frac{(-1+\omega)}{2}\frac{\partial u}{\partial x^j} &= (1-\omega)\frac{\partial\delta}{\partial x^j}+\left[3(1-\omega)\frac{\dot{a}}{a}+\frac{\dot{\omega}}{2\omega}\right]\\ &\quad\left[\frac{1}{4\pi G\bar{\rho}}\left(\frac{\dot{a}}{a}\frac{\partial\psi}{\partial x^j}+\frac{\partial\dot{\psi}}{\partial x^j}\right)+a^2\frac{\bar{\rho}_{dm}}{\bar{\rho}}\frac{\partial U}{\partial x^j}\right]\end{aligned} \tag{5.29}$$

While quintessence has extra terms in addition to those present in equation (5.29):

$$\begin{aligned}\frac{(-1+\omega)}{2}\frac{\partial u}{\partial x^j} &= (1-\omega)\frac{\partial\delta}{\partial x^j}+\left[3(1-\omega)\frac{\dot{a}}{a}+\frac{\dot{\omega}}{2\omega}\right]\\ &\quad\left[\frac{1}{4\pi G\bar{\rho}}\left(\frac{\dot{a}}{a}\frac{\partial\psi}{\partial x^j}+\frac{\partial\dot{\psi}}{\partial x^j}\right)+a^2\frac{\bar{\rho}_{dm}}{\bar{\rho}}\frac{\partial U}{\partial x^j}\right]\\ &\quad+\omega\left[\frac{3\dot{a}}{8\pi G\bar{\rho}a}\frac{\partial}{\partial x^j}\left(\frac{\dot{a}}{a}\psi+\dot{\psi}\right)+\frac{3\bar{\rho}_{dm}\dot{a}a}{2\bar{\rho}}\frac{\partial U}{\partial x^j}+\frac{1}{2}\frac{\partial\delta}{\partial x^j}\right]\end{aligned} \tag{5.30}$$

Observing the third line in the above equation and comparing it with the equation for tachyonic counterpart (5.29), we find that the difference between two models is encoded in the terms multiplied by $\omega=(1+\bar{w})$. For the models constrained by observations, this number is small, much smaller than unity. Effectively this

makes the differences between two models a second order term.

We relate u to familiar quantities:

$$\frac{(u+\delta)\bar{w}}{\delta} = \frac{(\delta p)}{(\delta \rho)} \tag{5.31}$$

The effective “velocity" perturbation (coming from 5.4) for scalar field is:

$$\theta = \frac{k^2(\delta\phi)}{a\dot{\phi}} \tag{5.32}$$

and the effective speed of sound is:

$$c_s^2 = \frac{(u+\delta)\bar{w} + 3\frac{\dot{a}}{a}(1+\bar{w})c_a^2\frac{(\delta\phi)}{\dot{\phi}}}{\delta + 3\frac{\dot{a}}{a}(1+\bar{w})\frac{(\delta\phi)}{\dot{\phi}}} \tag{5.33}$$

As stated earlier, we do not need to incorporate an effective c_s^2 while working with fields because we have an analytical expression that can be evaluated. But for comparison of models, we derive approximate effective c_s^2 for tachyonic field. Please note that c_s^2 for quintessence is unity.

For tachyonic field the Lagrangian density is:

$$L(X,\Phi) = -V(\Phi)\sqrt{1-2X} \tag{5.34}$$

In the comoving frame of a scalar field:

$$c_s^2 = \frac{p_{,X}}{\rho_{,X}} = \frac{L_{,X}}{L_{,X} + 2L_{,XX}X} \tag{5.35}$$

In case of tachyonic field:

$$c_s^2 = (1-2X) = -\bar{w} - (1+\bar{w})(\delta g^{00})_{rf} \approx -\bar{w} \tag{5.36}$$

In linear theory approximation c_s^2 is just $-\bar{w}$ as $(1+\bar{w}) \ll 1$ for models allowed by observations and the second term in eq.(5.36) is effectively of second order. Most of the comparisons of c_s^2 in literature are between very different values of c_s^2 like between 1, 0.1, 0.01,0, etc. While we see that for models allowed by background observations, tachyonic c_s^2 is not very different from quintessence value of 1.

In the following sections, we study the differences in the two models in linear theory using field perturbations. Note that one can either directly use equations derived from field perturbations or the fluid perturbations (u and δ) equations

derived in this section as these are equivalent approaches.

5.4 Results for field-based comparisons

We divide our discussion here into 2 subsections. In first we show comparisons for quantities, that influence observables, like metric potential (ψ) and its derivative ($\dot{\psi}$). In the second subsection, we show differences in dark energy perturbations.

5.4.1 Influence on observables

All observables are affected by metric coefficients. The influence of these coefficients on dark matter linear growth rate is used in calculating observational effects like matter clustering, σ_8, growth index, etc. Rate of change of potential ($\dot{\psi}$) affects CMB photons and causes observable effects like ISW [105, 130].

We present ψ and $\dot{\psi}$ for the following background evolutions (characterized by $\bar{w}(a)$):

- Constant $\bar{w}(z)$ for values: - 0.5 and -0.975
- Chevallier-Polarski-Linder (CPL) paramterization [148, 149]

$$\bar{w} = w_0 + w_a(1 - \frac{a}{a_0}) \tag{5.37}$$

  $\bar{w}(z)$ with parameters: $w_0 = -0.9$ and $w_a = -0.099$

Since differences in growth rate of perturbations with scale has been seen mainly at very large scales [127, 136, 137] we present results for length-scales: 2000 Mpc and 10000 Mpc. The differences between two models peak approximately around 10000 Mpc length-scales. At small scales, the growth of perturbations is suppressed, and at very large scales the growth rate is independent of the speed of sound. It is only in the transition region that we can expect to capture some differences between models with the same expansion history but a different c_s^2.

We show ψ and $\dot{\psi}$ in figures 5.1,5.2 and 5.3. In the notation used to annotate the curves, we use 'quin' for quintessence models and 'tach' for the tachyon models. Also, we use red color for quintessence and black for the tachyonic field. The length

scales are mentioned alongside. We find that tachyonic and quintessence models for $\bar{w} = -0.975$ and CPL cases are almost indistinguishable with differences of the order 0.01% in most cases. Corresponding differences for $\bar{w} = -0.5$ are more significant. These differences grow in a monotonic and continuous manner as we moves away from $w = -1$. We plot one extreme case $\bar{w} = -0.5$ that is observationally ruled out but gives an indication of the order of differences between the two classes of models. CPL and $\bar{w} = -0.975$ are observationally allowed [153, 175] but differences between the models are extremely small at all scales. For $w = -0.5$, differences in potentials and its time derivatives can be of the order 10%. $w = -0.975$ case shows negligible differences of the order 0.01% while CPL case has differences around 0.1%.

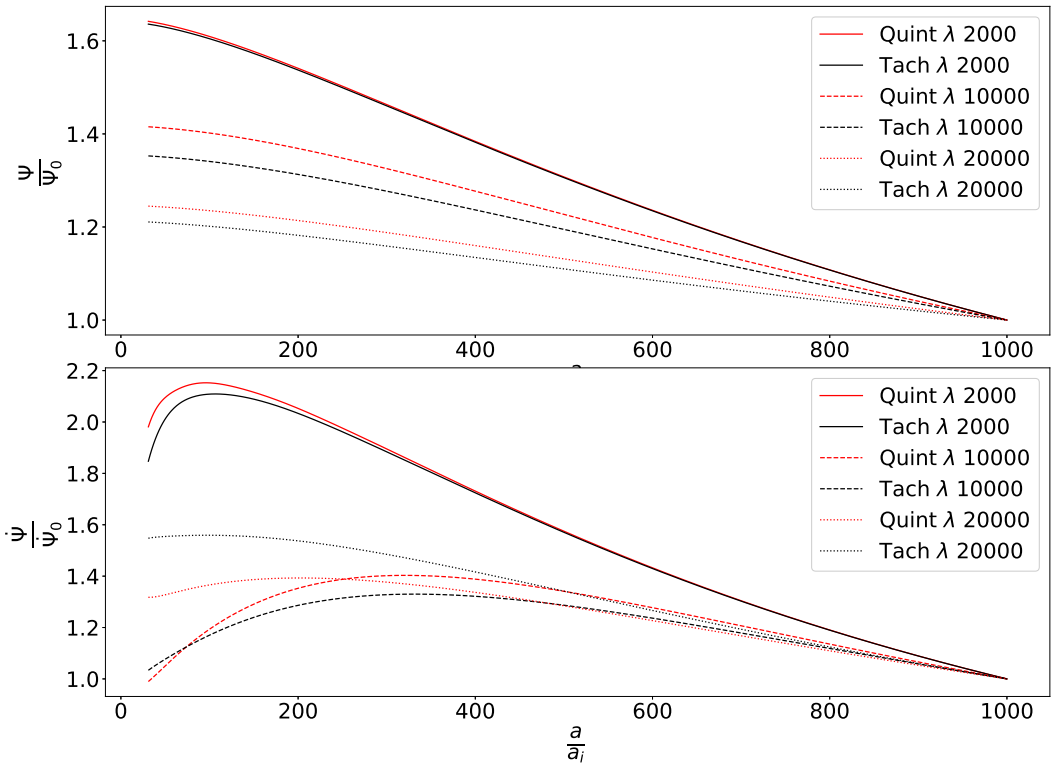

Figure 5.1: This figure shows the potential ψ and its time derivatives for $\bar{w} = -0.5$. The potentials have been normalized by their present day value. The difference in different models is higher for $\lambda \sim 10k$.

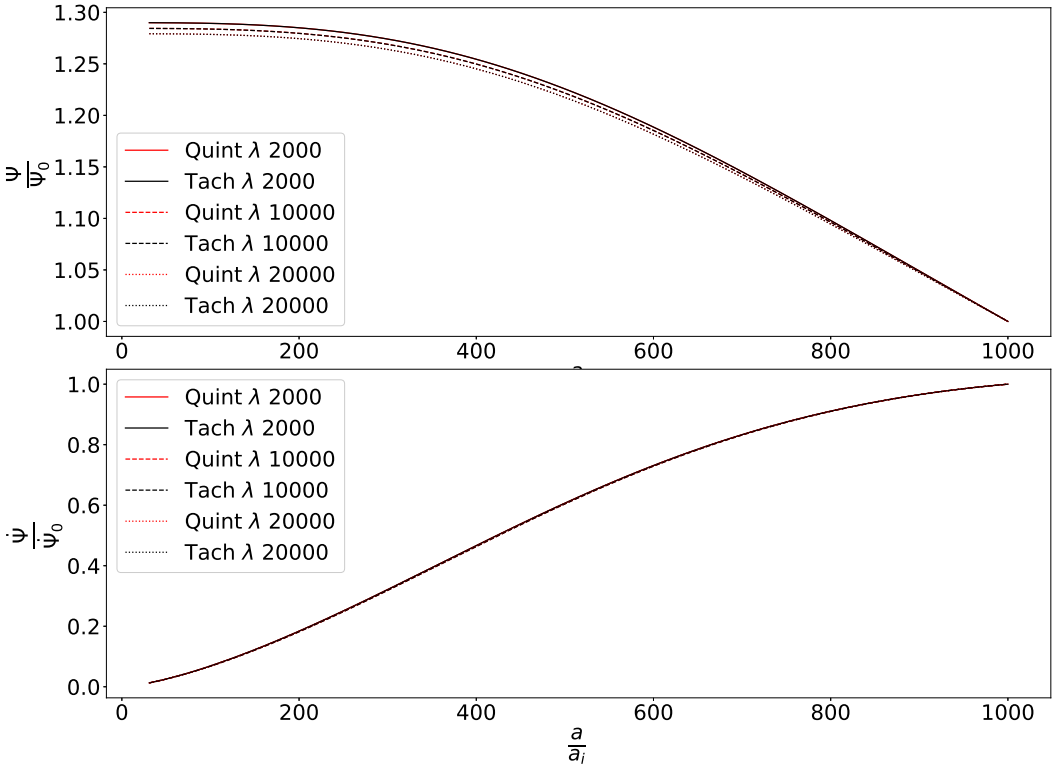

Figure 5.2: The plots show the potential ψ and its time derivatives for $\bar{w} = -0.975$ case. Clearly, the relative differences are much smaller than in the case of $w = -0.5$.

5.4.2 Scalar fields

While dark energy perturbations show more differences (figures 5.4, 5.5 and 5.6) than potentials, their effects on observables are not very significant as shown in the previous subsection. Fluctuations are stronger for cases that are significantly removed from $w = -1$. Since dark energy perturbations are not directly observable, the significance of fluctuations can only be evaluated through observables as in the last subsection. We have shown comparisons for dark energy perturbations in figures 5.4, 5.5 and 5.6. Although there are visible differences (between tachyon and quintessence cases) in the evolution of DE perturbations but these differences remain insignificant because the amplitude of perturbations is very small.

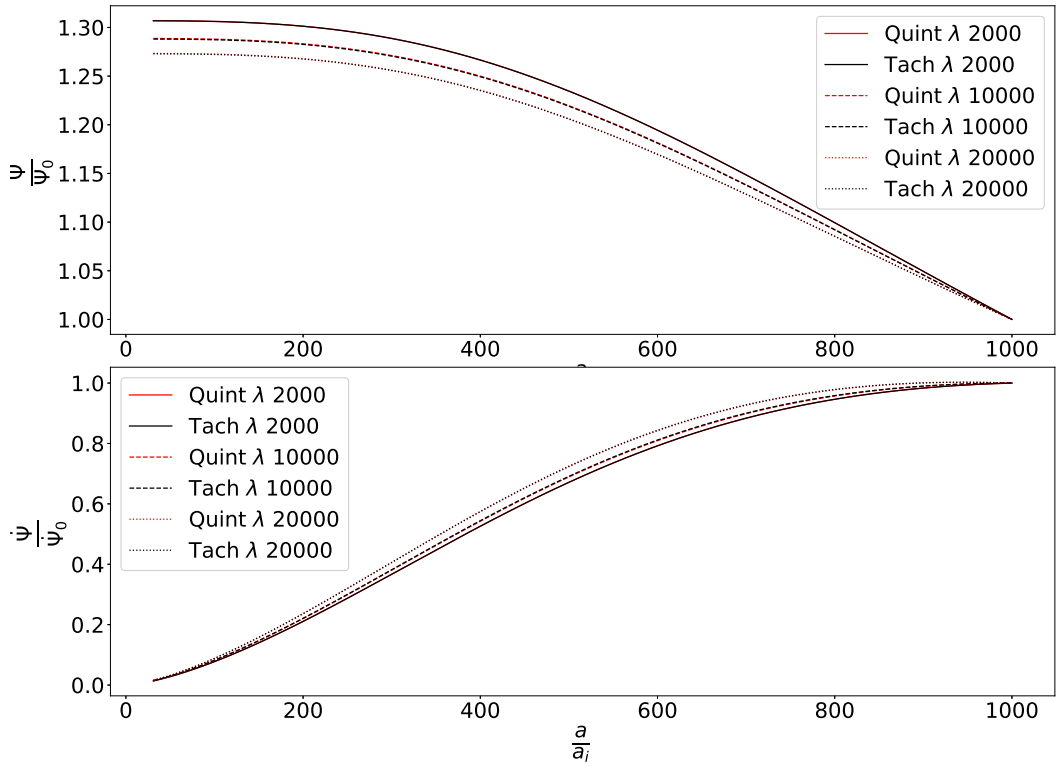

Figure 5.3: Here potential ψ and its time derivatives are plotted for the CPL model. Differences are much smaller than $w = -0.5$ and slightly stronger than $w = -0.975$ case. This is because in comparison to $w = -0.975$, the background evolution for the CPL model has a larger deviation from $w = -1$.

5.5 Constraining models with CMB anisotropy data

There are two popular public codes available for CMB anisotropy calculations: CAMB [176] and CLASS [177, 178, 179]. Both have support for implementing fluid models with effective c_s^2. Here we use CLASS to calculate CMB anisotropy power spectra for effective c_s^2 corresponding to tachyon models and quintessence models. This requires some minor tweaks in the default CLASS code as the standard version does not have time-dependent c_s^2. We modified the code to allow for a time-varying form of c_s^2 for tachyon models. There are various ways tachyonic models can be included in CLASS. We can write effective potentials for the tachyon field in terms of a chosen background DE (particular $w(a)$), or we can have an effective fluid description with c_s^2 as derived in eq.(5.36). While the former is a more apt and clean approach, the latter is easier to implement and is expected to

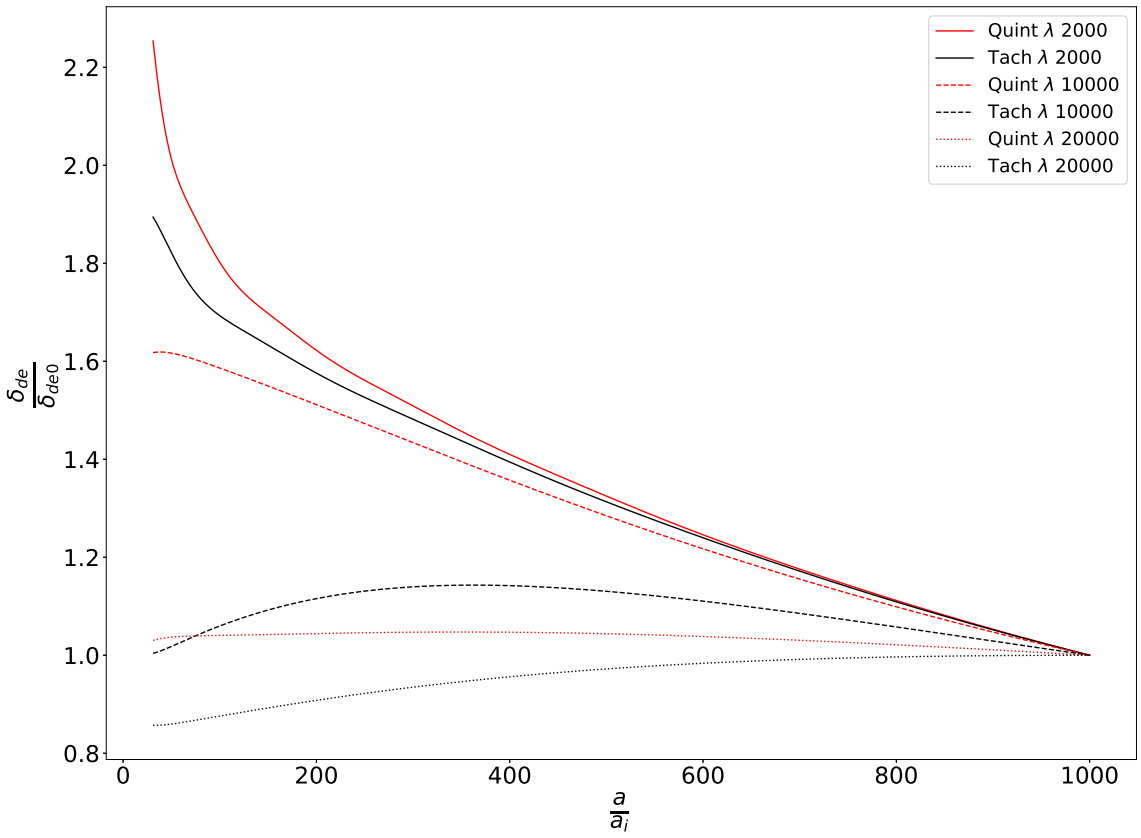

Figure 5.4: Dark energy (DE) density contrast for $\bar{w} = -0.5$ case. It shows growth of DE normalized by present value.

give same results for $(1 + \bar{w}) \ll 1$, which anyway is the region already constrained by background cosmology probes. In cases where one has well-motivated forms for potentials, these tachyonic models can be implemented in CLASS with some more effort. We do this in the next section where we constrain tachyon models for two well-studied potentials.

We adopt following parametric form for c_s^2:

$$c_s^2 = c1 * w + c0 \tag{5.38}$$

This is the simplest form that can capture both quintessence and tachyonic models. For quintessence, we have $c1 = 0$ and $c0 = 1$ and for tachyonic models $c1 = -1$ and $c0 = 0$. We then do an MCMC sampling using CLASS with MontePython [180, 181]. We use CMB (Planck 2018 high-l TT,TE,EE, low-l EE, low-l TT, lensing) [182] and BAO data (Boss Data Release 12 [183, 184], small-z BAO data

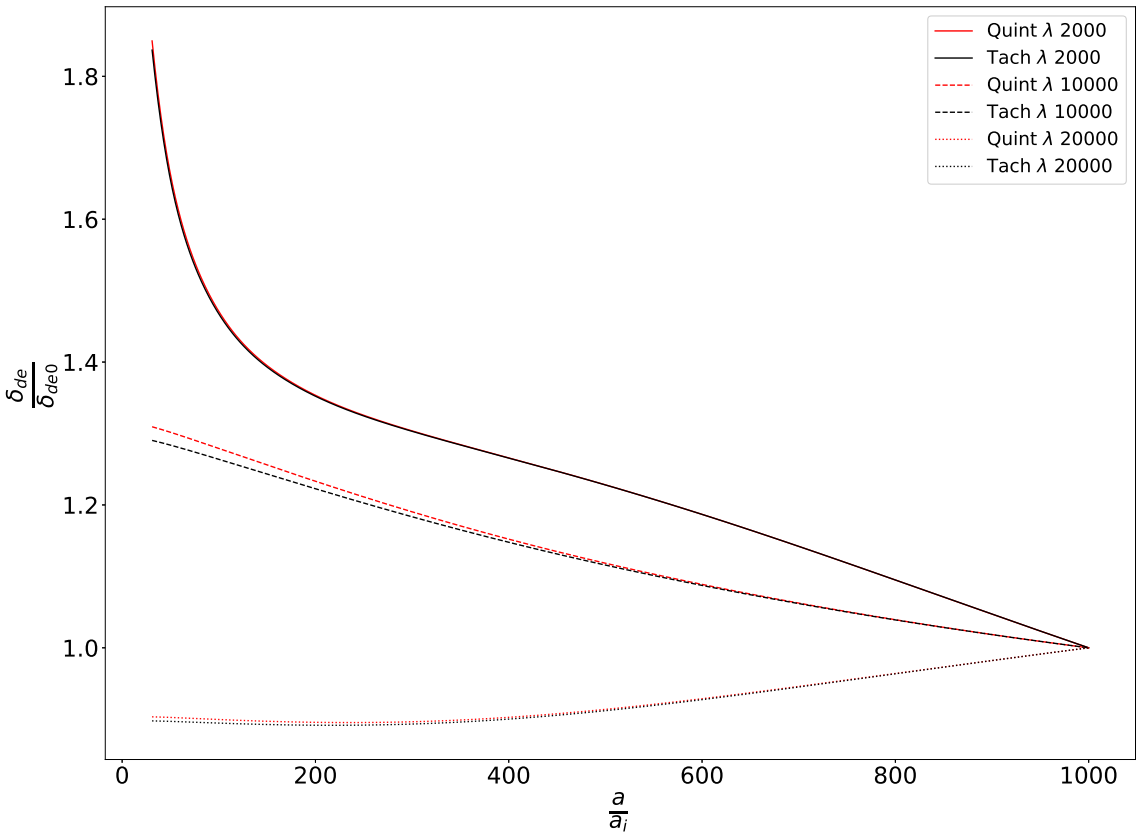

Figure 5.5: Dark energy (DE) density contrast for $\bar{w} = -0.975$ case. Relative differences between quintessence and tachyonic models are small in comparison with $w = -0.5$ case.

from 6dF Galaxy Survey [185] and SDSS DR7 main Galaxy sample [186]). We find that the two parameters $c1$ and $c0$ remain unconstrained. In fig 5.7, we show triangle plots for 2d marginalized credible intervals. Parameters relating to DE speed of sound are unconstrained. This result is similar to analyses with constant c_s^2 have obtained earlier [169, 170, 171, 172]. While the previous work deals with either constant c_s^2 or some particularly chosen form, here we have chosen an explicit parameterized form for it, which encapsulates both quintessence and tachyonic field. In figure 5.8, we plot the marginalised posteriors.

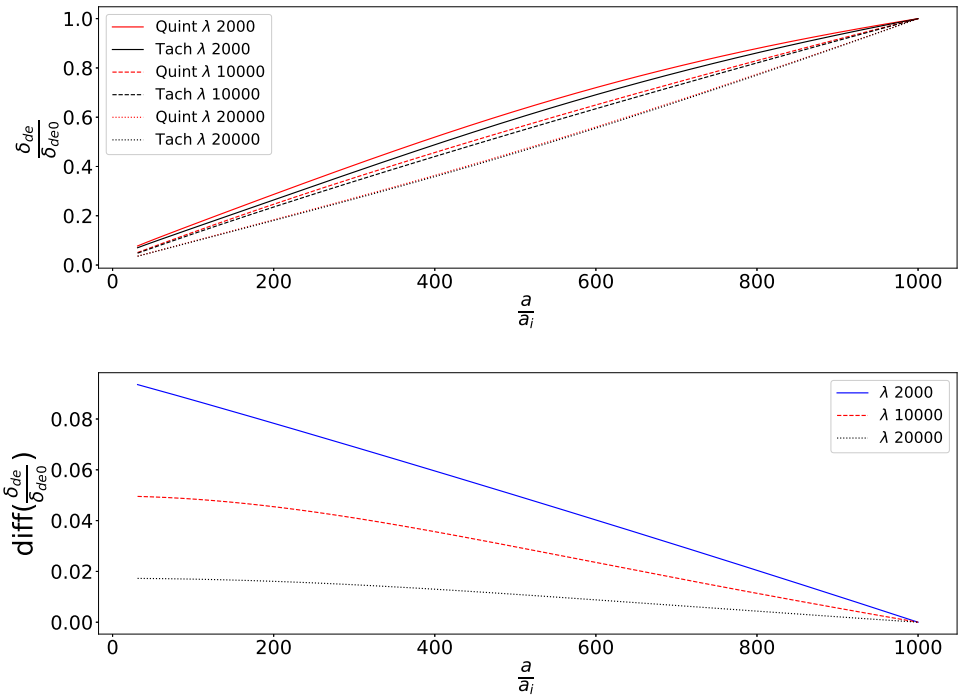

Figure 5.6: Dark energy (DE) density contrast for the CPL case. Curves are neatly clustered here by field type. This suggests that for this particular background evolution, tachyonic field and quintessence field evolve similarly for a particular lengthscale.

5.6 CMB data and tachyonic models

We modify CLASS to implement tachyonic models as a scalar field at linear level, where equations are obtained from Lagrangian corresponding to tachyonic dark energy (The equations and modifications related information is provided in B). Two potentials which we code in CLASS are:

- Exponential potential

$$V(\phi) = V_0 \exp(-\frac{\phi}{\phi_a}) \tag{5.39}$$

- Inverse Square Potential

$$V(\phi) = \frac{n}{4\pi G}\left(1 - \frac{2}{3n}\right)^{\frac{1}{2}} \frac{1}{\phi^2} \tag{5.40}$$

These two potentials have some interesting features and have been studied in detail [43, 61]. These potentials have been constrained using low red-shift data

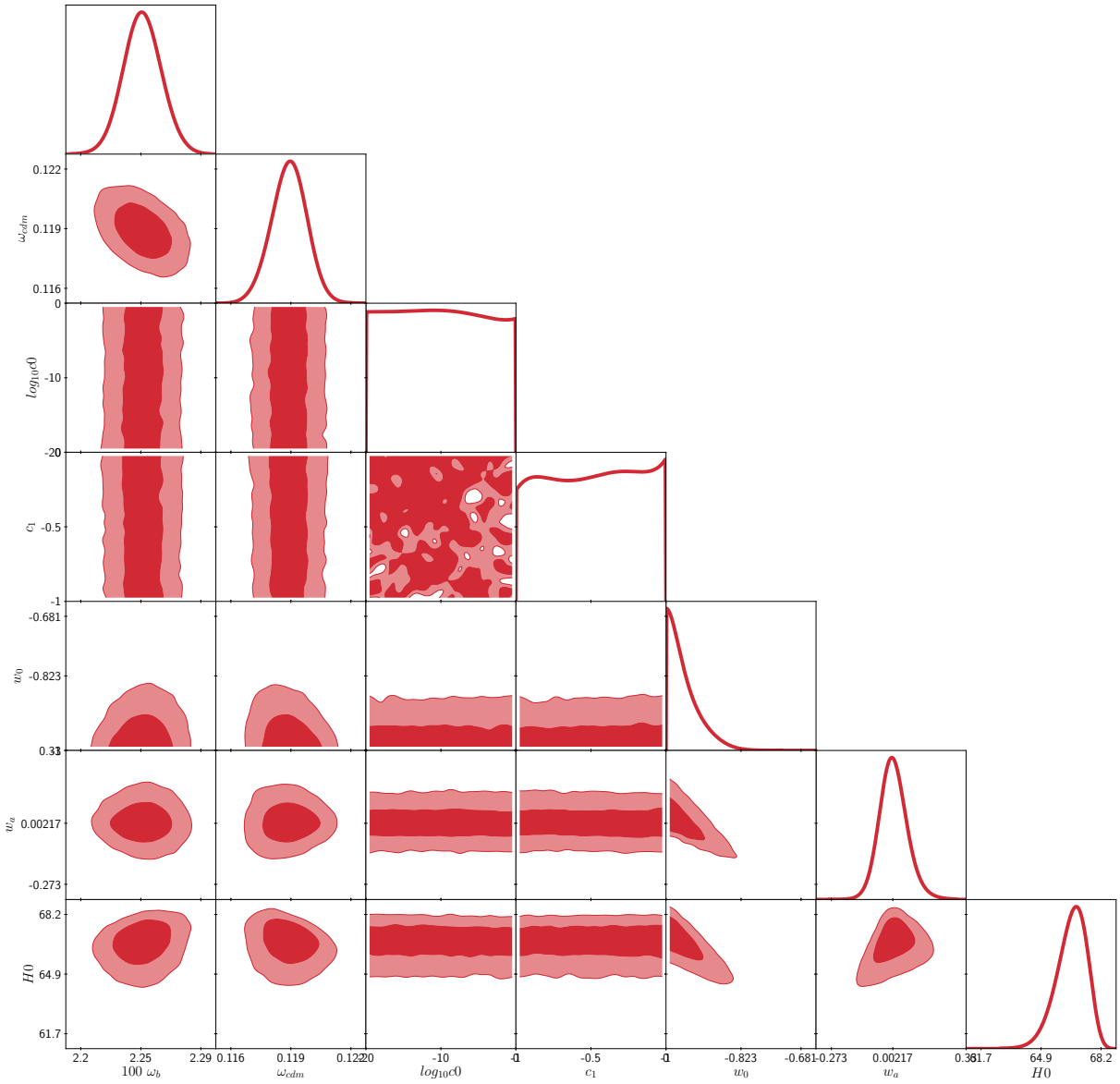

Figure 5.7: Triangle plot: While background cosmological parameters like density parameters, H_0, w_0,etc. are well constrained, perturbation related parameters like c_s^2 remain unconstrained.

in [63, 64]. In [63], tachyonic models were constrained using low redshift data from supernova, Hubble parameter measurements, and BAO data. Evolution of perturbations was considered in [64] and redshift space distortion data was used for model comparisons. These models have not yet been constrained using CMB data. We use CLASS with MontePython to constrain the tachyonic models (with the above-mentioned potentials) using Planck 2018 data [187]. We use the following combinations of data:

- CMB (Planck 2018 high-l TT,TE,EE, low-l EE, low-l TT, lensing) [182]
- BAO (Boss Data Release 12 [183, 184], small-z BAO data from 6dF Galaxy

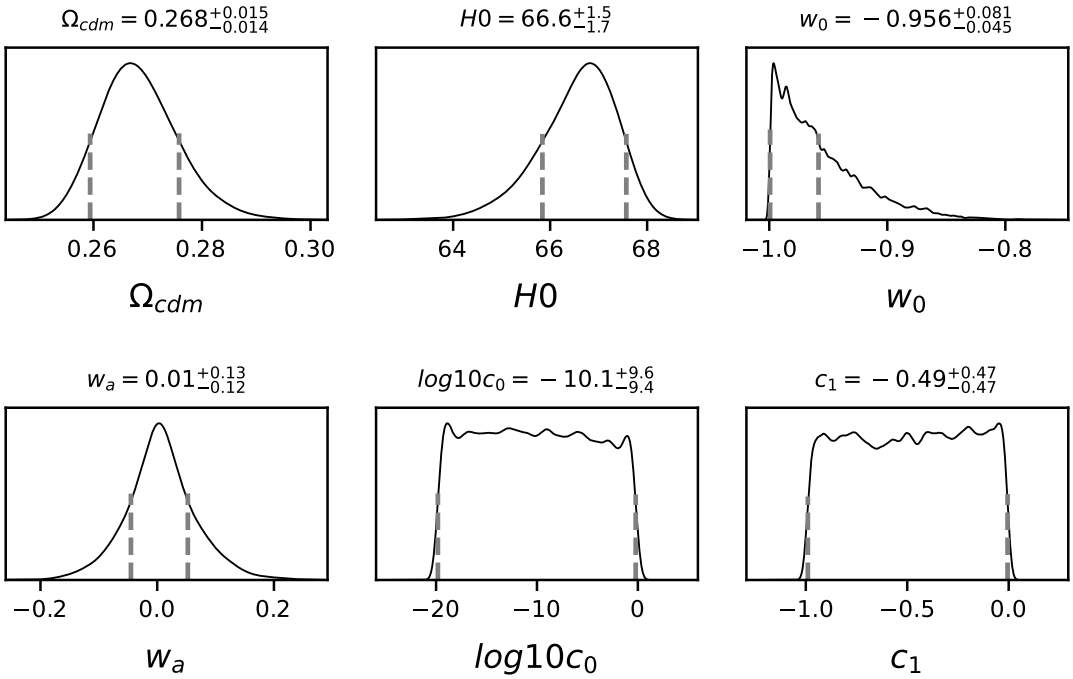

Figure 5.8: 1-dimensional posterior distributions. Vertical dashed lines mark half-maximum x-coordinates while the limits quoted at top are 2σ limits.

Survey [185] and SDSS DR7 main Galaxy sample [186])

- Combination of the above-mentioned CMB and BAO data.
- JLA data [188].

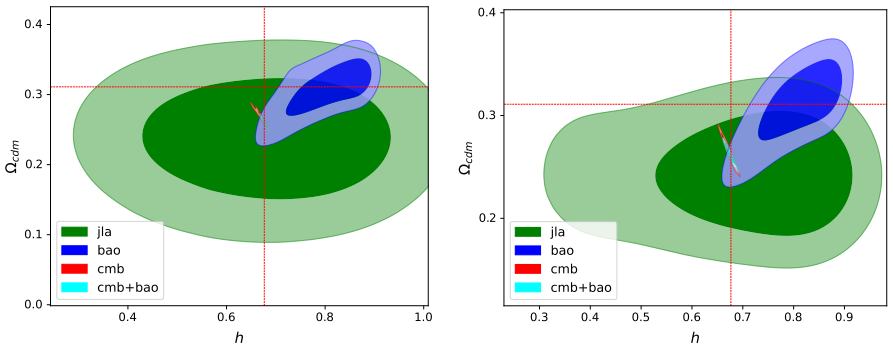

Figure 5.9: 2-d plots for present day matter density parameter Ω_{cdm} and Hubble parameter (h). Left panel is for exponential potential while right one is for inverse square. Red lines show the best-fit values for ΛCDM model from Planck 2018 [182]. CMB data, as already known, shrinks the constrained region. H_0 tension is not resolved by tachyonic models considered here.

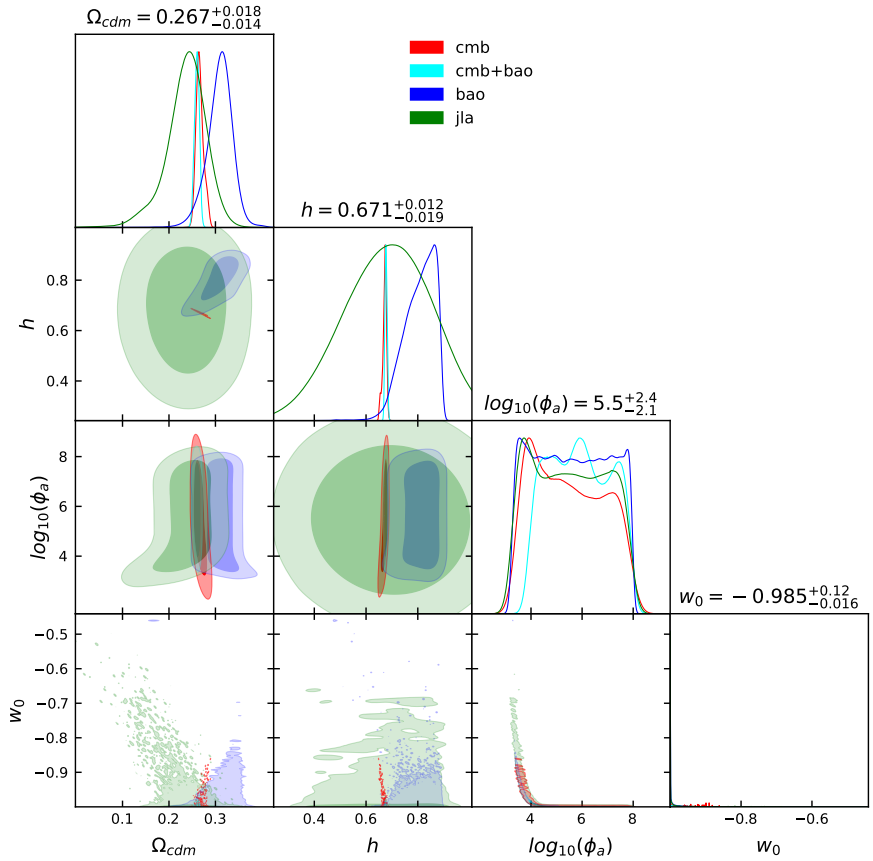

Figure 5.10: Triangle plot using four combinations of data, for exponential potential. Potential parameter ϕ_a is slightly constrained to be greater with certain minima. While ϕ_a appears to have nonlinear correlations with w_0, w_0 is constrained be close to -1.

5.6.1 Results

We first consider constraints on parameters that only concern background evolution and are needed irrespective of potentials: density parameter for dark matter and the Hubble constant. In figure 5.9, we plot contours for present-day matter density contrast (Ω_{cdm}) and dimensionless Hubble constant (h). CMB data provides tight constraints. The best fit values of these parameters, from the ΛCDM model based CMB constraint in Planck 2018 cosmo parameters paper, is represented by red lines in the figure. We find that the best-fit value (2-d) lies in the 1-sigma region of the JLA data, but it is out of 2-sigma regions for CMB and BAO data constraints. While h is consistent (within 2-sigma regions), it is Ω_{cdm}, which is lower for these tachyonic field based cosmological models. So, inference of dark matter content of the Universe shows dark energy model dependence, when considering extensions beyond Λ. In figure 5.10, we present the triangle plot for exponential (exp) potential with potential parameter ϕ_a and present-day equation

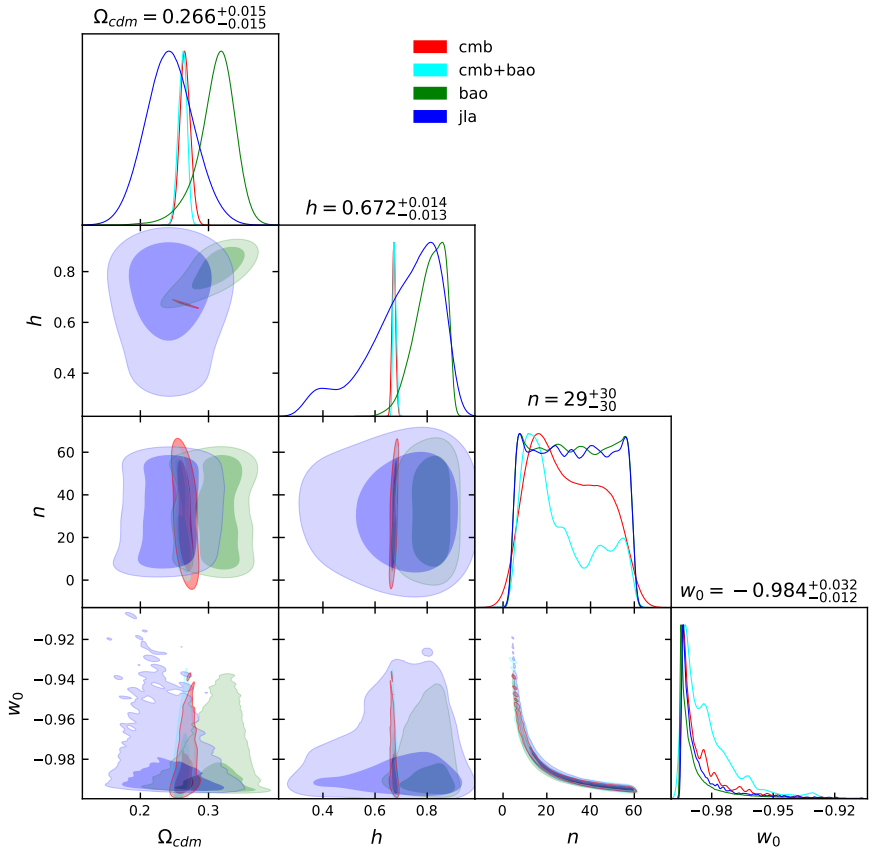

Figure 5.11: Triangle plot using four combinations of data, for inverse square potential. Results are somewhat similar to that for exponential case as potential parameter n is slightly constrained and is correlated to w_0. A particular value of w_0 is favoured, which is not -1, but is close to it.

of state w_0, included along with density and Hubble parameter. w_0 is constrained to be close to -1. The potential parameter ϕ_a is not constrained by any of the used data. Triangle plot for inverse-square (insq) potential is presented in figure 5.11. Again, potential parameter n is allowed a very wide region and w_0 is very close to -1. Plots with σ_8 are shown in figures 5.12 and 5.13. The constraints for σ_8 for two potentials agree with each other as well as with that for ΛCDM. This is again a manifestation of the fact that the models which have same background evolution and are close to Λ are extremely difficult to distinguish.

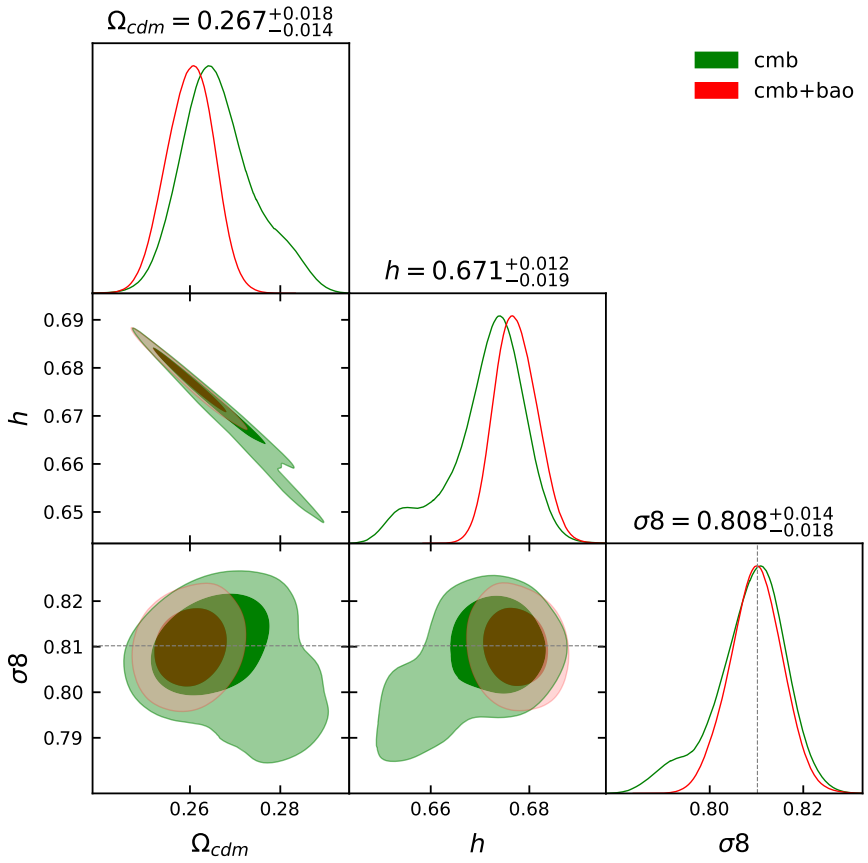

Figure 5.12: Triangle plot with σ_8 for the exponetial potential. The value of σ_8 is compatible with that for ΛCDM from Planck 2018 (plotted as line in this figure).

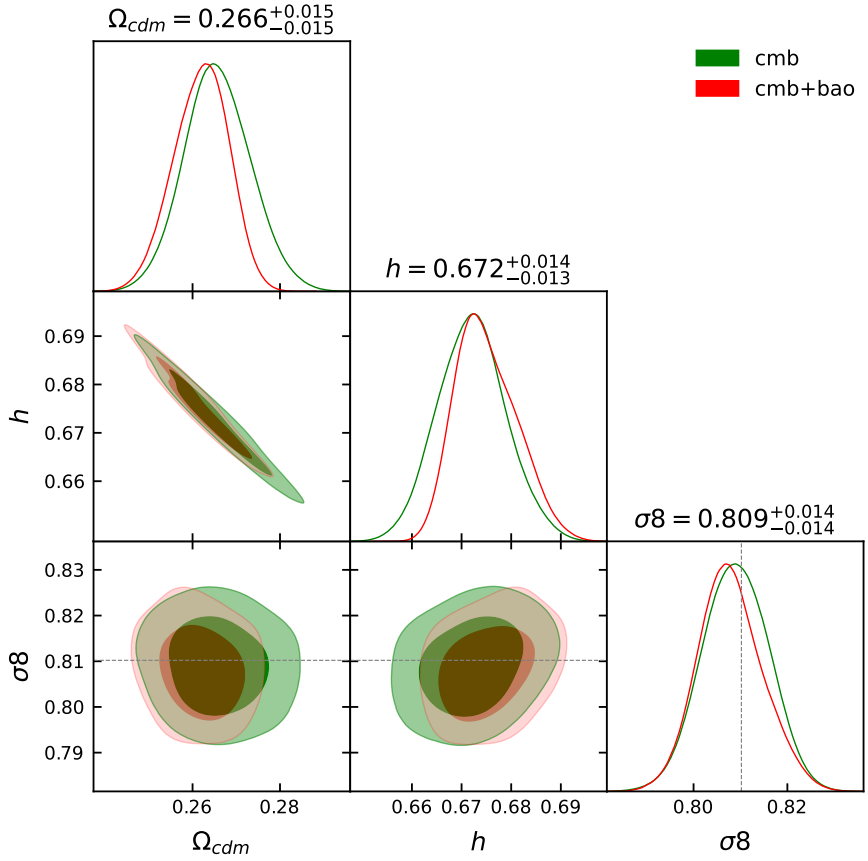

Figure 5.13: Triangle plot with σ_8 for the inverse square potential. The constraints are comparable with those for exponential potential as well as ΛCDM

5.7 Summary

We have studied the prospects of using linear perturbation theory to distinguish two different models of dark energy: quintessence and tachyonic field. Specifically, we investigate the differences in dynamics of perturbations for the same background expansion in both models. This helps us separate the effects coming from different background expansions and differences due to perturbations.

We recast linear theory equations in a form that provides insight into how the systems of perturbations differ in two theories. We show that when the equations for both are written in fluid terms, substituting for corresponding field terms, one of the equations has extra terms for quintessence. These first-order terms are multiplied by $\omega \equiv (1 + w)$. This implies that if the background expansion is close to $w = -1$, differences between the two models diminish.

We calculated and showed the evolution of quantities like ψ and its derivative, which affects the observables. These numerical calculations demonstrate the theoretical dependence on the factor of $(1 + w)$.

We find that the differences between models while being small at all scales are largest around the scale of 10000 Mpc. We believe that this is due to the difference between the effective speed of sound in two models and that this difference is seen in the transition scales from suppression of perturbations at small scales to growth at large scales.

We used the definition of effective c_s^2 for two models to write a parametric form for $c_s^2 (\equiv c1 * w + c0)$ which incorporates both fields as instances of particular values of the parameters. We then used CMB data to constrain this parametric form to see if we can distinguish two models and find that two parameters $c0$ and $c1$ remain unconstrained.

We modified the CMB anisotropy code CLASS to incorporate tachyon models. We then used it to constrain common tachyonic potentials: $V \propto \exp(-\frac{\phi}{\phi_a})$ and $V \propto \phi^{-2}$ using CMB and other data. We find that the parameters are very weakly constrained.

We have shown that it is very difficult to distinguish between these two classes of models at large scales where linear perturbation theory is applicable. We have also shown that this is primarily because only models with $(1+w) \ll 1$ are allowed and in this regime, the differences between the two classes of models are effectively

of second order. Combined with our earlier work where we have explored these models at small scales using spherical collapse, it appears that there are no obvious observables available at present that may be used to distinguish between these two classes of models if the expansion history is the same. We can conclude that at least for these two classes of dark energy, as also for a fluid model of dark energy, the choice of class of models is irrelevant and calculation of observables may be done in any model. On one hand, this is a potential simplification of calculations, on the other hand, it means that we cannot know which of the models is the true model for dark energy.

Chapter 6

Summary and Prospects

This chapter summarizes this thesis, highlights main results and touches upon future prospects.

6.1 Summary

The work in this thesis was done for studying the effects of perturbations in scalar field dark energy models. We simulated cosmological models with dark matter and dark energy perturbations. First we studied nonlinear perturbations, in spherical symmetry, with dark energy represented by canonical scalar field called "quintessence". Then we developed the techniques for numerical reconstruction of potentials in quintessence and tachyonic models, given some background cosmology. This was followed by spherically symmetric simulations with tachyonic dark energy and subsequent comparison with quintessence for same background expansion. Comparisons make use of reconstruction techniques developed in previous part. Next, we did comparative studies of perturbations in two models using (linear) cosmological perturbation theory. Further we used CMB data to check the prospects of distinguishing two models. Also, we tried to constrain cosmology with tachyonic dark energy using CMB and other data sets.

The main results of these studies are:

- For both, tachyonic fields and quintessence, perturbations in dark energy field are induced by metric perturbations. These grow in time.

- The induced perturbations remain small, even when the matter perturbations have become highly nonlinear.
- Scale of perturbations is very important for growth of dark energy perturbations. Larger perturbations with small amplitudes evolve to be stronger than those with bigger amplitudes but smaller lengthscales.
- Even though dark energy perturbations are induced and they grow with time, their effect on dark matter or metric is insignificant. This can be attributed to the fact that background, for the most part of expansion history, is dominated by dark matter, while dark energy domination is a relatively recent phenomenon.
- Rate of growth of dark energy perturbations is higher (particularly at late times) in nonlinear evolution as compared to linear calculations.
- Effective equation of state (w) becomes a function of space-time.
- Dynamics of DE perturbations is stronger in large voids and these can be plausible systems for diagnostics of DE perturbations. This is because dark energy component dominates over dark matter in these regions. Further these are large and dark energy perturbations have an opportunity to grow.
- Comparing linear as well as nonlinear perturbations in tachyonic models and quintessence models, we find that the differences in perturbations are dependent on relative differences in background. We simulated perturbations in two models with exactly same background. For backgrounds close to ΛCDM ($w \sim -1$), differences are small and increase as we go away from $w = -1$. Dark matter/metric perturbations do not exhibit any significant differences for two different Lagrangians. Dark energy fluctuations do show differences, but these differences diminish as background expansion is tuned closer to $w = -1$. For background expansion history (or w) constrained by current observations, observables do not show any significant distinguishing features.
- We used linear theory formalism to provide insight into how differences depend on background expansion. Specifically, there is an extra term in equations for quintessence which contains terms of linear order and is prefixed by $(1 + w)$. Effectively this makes the difference between quintessence and tachyon models as second order if $(1 + w) \ll 1$.
- We used effective speed of sound (of dark energy: c_s^2) formalism to constrain a parametric form of c_s^2 using CMB data (Planck 2018 data release). We find

that the parameters are not constrained well enough to distinguish tachyonic models from quintessence.

- We also constrained cosmology for two specific tachyonic models: Inverse-square potential and exponential potential. Parameters of potentials are weakly constrained, while value of Ω's is different from what one would obtain from ΛCDM parameter estimation. This demonstrates the fact the parameter values are dependent on dark energy model assumed.

6.2 Prospects

Most of the cosmological simulations are based on a split of space-time into background and perturbations. Perturbations may be treated in linear approximation or in some other approximation (e.g. symmetry). In such calculations, large perturbations of a component, which is not dominant at background level, do not affect the space-time evolution significantly . At all times there is an assumption about uniform background's composition. On the contrary, in a more realistic situation there may be possibilities of regions where a particular component comes to domination, but is not the most significant in terms of global averaging. This calls for simulations that avoid this splitting and which simulate space-time as a whole. Further simulations need to be developed which are based on relativistic formulations rather than Newtonian approximations or linear equations. There are some efforts in this direction[86, 87, 88]. Further investigations and work would be needed for these types of simulations to evolve and achieve multiphysics capacity as achieved by traditional N-body simulations.

Along these lines, in future work, we would be exploring relativistic N-body simulations and cosmological simulations based on numerical relativity formalism. Also, there is possibility of extending the linear theory calculations comparing perturbations in different Lagrangians of dark energy by assuming a general form for Lagrangian and then expanding it around its homogeneous and isotropic form.

Study of voids dominated by dark energy and formation of dark energy halos is another prospect that can be explored particularly using gravitational lensing.

Working out forecasts to find out the sensitivity of observations required to differentiate between the class of models. This will help us know if upcoming surveys would be capable of distinguishing between these models.

Appendix A

Methods for Chapter 2

A.1 T^{μ}_{ν} for scalar field

In order to get Einstein's equation in the familiar form, we define the stress-energy tensor as follows:

$$T_{\mu\nu} = -2c\left[\frac{\partial L_{\psi}}{\partial g^{\mu\nu}} - \frac{1}{2}L_{\psi}g_{\mu\nu}\right] \tag{A.1}$$

Owing to spherical symmetry we get the following non-vanishing components.

$$T_{\mu\nu} = c\left[\partial_{\mu}\psi\partial_{\nu}\psi \; - \; L_{\psi}g_{\mu\nu}\right] \tag{A.2}$$

$$T^{0}_{0} = c\left[\frac{\dot{\psi}^{2}}{2c^{2}} + \frac{e^{-2B}\psi'^{2}}{2} + V\right] \tag{A.3}$$

$$T^{1}_{1} = -c\left[\frac{\dot{\psi}^{2}}{2c^{2}} + \frac{e^{-2B}\psi'^{2}}{2} - V\right] \tag{A.4}$$

$$T^{2}_{2} = T^{3}_{3} = -c\left[\frac{\dot{\psi}^{2}}{2c^{2}} - \frac{e^{-2B}\psi'^{2}}{2} - V\right] \tag{A.5}$$

$$T^{1}_{0} = -ce^{-2B}\dot{\psi}\psi' \tag{A.6}$$

$$T^{0}_{1} = \frac{\dot{\psi}\psi'}{c} \tag{A.7}$$

Vanishing of four divergence of stress energy tensor gives us the equation of motion for the scalar field:

$$T^{\mu}_{0}{}_{,\mu} = c\dot{\psi}\left[e^{-2B}\left(B'\psi' - \psi'' - 2\frac{R'}{R}\psi'\right) + \frac{\dot{B}\dot{\psi}}{c^{2}} + \frac{2\dot{\psi}\dot{R}}{Rc^{2}} + \frac{\ddot{\psi}}{c^{2}} + V_{,\psi}\right] = 0 \tag{A.8}$$

A.2 Einstein Equations

Variation of Einstein-Hilbert action gives us:

$$\delta I_{Ein-Hilb} = \frac{c^3}{16\pi G}\int (drd\theta d\phi dt)\sqrt{-g}\left[R_{\mu\nu} - \frac{1}{2}g_{\mu\nu}R_E\right]\delta g^{\mu\nu}$$

where Ricci scalar is represented as R_E to distinguish it from metric coefficient R. Combining this variation with the stress- energy tensor for ψ in previous sub-subsection, we get Einstein's equations

$$G^{\mu}_{\nu} = R^{\mu}_{\nu} - \frac{1}{2}\delta^{\mu}_{\nu}R_E = \frac{8\pi G}{c^4}T^{\mu}_{\nu}$$

$\binom{1}{1}$ component

$$\left[\frac{1}{R^2} - e^{-2B}\frac{R'^2}{R^2} + \frac{\dot{R}^2}{c^2R^2} + \frac{2\ddot{R}}{c^2R}\right] = -\frac{8\pi G}{c^3}\left[\frac{\dot{\psi}^2}{2c^2} + \frac{e^{-2B}\psi'^2}{2} - V\right] \tag{A.9}$$

$\binom{2}{2}$ and $\binom{3}{3}$ component

$$e^{-2B}\left[\frac{R'B'}{R} - \frac{R''}{R}\right] + \frac{1}{c^2}\left[\frac{\dot{R}\dot{B}}{R} + \frac{\ddot{R}}{R} + \dot{B}^2 + \ddot{B}\right] = -\frac{8\pi G}{c^3}\left[\frac{\dot{\psi}^2}{2c^2} - \frac{e^{-2B}\psi'^2}{2} - V\right] \tag{A.10}$$

$\binom{0}{0}$ component

$$\begin{aligned} -e^{-2B}\left[\left(\frac{R'}{R}\right)^2 - \frac{2R'B'}{R} + \frac{2R''}{R}\right] + \frac{1}{R^2} + \frac{\dot{R}^2}{c^2R^2} + \frac{2\dot{R}\dot{B}}{c^2R} = \\ \frac{8\pi G\rho}{c^2} + \frac{8\pi G}{c^3}\left[\frac{\dot{\psi}^2}{2c^2} + \frac{e^{-2B}\psi'^2}{2} + V\right] \end{aligned} \tag{A.11}$$

$\binom{1}{0}$ and $\binom{0}{1}$ components yield same equation

$$R'\dot{B} - \dot{R}' = \frac{4\pi G}{c^3}\dot{\psi}\psi' R \tag{A.12}$$

Combining equations for $\binom{0}{0}$,$\binom{1}{1}$ and $\binom{2}{2}$ components, we obtain:

$$\ddot{B} = \frac{8\pi G}{c}\left[e^{-2B}\psi'^2 + V + \frac{\rho c}{2}\right] + 2e^{-2B}c^2\left[\frac{R''}{R} - \frac{R'B'}{R}\right] - \frac{2\dot{B}\dot{R}}{R} - \dot{B}^2 \tag{A.13}$$

or equivalently we can obtain

$$\ddot{B} = -c^2e^{-2B}\frac{R'^2}{R^2} + \frac{c^2}{R^2} + \frac{\dot{R}^2}{R^2} - \dot{B}^2 - 4\pi G\rho - \frac{8\pi G}{c}\left[\frac{\dot{\psi}^2}{2c^2} - e^{-2B}\frac{\psi'^2}{2}\right] \tag{A.14}$$

and from $\binom{1}{1}$, we already have eqn.(A.9). Rewriting it again

$$\frac{\ddot{R}}{R} = -\frac{4\pi G}{c}\left[\frac{\dot{\psi}^2}{2c^2} + \frac{e^{-2B}\psi'^2}{2} - V\right] - \frac{1}{2}\frac{\dot{R}^2}{R^2} + \frac{c^2}{2}\left[e^{-2B}\frac{R'^2}{R^2} - \frac{1}{R^2}\right] \tag{A.15}$$

A.3 Numerical Methods

Three second order partial differential equations, eq (2.3),(2.4) and (2.5), can be written as 6 first order partial differential equations and we have two first order partial differential equations for ρ and R' giving us total of 8 first order partial differential equations.

$$\dot{x}_i(r) = f_i\left[x_1(r), x_2(r), .., x_8(r), x_1'(r), x_1''(r), x_3'(r)\right] \tag{A.16}$$

$$\{x_1, x_2, x_3, x_4, x_5, x_6, x_7, x_8\} = \left\{\psi, R, B, \dot{\psi}, \dot{R}, \dot{B}, \rho, R'\right\} \tag{A.17}$$

But solving these equations using time 't' as parameter turns out to be time consuming, so we switch to background scale factor 'a(t)' as independent parameter. Switching from 't' to 'a' requires simultaneously solving two more equations for $\dot{a}$ and $\ddot{a}$:

Having structured equations in above form, we used a RK4 algorithm to solve the equations in following flow:

- Initialise all variables
- Loop over "a" begins

  Calculate spatial derivatives

  RK4 first predictor step to calculate $x_i k1$'s

  Calculate spatial derivatives

  RK4 second predictor step to calculate $x_i k2$'s

  Calculate spatial derivatives

  RK4 third predictor step to calculate $x_i k3$'s

  Calculate spatial derivatives

  RK4 fourth predictor step to calculate $x_i k4$'s and correction.
- Loop over "a" ends

We have tested the algorithm for numerical convergence by varying Δt and Δr. Further, the epoch of virialisation scales correctly with initial density contrasts. We have also solved the equations in the case of ΛCDM and compared with the solutions obtained using the first integral. These tests have been used to validate the code.

Appendix B

Linear Theory Equations for modification of CLASS for Chapter 5

B.1 Equations in Synchronous Gauge

Here we present the equations required for modification of CLASS for tachyonic field. Since synchronous gauge is the default gauge in CLASS, we write the equations in this gauge. Quintessence with some potentials are already implemented in CLASS, one can simply follow the same structure for incorporating the tachyonic models. Here, we present equations for both quintessence and tachyonic field because this helps on modifications comparing with quintessence implementation.

Note: In this section, we use conformal time and prime represents derivative wrt to conformal time.

Field dynamics equation: For tachyonic models

$$\begin{aligned}(\delta\phi)'' &= \left[1-\frac{\phi'^2}{a^2}\right]\left[a^2(\delta\phi)\left\{\frac{(V_{,\phi})^2}{V^2}-\frac{(V_{,\phi\phi})^2}{V^2}\right\}+\nabla^2(\delta\phi)-\frac{\phi' h'}{2}\right] \\ &\quad +(\delta\phi)'\left[-\frac{2a'}{a}+9\frac{a'}{a}\frac{\phi'^2}{a^2}+2\frac{V_{,\phi}}{V^2}\phi'^2\right] \end{aligned} \tag{B.1}$$

For quintessence

$$(\delta\phi)'' = -a^2(\delta\phi)(V_{,\phi\phi})-\frac{\phi' h'}{2}-\frac{2a'}{a}(\delta\phi)'+\nabla^2(\delta\phi) \tag{B.2}$$

Density ($\delta\rho$) and pressure perturbations (δp): For tachyonic field

$$(\delta\rho) = \frac{(\delta\phi)(V_{,\phi})}{\sqrt{1-\frac{\phi'^2}{a^2}}} + \frac{V\phi'(\delta\phi)'}{a^2\left[1-\frac{\phi'^2}{a^2}\right]^{3/2}} \tag{B.3}$$

$$(\delta p) = -(\delta\phi)(V_{,\phi})\sqrt{1-\frac{\phi'^2}{a^2}} + \frac{V\phi'(\delta\phi)'}{a^2\sqrt{1-\frac{\phi'^2}{a^2}}} \tag{B.4}$$

For quintessence

$$(\delta\rho) = (\delta\phi)(V_{,\phi}) + \frac{\phi'(\delta\phi)'}{a^2} \tag{B.5}$$

$$(\delta p) = -(\delta\phi)(V_{,\phi}) + \frac{\phi'(\delta\phi)'}{a^2} \tag{B.6}$$

Effective velocity perturbations:
For tachyonic field

$$(\bar{\rho}+\bar{p})\theta = ik^j(\delta T)^0_j = \frac{\phi'}{a^2}k^2(\delta\phi)\frac{V}{\sqrt{1-\frac{\phi'^2}{a^2}}} \tag{B.7}$$

For quintessence

$$(\bar{\rho}+\bar{p})\theta = \frac{\phi'}{a^2}k^2(\delta\phi) \tag{B.8}$$

Bibliography

[1] A. Einstein, *The Field Equations of Gravitation*, *Sitzungsber. Preuss. Akad. Wiss. Berlin (Math. Phys.)* **1915** (1915) 844.

[2] A. Einstein, *Cosmological considerations on the general theory of relativity*, pp. 175–188. 1952.

[3] A. Einstein, *Cosmological Considerations in the General Theory of Relativity*, *Sitzungsber. Preuss. Akad. Wiss. Berlin (Math. Phys.)* **1917** (1917) 142.

[4] V. M. Slipher, *Spectrographic Observations of Nebulae*, *Popular Astronomy* **23** (1915) 21.

[5] E. Hubble, *A relation between distance and radial velocity among extra-galactic nebulae*, *Proceedings of the National Academy of Sciences* **15** (1929) 168 [https://www.pnas.org/content/15/3/168.full.pdf].

[6] C. O'Raifeartaigh, M. O'Keeffe, W. Nahm and S. Mitton, *Einstein's 1917 static model of the universe: a centennial review*, *European Physical Journal H* **42** (2017) [1701.07261].

[7] I. Newton, *Philosophiae naturalis principia mathematica, vol. 1 - 4*. 1760.

[8] A. Einstein, *Zur elektrodynamik bewegter körper*, *Annalen der Physik* **322** (1905) 891 [https://onlinelibrary.wiley.com/doi/pdf/10.1002/andp.1905322100

[9] A. Einstein, *On the electrodynamics of moving bodies*, *Annalen Phys.* **17** (1905) 891.

[10] G. F. R. Ellis, *Issues in the Philosophy of Cosmology*, *arXiv e-prints* (2006) astro [astro-ph/0602280].

[11] A. G. Lemaître, *A Homogeneous Universe of Constant Mass and Increasing Radius accounting for the Radial Velocity of Extra-galactic Nebulæ*, *Monthly Notices of the Royal Astronomical Society* **91** (1931) 483 [https://academic.oup.com/mnras/article-pdf/91/5/483/3079971/mnras91-0

[12] G. Lemaître, *L'Univers en expansion*, *Annales de la Société Scientifique de Bruxelles* **53** (1933) 51.

[13] H. P. Robertson, *Kinematics and World-Structure*, *ApJ* **82** (1935) 284.

[14] H. P. Robertson, *Kinematics and World-Structure II.*, *ApJ* **83** (1936) 187.

[15] H. P. Robertson, *Kinematics and World-Structure III.*, *ApJ* **83** (1936) 257.

[16] A. G. Walker, *On Milne's Theory of World-Structure*, *Proceedings of the London Mathematical Society* **42** (1937) 90.

[17] A. Einstein and W. de Sitter, *On the Relation between the Expansion and the Mean Density of the Universe*, *Contributions from the Mount Wilson Observatory* **3** (1932) 51.

[18] D. W. Hogg, *Distance measures in cosmology*, astro-ph/9905116.

[19] A. G. Riess, A. V. Filippenko, P. Challis, A. Clocchiatti, A. Diercks, P. M. Garnavich et al., *Observational evidence from supernovae for an accelerating universe and a cosmological constant*, *The Astronomical Journal* **116** (1998) 1009.

[20] S. Perlmutter, G. Aldering, G. Goldhaber, R. A. Knop, P. Nugent, P. G. Castro et al., *Measurements of* Ω *and* Λ *from 42 high-redshift supernovae*, *The Astrophysical Journal* **517** (1999) 565.

[21] B. P. Schmidt, N. B. Suntzeff, M. M. Phillips, R. A. Schommer, A. Clocchiatti, R. P. Kirshner et al., *The High-Z Supernova Search: Measuring Cosmic Deceleration and Global Curvature of the Universe Using Type IA Supernovae*, *ApJ* **507** (1998) 46 [astro-ph/9805200].

[22] C. O'Raifeartaigh, M. O'Keeffe, W. Nahm and S. Mitton, *Einstein's 1917 static model of the universe: a centennial review*, *Eur. Phys. J. H* **42** (2017) 431 [1701.07261].

[23] J. Ostriker and P. J. Steinhardt, *The Observational case for a low density universe with a nonzero cosmological constant*, *Nature* **377** (1995) 600.

[24] M. Davis, G. Efstathiou, C. S. Frenk and S. D. M. White, *The evolution of large-scale structure in a universe dominated by cold dark matter*, *ApJ* **292** (1985) 371.

[25] G. Efstathiou, W. J. Sutherland and S. J. Maddox, *The cosmological constant and cold dark matter*, *Nature* **348** (1990) 705.

[26] J. Bagla, T. Padmanabhan and J. Narlikar, *Crisis in cosmology: Observational constraints on omega and h(0)*, *Comments Astrophys.* **18** (1996) 275 [astro-ph/9511102].

[27] G. E. Addison, G. Hinshaw and M. Halpern, *Cosmological constraints from baryon acoustic oscillations and clustering of large-scale structure*, *MNRAS* **436** (2013) 1674 [1304.6984].

[28] D. M. Scolnic, D. O. Jones, A. Rest, Y. C. Pan, R. Chornock, R. J. Foley et al., *The Complete Light-curve Sample of Spectroscopically Confirmed SNe Ia from Pan-STARRS1 and Cosmological Constraints from the Combined Pantheon Sample*, *ApJ* **859** (2018) 101 [1710.00845].

[29] N. Aghanim, Y. Akrami, M. Ashdown, J. Aumont, C. Baccigalupi, M. Ballardini et al., *Planck 2018 results*, *Astronomy & Astrophysics* **641** (2020) A6.

[30] S. Weinberg, *The Cosmological Constant Problem*, *Rev. Mod. Phys.* **61** (1989) 1.

[31] L. Lombriser, *On the cosmological constant problem*, *Physics Letters B* **797** (2019) 134804.

[32] J. Martin, *Everything you always wanted to know about the cosmological constant problem (but were afraid to ask)*, *Comptes Rendus Physique* **13** (2012) 566 .

[33] T. Clifton, P. G. Ferreira, A. Padilla and C. Skordis, *Modified Gravity and Cosmology*, *Phys. Rept.* **513** (2012) 1 [1106.2476].

[34] B. Boisseau, G. Esposito-Farese, D. Polarski and A. A. Starobinsky, *Reconstruction of a scalar tensor theory of gravity in an accelerating universe*, *Phys. Rev. Lett.* **85** (2000) 2236 [gr-qc/0001066].

[35] T. P. Sotiriou and V. Faraoni, *f(R) Theories Of Gravity*, *Rev. Mod. Phys.* **82** (2010) 451 [0805.1726].

[36] S. Nojiri, S. Odintsov and V. Oikonomou, *Modified Gravity Theories on a Nutshell: Inflation, Bounce and Late-time Evolution*, *Phys. Rept.* **692** (2017) 1 [1705.11098].

[37] G. Dvali, G. Gabadadze and M. Porrati, *4d gravity on a brane in 5d minkowski space*, *Physics Letters B* **485** (2000) 208 .

[38] V. Sahni and Y. Shtanov, *Brane world models of dark energy*, *JCAP* **11** (2003) 014 [astro-ph/0202346].

[39] S. M. Carroll, *Quintessence and the rest of the world: Suppressing long-range interactions*, *Physical Review Letters* **81** (1998) 3067–3070.

[40] P. J. E. Peebles and B. Ratra, *Cosmology with a Time-Variable Cosmological "Constant"*, *ApJL* **325** (1988) L17.

[41] C. Wetterich, *An asymptotically vanishing time-dependent cosmological "constant"*., *A&A* **301** (1995) 321 [hep-th/9408025].

[42] S. Tsujikawa, *Quintessence: A Review*, *Class. Quant. Grav.* **30** (2013) 214003 [1304.1961].

[43] T. Padmanabhan, *Accelerated expansion of the universe driven by tachyonic matter*, *Phys. Rev. D* **66** (2002) 021301 [hep-th/0204150].

[44] J. Bagla, H. K. Jassal and T. Padmanabhan, *Cosmology with tachyon field as dark energy*, *Phys. Rev. D* **67** (2003) 063504 [astro-ph/0212198].

[45] T. Chiba, T. Okabe and M. Yamaguchi, *Kinetically driven quintessence*, *Phys. Rev. D* **62** (2000) 023511.

[46] C. Armendariz-Picon, V. Mukhanov and P. J. Steinhardt, *Dynamical Solution to the Problem of a Small Cosmological Constant and Late-Time Cosmic Acceleration*, *Phys. Rev. Lett.* **85** (2000) 4438 [astro-ph/0004134].

[47] C. Armendariz-Picon, V. Mukhanov and P. J. Steinhardt, *Essentials of k-essence*, *Phys. Rev. D* **63** (2001) 103510 [astro-ph/0006373].

[48] M. Bento, O. Bertolami and A. Sen, *Generalized Chaplygin gas, accelerated expansion and dark energy matter unification*, *Phys. Rev. D* **66** (2002) 043507 [gr-qc/0202064].

[49] J. K. Erickson, R. R. Caldwell, P. J. Steinhardt, C. Armendariz-Picon and V. Mukhanov, *Measuring the speed of sound of quintessence*, *Phys. Rev. Lett.* **88** (2002) 121301.

[50] A. Joyce, L. Lombriser and F. Schmidt, *Dark Energy Versus Modified Gravity*, *Annual Review of Nuclear and Particle Science* **66** (2016) 95 [1601.06133].

[51] R. Caldwell, R. Dave and P. J. Steinhardt, *Cosmological imprint of an energy component with general equation of state*, *Phys. Rev. Lett.* **80** (1998) 1582 [astro-ph/9708069].

[52] A. H. Guth, *Inflationary universe: A possible solution to the horizon and flatness problems*, *Phys. Rev. D* **23** (1981) 347.

[53] A. Linde, *A new inflationary universe scenario: A possible solution of the horizon, flatness, homogeneity, isotropy and primordial monopole problems*, *Physics Letters B* **108** (1982) 389 .

[54] A. Albrecht and P. J. Steinhardt, *Cosmology for grand unified theories with radiatively induced symmetry breaking*, *Phys. Rev. Lett.* **48** (1982) 1220.

[55] B. Ratra and P. Peebles, *Cosmological Consequences of a Rolling Homogeneous Scalar Field*, *Phys. Rev. D* **37** (1988) 3406.

[56] L. Amendola and S. Tsujikawa, *Dark Energy: Theory and Observations*. Cambridge University Press, 2010, 10.1017/CBO9780511750823.

[57] R. Caldwell and E. V. Linder, *The Limits of quintessence*, *Phys. Rev. Lett.* **95** (2005) 141301 [astro-ph/0505494].

[58] E. J. Copeland, A. R. Liddle and D. Wands, *Exponential potentials and cosmological scaling solutions*, *Phys. Rev. D* **57** (1998) 4686.

[59] I. Zlatev, L. Wang and P. J. Steinhardt, *Quintessence, cosmic coincidence, and the cosmological constant*, *Phys. Rev. Lett.* **82** (1999) 896.

[60] P. J. Steinhardt, L. Wang and I. Zlatev, *Cosmological tracking solutions*, *Physical Review D* **59** (1999) .

[61] A. Sen, *Rolling tachyon*, *Journal of High Energy Physics* **2002** (2002) 048.

[62] T. Padmanabhan and T. Choudhury, *Can the clustered dark matter and the smooth dark energy arise from the same scalar field?*, *Phys. Rev. D* **66** (2002) 081301 [hep-th/0205055].

[63] A. Singh, A. Sangwan and H. Jassal, *Low redshift observational constraints on tachyon models of dark energy*, *Journal of Cosmology and Astroparticle Physics* **2019** (2019) 047.

[64] A. Singh, H. Jassal and M. Sharma, *Perturbations in tachyon dark energy and their effect on matter clustering*, *Journal of Cosmology and Astroparticle Physics* **2020** (2020) 008–008.

[65] A. Vilenkin and E. P. S. Shellard, *Cosmic Strings and Other Topological Defects*. 2000.

[66] A. A. Penzias and R. W. Wilson, *A Measurement of Excess Antenna Temperature at 4080 Mc/s.*, *ApJ* **142** (1965) 419.

[67] R. H. Dicke, P. J. E. Peebles, P. G. Roll and D. T. Wilkinson, *Cosmic Black-Body Radiation.*, *ApJ* **142** (1965) 414.

[68] W. Hu and S. Dodelson, *Cosmic microwave background anisotropies*, *Annual Review of Astronomy and Astrophysics* **40** (2002) 171 [https://doi.org/10.1146/annurev.astro.40.060401.093926].

[69] H. Kodama and M. Sasaki, *Cosmological Perturbation Theory*, *Prog. Theor. Phys. Suppl.* **78** (1984) 1.

[70] V. F. Mukhanov, H. A. Feldman and R. H. Brandenberger, *Theory of cosmological perturbations*, *Phys. Reports* **215** (1992) 203.

[71] C.-P. Ma and E. Bertschinger, *Cosmological perturbation theory in the synchronous and conformal newtonian gauges*, *The Astrophysical Journal* **455** (1995) 7.

[72] D. Wands, K. A. Malik, D. H. Lyth and A. R. Liddle, *New approach to the evolution of cosmological perturbations on large scales*, *Phys. Rev. D* **62** (2000) 043527 [astro-ph/0003278].

[73] A. L. Erickcek, S. M. Carroll and M. Kamionkowski, *Superhorizon perturbations and the cosmic microwave background*, *Phys. Rev. D* **78** (2008) 083012 [0808.1570].

[74] *The early universe and observational cosmology*, *Lecture Notes in Physics* (2004) .

[75] J. M. Bardeen, *Gauge-invariant cosmological perturbations*, *Phys. Rev. D* **22** (1980) 1882.

[76] U. H. Gerlach and U. K. Sengupta, *Relativistic equations for aspherical gravitational collapse*, *Phys. Rev. D* **18** (1978) 1789.

[77] K. A. Malik and D. Wands, *Evolution of second-order cosmological perturbations*, *Class. Quant. Grav.* **21** (2004) L65 [astro-ph/0307055].

[78] K. Nakamura, *Second-Order Gauge Invariant Cosmological Perturbation Theory: — Einstein Equations in Terms of Gauge Invariant Variables —*, *Progress of Theoretical Physics* **117** (2007) 17 [https://academic.oup.com/ptp/article-pdf/117/1/17/19572268/117-1

[79] R. K. Sheth, H. J. Mo and G. Tormen, *Ellipsoidal collapse and an improved model for the number and spatial distribution of dark matter haloes*, *Monthly Notices of the Royal Astronomical Society* **323** (2001) 1 [https://academic.oup.com/mnras/article-pdf/323/1/1/3204200/323-1

[80] V. Desjacques, *Environmental dependence in the ellipsoidal collapse model*, *Monthly Notices of the Royal Astronomical Society* **388** (2008) 638 [https://academic.oup.com/mnras/article-pdf/388/2/638/2997902/mni

[81] G. Efstathiou, M. Davis, S. D. M. White and C. S. Frenk, *Numerical techniques for large cosmological N-body simulations*, *ApJS* **57** (1985) 241.

[82] J. S. Bagla, *Cosmological n-body simulation: Techniques, scope and status*, *Current Science* **88** (2005) 1088.

[83] J. G. Stadel, *Cosmological N-body simulations and their analysis*, Ph.D. thesis, UNIVERSITY OF WASHINGTON, Jan., 2001.

[84] S. J. Maddox, G. Efstathiou, W. J. Sutherland and J. Loveday, *Galaxy correlations on large scales.*, *MNRAS* **242** (1990) 43.

[85] M. Baldi, *Dark energy simulations*, *Physics of the Dark Universe* **1** (2012) 162 .

[86] J. Adamek, D. Daverio, R. Durrer and M. Kunz, *General relativistic n-body simulations in the weak field limit*, *Phys. Rev. D* **88** (2013) 103527.

[87] J. Adamek, D. Daverio, R. Durrer and M. Kunz, *General relativity and cosmic structure formation*, *Nature Physics* **12** (2016) 346 [1509.01699].

[88] C. Barrera-Hinojosa and B. Li, *GRAMSES: a new route to general relativistic n-body simulations in cosmology. part i. methodology and code description*, *Journal of Cosmology and Astroparticle Physics* **2020** (2020) 007.

[89] G. Lemaitre, *A Homogeneous Universe of Constant Mass and Growing Radius Accounting for the Radial Velocity of Extragalactic Nebulae*, *Gen. Rel. Grav.* **45** (2013) 1635.

[90] H. Bondi, *Spherically symmetrical models in general relativity*, *Mon. Not. Roy. Astron. Soc.* **107** (1947) 410.

[91] R. C. Tolman, *Effect of imhomogeneity on cosmological models*, *Proc. Nat. Acad. Sci.* **20** (1934) 169.

[92] J. E. Gunn and I. Gott, J. Richard, *On the Infall of Matter into Clusters of Galaxies and Some Effects on Their Evolution*, *Astrophys. J.* **176** (1972) 1.

[93] W. H. Press and P. Schechter, *Formation of Galaxies and Clusters of Galaxies by Self-Similar Gravitational Condensation*, *ApJ* **187** (1974) 425.

[94] J. R. Bond, S. Cole, G. Efstathiou and N. Kaiser, *Excursion Set Mass Functions for Hierarchical Gaussian Fluctuations*, *ApJ* **379** (1991) 440.

[95] H. Mo, F. C. van den Bosch and S. White, *Galaxy Formation and Evolution*. 2010.

[96] I. Maor and O. Lahav, *On virialization with dark energy*, *Journal of Cosmology and Astroparticle Physics* **2005** (2005) 003 [astro-ph/0505308].

[97] M. Pratap Rajvanshi, T. Chakraborty and J. S. Bagla, *Gravitational collapse and structure formation in an expanding universe with dark energy*, *arXiv e-prints* (2018) arXiv:1803.04267 [1803.04267].

[98] J. D. Barrow and P. Saich, *Growth of large-scale structure with a cosmological constant*, *MNRAS* **262** (1993) 717.

[99] R. K. Sheth, H. J. Mo and G. Tormen, *Ellipsoidal collapse and an improved model for the number and spatial distribution of dark matter haloes*, *Monthly Notices of the Royal Astronomical Society* **323** (2001) 1–12.

[100] A. Cooray and R. Sheth, *Halo models of large scale structure*, *Phys. Reports* **372** (2002) 1 [astro-ph/0206508].

[101] A. J. Benson, S. Cole, C. S. Frenk, C. M. Baugh and C. G. Lacey, *The nature of galaxy bias and clustering*, *Monthly Notices of the Royal Astronomical Society* **311** (2000) 793 [https://academic.oup.com/mnras/article-pdf/311/4/793/4866800/311-4-79

[102] V. Desjacques, D. Jeong and F. Schmidt, *Large-scale galaxy bias*, *Physics Reports* **733** (2018) 1 .

[103] S. Dodelson, *Modern Cosmology*. Academic Press, Amsterdam, 2003.

[104] N. Kaiser, *Clustering in real space and in redshift space*, *Mon. Not. Roy. Astron. Soc.* **227** (1987) 1.

[105] R. K. Sachs and A. M. Wolfe, *Perturbations of a Cosmological Model and Angular Variations of the Microwave Background*, *ApJ* **147** (1967) 73.

[106] V. Marra and M. Pääkkönen, *Exact spherically-symmetric inhomogeneous model with n perfect fluids*, *Journal of Cosmology and Astroparticle Physics* **2012** (2012) 025 [1105.6099].

[107] D. F. Mota and C. van de Bruck, *On the spherical collapse model in dark energy cosmologies*, *A&A* **421** (2004) 71 [astro-ph/0401504].

[108] F. Pace, J. C. Waizmann and M. Bartelmann, *Spherical collapse model in dark-energy cosmologies*, *MNRAS* **406** (2010) 1865 [1005.0233].

[109] L. R. Abramo, R. C. Batista, L. Liberato and R. Rosenfeld, *Structure formation in the presence of dark energy perturbations*, *Journal of Cosmology and Astroparticle Physics* **2007** (2007) 012 [0707.2882].

[110] L. R. Abramo, R. C. Batista, L. Liberato and R. Rosenfeld, *Physical approximations for the nonlinear evolution of perturbations in inhomogeneous dark energy scenarios*, *Phys. Rev. D* **79** (2009) 023516 [0806.3461].

[111] Z. Roupas, M. Axenides, G. Georgiou and E. N. Saridakis, *Galaxy clusters and structure formation in quintessence versus phantom dark energy universe*, *Phys. Rev. D* **89** (2014) 083002 [1312.4893].

[112] P. Creminelli, G. D'Amico, J. Noreña, L. Senatore and F. Vernizzi, *Spherical collapse in quintessence models with zero speed of sound*, *Journal of Cosmology and Astroparticle Physics* **2010** (2010) 027 [0911.2701].

[113] G. Ballesteros and J. Lesgourgues, *Dark energy with non-adiabatic sound speed: initial conditions and detectability*, *Journal of Cosmology and Astroparticle Physics* **2010** (2010) 014 [1004.5509].

[114] S. Anselmi, G. Ballesteros and M. Pietroni, *Non-linear dark energy clustering*, *Journal of Cosmology and Astroparticle Physics* **2011** (2011) 014 [1106.0834].

[115] M. Tsizh and B. Novosyadlyj, *Dynamics of dark energy in collapsing halo of dark matter*, *Advances in Astronomy and Space Physics* **5** (2015) 51 [1508.05518].

[116] C. Fidler, T. Tram, C. Rampf, R. Crittenden, K. Koyama and D. Wands, *Relativistic interpretation of Newtonian simulations for cosmic structure formation*, *Journal of Cosmology and Astroparticle Physics* **2016** (2016) 031 [1606.05588].

[117] J. Rekier, A. Füzfa and I. Cordero-Carrión, *Nonlinear cosmological spherical collapse of quintessence*, *Phys. Rev. D* **93** (2016) 043533.

[118] D. Herrera, I. Waga and S. E. Jorás, *Calculation of the critical overdensity in the spherical-collapse approximation*, *Phys. Rev. D* **95** (2017) 064029.

[119] S. Tian, S. Cao and Z.-H. Zhu, *The Dynamics of Inhomogeneous Dark Energy*, *ApJ* **841** (2017) 63 [1705.09908].

[120] I. Achitouv, *Improved model of redshift-space distortions around voids: Application to quintessence dark energy*, *Phys. Rev. D* **96** (2017) 083506 [1707.08121].

[121] C.-C. Chang, W. Lee and K.-W. Ng, *Spherical collapse models with clustered dark energy*, *Physics of the Dark Universe* **19** (2018) 12 [1711.00435].

[122] T. Basse, O. Eggers Bjælde and Y. Y. Y. Wong, *Spherical collapse of dark energy with an arbitrary sound speed*, *Journal of Cosmology and Astroparticle Physics* **2011** (2011) 038 [1009.0010].

[123] F. Pace, S. Meyer and M. Bartelmann, *On the implementation of the spherical collapse model for dark energy models*, *Journal of Cosmology and Astroparticle Physics* **2017** (2017) 040 [1708.02477].

[124] D. Lynden-Bell and J. Bičák, *Pressure in Lemaître–Tolman–Bondi solutions and cosmologies*, *Class. Quant. Grav.* **33** (2016) 075001 [1603.01479].

[125] A. Friedman, *On the Curvature of space*, *Z. Phys.* **10** (1922) 377.

[126] A. G. Walker, *On Riemannian spaces with spherical symmetry about a line, and the conditions for isotropy in general relativity*, *The Quarterly Journal of Mathematics* **1** (1935) 81.

[127] S. Unnikrishnan, H. K. Jassal and T. R. Seshadri, *Scalar field dark energy perturbations and their scale dependence*, *Phys. Rev. D* **78** (2008) 123504 [0801.2017].

[128] R. C. Batista and V. Marra, *Clustering dark energy and halo abundances*, *Journal of Cosmology and Astroparticle Physics* **2017** (2017) 048 [1709.03420].

[129] L. R. Abramo, R. C. Batista, L. Liberato and R. Rosenfeld, *Dynamical mutation of dark energy*, *Phys. Rev. D* **77** (2008) 067301 [0710.2368].

[130] H. K. Jassal, *Scalar field dark energy perturbations and the integrated Sachs-Wolfe effect*, *Phys. Rev. D* **86** (2012) 043528 [1203.5171].

[131] Y. T. Wang, L. X. Xu and Y. X. Gui, *Integrated Sachs-Wolfe effect in a quintessence cosmological model: Including anisotropic stress of dark energy*, *Phys. Rev. D* **82** (2010) 083522.

[132] J. Mifsud and C. van de Bruck, *Probing the imprints of generalized interacting dark energy on the growth of perturbations*, *Journal of Cosmology and Astroparticle Physics* **2017** (2017) 001 [1707.07667].

[133] F. de Bernardis, M. Martinelli, A. Melchiorri, O. Mena and A. Cooray, *Future weak lensing constraints in a dark coupled universe*, *Phys. Rev. D* **84** (2011) 023504 [1104.0652].

[134] V. Pettorino and C. Baccigalupi, *Coupled and extended quintessence: Theoretical differences and structure formation*, *Phys. Rev. D* **77** (2008) 103003 [0802.1086].

[135] W. Yang, H. Li, Y. Wu and J. Lu, *Cosmological constraints on coupled dark energy*, *Journal of Cosmology and Astroparticle Physics* **2016** (2016) 007 [1608.07039].

[136] M. Pratap Rajvanshi and J. S. Bagla, *Nonlinear spherical perturbations in quintessence models of dark energy*, *Journal of Cosmology and Astroparticle Physics* **2018** (2018) 018 [1802.05840].

[137] M. Pratap Rajvanshi and J. S. Bagla, *Erratum: Nonlinear spherical perturbations in quintessence models of dark energy*, *Journal of Cosmology and Astroparticle Physics* **2020** (2020) E01.

[138] P. Wu and H. Yu, *Reconstructing the properties of dark energy from recent observations*, *Journal of Cosmology and Astroparticle Physics* **2007** (2007) 014 [0710.1958].

[139] V. Sahni and A. Starobinsky, *Reconstructing Dark Energy*, *International Journal of Modern Physics D* **15** (2006) 2105 [astro-ph/0610026].

[140] T. D. Saini, S. Raychaudhury, V. Sahni and A. A. Starobinsky, *Reconstructing the Cosmic Equation of State from Supernova Distances*, *Phys. Rev. Lett.* **85** (2000) 1162 [astro-ph/9910231].

[141] D. Huterer and M. S. Turner, *Prospects for probing the dark energy via supernova distance measurements*, *Phys. Rev. D* **60** (1999) 081301 [astro-ph/9808133].

[142] C. Li, D. E. Holz and A. Cooray, *Direct reconstruction of the dark energy scalar-field potential*, *Phys. Rev. D* **75** (2007) 103503 [astro-ph/0611093].

[143] B. F. Gerke and G. Efstathiou, *Probing quintessence: reconstruction and parameter estimation from supernovae*, *MNRAS* **335** (2002) 33 [astro-ph/0201336].

[144] C. Clarkson and C. Zunckel, *Direct Reconstruction of Dark Energy*, *Phys. Rev. Lett.* **104** (2010) 211301 [1002.5004].

[145] D. Huterer and D. L. Shafer, *Dark energy two decades after: observables, probes, consistency tests*, *Reports on Progress in Physics* **81** (2018) 016901 [1709.01091].

[146] R. J. Scherrer, *Mapping the Chevallier-Polarski-Linder parametrization onto physical dark energy Models*, *Phys. Rev. D* **92** (2015) 043001 [1505.05781].

[147] R. A. Battye and F. Pace, *Approximation of the potential in scalar field dark energy models*, *Phys. Rev. D* **94** (2016) 063513 [1607.01720].

[148] M. Chevallier and D. Polarski, *Accelerating Universes with Scaling Dark Matter*, *International Journal of Modern Physics D* **10** (2001) 213 [gr-qc/0009008].

[149] E. V. Linder, *Exploring the Expansion History of the Universe*, *Phys. Rev. Lett.* **90** (2003) 091301 [astro-ph/0208512].

[150] P. W., *Computation of hypergeometric functions*, 2009.

[151] E. W. Weisstein, ""incomplete beta function." from mathworld–a wolfram web resource."

[152] A. Sangwan, A. Mukherjee and H. K. Jassal, *Reconstructing the dark energy potential*, *Journal of Cosmology and Astroparticle Physics* **2018** (2018) 018 [1712.05143].

[153] A. Tripathi, A. Sangwan and H. K. Jassal, *Dark energy equation of state parameter and its evolution at low redshift*, *Journal of Cosmology and Astroparticle Physics* **2017** (2017) 012 [1611.01899].

[154] H. M. Antia, *Numerical methods for scientists and engineers*. Hindustan Book Agency, 2012, 10.1007/978-93-86279-52-1.

[155] L. Amendola, *Coupled quintessence*, *Phys. Rev. D* **62** (2000) 043511 [astro-ph/9908023].

[156] M. Shahalam, S. D. Pathak, M. M. Verma, M. Y. Khlopov and R. Myrzakulov, *Dynamics of interacting quintessence*, *European Physical Journal C* **75** (2015) 395 [1503.08712].

[157] B. J. Barros, L. Amendola, T. Barreiro and N. J. Nunes, *Coupled quintessence with a ΛCDM background: removing the σ_8 tension*, *Journal of Cosmology and Astroparticle Physics* **2019** (2019) 007 [1802.09216].

[158] L. Heisenberg, M. Bartelmann, R. Brandenberger and A. Refregier, *Dark energy in the swampland*, *Phys. Rev. D* **98** (2018) 123502 [1808.02877].

[159] P. Agrawal, G. Obied, P. J. Steinhardt and C. Vafa, *On the cosmological implications of the string Swampland*, *Physics Letters B* **784** (2018) 271 [1806.09718].

[160] Y. Akrami, R. Kallosh, A. Linde and V. Vardanyan, *The Landscape, the Swampland and the Era of Precision Cosmology*, *Fortschritte der Physik* **67** (2019) 1800075 [1808.09440].

[161] M. Doran, C. M. Müller, G. Schäfer and C. Wetterich, *Gauge-invariant initial conditions and early time perturbations in quintessence universes*, *Phys. Rev. D* **68** (2003) 063505 [astro-ph/0304212].

[162] M. Malquarti and A. R. Liddle, *Evolution of large-scale perturbations in quintessence models*, *Phys. Rev. D* **66** (2002) 123506 [astro-ph/0208562].

[163] L. R. Abramo and F. Finelli, *Attractors and isocurvature perturbations in quintessence models*, *Phys. Rev. D* **64** (2001) 083513 [astro-ph/0101014].

[164] H. K. Jassal, *Comparison of perturbations in fluid and scalar field models of dark energy*, *Phys. Rev. D* **79** (2009) 127301 [0903.5370].

[165] A. Sen, *Tachyon Matter*, *Journal of High Energy Physics* **2002** (2002) 065 [hep-th/0203265].

[166] M. P. Rajvanshi and J. S. Bagla, *Reconstruction of dynamical dark energy potentials: Quintessence, tachyon and interacting models*, *Journal of Astrophysics and Astronomy* **40** (2019) 44 [1905.01103].

[167] H. K. Jassal, *Evolution of perturbations in distinct classes of canonical scalar field models of dark energy*, *Phys. Rev. D* **81** (2010) 083513.

[168] J.-c. Hwang and H. Noh, *Quintessential perturbations during scaling regime*, *Phys. Rev. D* **64** (2001) 103509.

[169] A. Mehrabi, S. Basilakos and F. Pace, *How clustering dark energy affects matter perturbations*, *MNRAS* **452** (2015) 2930 [1504.01262].

[170] R. Bean and O. Dore, *Probing dark energy perturbations: The Dark energy equation of state and speed of sound as measured by WMAP*, *Phys. Rev. D* **69** (2004) 083503 [astro-ph/0307100].

[171] R. de Putter, D. Huterer and E. V. Linder, *Measuring the speed of dark: Detecting dark energy perturbations*, *Phys. Rev. D* **81** (2010) 103513.

[172] J. Weller and A. M. Lewis, *Large-scale cosmic microwave background anisotropies and dark energy*, *MNRAS* **346** (2003) 987 [astro-ph/0307104].

[173] R. Batista and F. Pace, *Structure formation in inhomogeneous Early Dark Energy models*, *JCAP* **06** (2013) 044 [1303.0414].

[174] S. DeDeo, R. R. Caldwell and P. J. Steinhardt, *Effects of the sound speed of quintessence on the microwave background and large scale structure*, *Phys. Rev. D* **67** (2003) 103509 [astro-ph/0301284].

[175] Planck Collaboration, P. A. R. Ade, N. Aghanim, M. Arnaud, M. Ashdown, J. Aumont et al., *Planck 2015 results. XIII. Cosmological parameters*, *A&A* **594** (2016) A13 [1502.01589].

[176] A. Lewis, A. Challinor and A. Lasenby, *Efficient Computation of Cosmic Microwave Background Anisotropies in Closed Friedmann-Robertson-Walker Models*, *ApJ* **538** (2000) 473 [astro-ph/9911177].

[177] J. Lesgourgues, *The Cosmic Linear Anisotropy Solving System (CLASS) I: Overview*, *arXiv e-prints* (2011) arXiv:1104.2932 [1104.2932].

[178] D. Blas, J. Lesgourgues and T. Tram, *The Cosmic Linear Anisotropy Solving System (CLASS). Part II: Approximation schemes*, *Journal of Cosmology and Astroparticle Physics* **2011** (2011) 034 [1104.2933].

[179] J. Lesgourgues, *The Cosmic Linear Anisotropy Solving System (CLASS) III: Comparision with CAMB for LambdaCDM*, *arXiv e-prints* (2011) arXiv:1104.2934 [1104.2934].

[180] B. Audren, J. Lesgourgues, K. Benabed and S. Prunet, *Conservative Constraints on Early Cosmology: an illustration of the Monte Python cosmological parameter inference code*, *JCAP* **1302** (2013) 001 [1210.7183].

[181] T. Brinckmann and J. Lesgourgues, *MontePython 3: boosted MCMC sampler and other features*, 1804.07261.

[182] Planck Collaboration and A. et. al, *Planck 2018 results. VI. Cosmological parameters*, *A&A* **641** (2020) A6 [1807.06209].

[183] A. et. al*MNRAS* **470** (2017) 2617 [1607.03155].

[184] M. A. Buen-Abad, M. Schmaltz, J. Lesgourgues and T. Brinckmann, *Interacting dark sector and precision cosmology*, *Journal of Cosmology and Astroparticle Physics* **2018** (2018) 008 [1708.09406].

[185] F. Beutler, C. Blake, M. Colless, D. H. Jones, L. Staveley-Smith, L. Campbell et al., *The 6dF Galaxy Survey: baryon acoustic oscillations and the local Hubble constant*, *MNRAS* **416** (2011) 3017 [1106.3366].

[186] A. J. Ross, L. Samushia, C. Howlett, W. J. Percival, A. Burden and M. Manera, *The clustering of the SDSS DR7 main Galaxy sample - I. A 4 per cent distance measure at z = 0.15*, *MNRAS* **449** (2015) 835 [1409.3242].

[187] Planck Collaboration and e. a. Aghanim, *Planck 2018 results. I. Overview and the cosmological legacy of Planck*, *A&A* **641** (2020) A1 [1807.06205].

[188] B. et. al, *Improved cosmological constraints from a joint analysis of the SDSS-II and SNLS supernova samples*, *A&A* **568** (2014) A22 [1401.4064].